AD NUMBER: AD0826139
LIMITATION CHANGES
TO: Approved for public release; distribution is unlimited.
FROM: Qualified requesters may obtain copies of this report from DDC. Foreign announcements and dissemination of this report by DDC is limited.
AUTHORITY
ST-A ONR NOTICE, 27 JUL 1971

SU-SEL-67-086

STANFORD UNIVERSITY

CENTER FOR SYSTEMS RESEARCH

Inductorless Filters

by

Desmond F. Sheahan

Technical Report No. 6560-15

Systems Theory Laboratory

September 1967

The research described in this report was supported wholly by Lenkurt Electric Company, Inc. Preparation of this report was supported by the Joint Services Electronics Program (U. S. Army, U. S. Navy and U. S. Air Force) Under Contract Nonr-225(83), NR 373 360

SEL-67-086

INDUCTORLESS FILTERS

by

Desmond Francis Sheahan

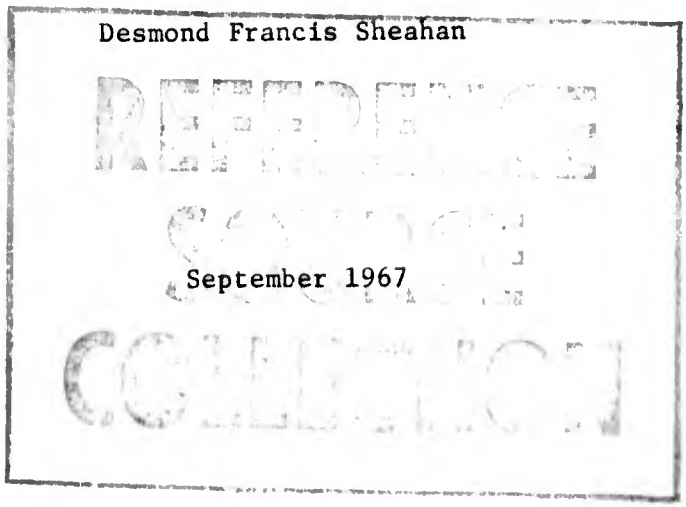

September 1967

Technical Report No. 6560-15

The research described in this report was supported wholly by Lenkurt Electric Company, Inc.

Preparation of this report was supported by the Joint Services Electronics Program (U.S. Army, U. S. Navy and U. S. Air Force) under Contract Nonr-225(83), NR 373 360

Systems Theory Laboratory
Stanford Electronics Laboratories
Stanford University Stanford, California

INDUCTORLESS FILTERS

In recent years integrated circuit technology has been used in the construction of many types of miniaturized electronic systems but it has not, as yet, found much application to the precision, electrical filters used by the telephone industry at frequencies up to a few hundred kilohertz. These filters require very high quality inductors, and those presently available are heavy, bulky items. Great savings in the size and weight of telephone systems would be obtained if suitable inductors could be made by integrated circuit techniques, but so far this has not been possible. One alternative is to make the filters by using those components which are available in integrable form.

Various schemes have been proposed for doing this, but most of them require component tolerances too tight to be practical. Many of the schemes use negative impedance converters in circuits whose transmission properties are determined by a critical match between a positive and a negative impedance; as a result of this matching process the transmission properties are very sensitive to component tolerances. The conventional, doubly terminated, inductor-capacitor filter, on the other hand is relatively insensitive to component tolerances, and it is proposed in the dissertation that this desirable property be retained by making an integrated circuit which simulates, in an inductorless fashion, the detailed behavior of the LC filter structure. Two distinct methods are described.

The first of these uses exactly the conventional LC filter structure and merely replaces each inductor by an integrable circuit that behaves like an inductor. The circuit takes the form of a frequency-independent, two-port network which, when terminated at one port by a capacitor, presents an

inductive behavior at the other port. This impedance inverting network, or gyrator , can be constructed from a pair of controlled sources. The dissertation analyzes this type of gyrator, derives a set of requirements for high-quality performance and describes a specific circuit which meets them. Experiments on a complex band-pass filter confirm that it is possible to obtain low sensitivity filters by this means.

The second method simulates the LC filter structure by making a complete model in the manner of an analog computer. Conventional analog computer circuitry proved inadequate and it was necessary to devise two special circuits to perform, very precisely, the operations of subtraction and integration. These were designated the Difference Amplifier and the Difference Integrator. In an attempt to produce a universal circuit arrangement that would be applicable to all classes of filter, these basic units were used to build the principal canonical tandem section due to Darlington and Brune. These simulated Brune sections were used to construct a low-pass, a high-pass, and a band-pass filter. Experiments on these filters showed that this also is a suitable way to produce low sensitivity filters.

It was found for both techniques, that, in order for the simulation to be successful, the original LC design should not have widely different L/C ratios in its resonant circuits. The dissertation compares the two techniques from several points of view and notes that the inductor simulation technique has a distinct practical advantage in that the filter capacitors isolate the bias circuits of the separate gyrators.

The two techniques are completely integrable as they use only resistors, capacitors, transistors and diodes. The tolerance and stability required of the resistors and capacitors can be achieved with modern thin-film

technology. Both techniques clearly show that complex filters can now be built in integrable form.

TABLE OF CONTENTS

LIST OF ILLUSTRATIONS

ACKNOWLEDGMENTS

I would like to acknowledge my deep debt of gratitude to H. J. Orchard and R. W. Newcomb for their inspiration and encouragement of this work. I would also like to express my grateful thanks to the management of Lenkurt Electric Co., Inc. for their support of this research, all of which was performed in the company's laboratories.

Desmond F. Sheahan

CHAPTER 1. THE CASE FOR INDUCTORLESS FILTERS

In recent years integrated circuit technology has permitted complex electronic circuits to be built smaller, lighter, and more economically that was formerly possible with discrete components. Up to now, however, these advantages have been applied mainly to non-linear digital circuits. This is partly due to the fact that this new technology as it exists today is incapable of making inductors, and the inductor is much more a fundamental component for linear than for digital circuits.

The greatest usage for inductors in linear circuitry is probably to be found in the manufacture of circuits designed to accept or reject signals of certain frequencies. Such circuits called electrical filters are used in vast quantities by the telephone industry to combine and separate individual telephone channels, for transmission over long distance carrier and microwave radio links. The frequency range of greatest interest for these filters is the spectrum below 100 kHz. This application for inductors in telephone-channel filters also happens to be one of the most demanding on the quality of inductor required.

Telephone-channel filters take up a great deal of space and weight in carrier systems, and much effort has been expended in trying to reduce their size. Considerable size reductions have been made in inductors as magnetic materials have been improved over the years, but it does appear to be true that the size of inductors cannot be decreased indefinitely, without suffering a lowering of inductor quality.

On the one hand, therefore, we have the tantalizing size and weight

capabilities of integrated circuits and on the other the size limitations of inductors, plus the fact that they cannot be integrated. It is thus worthwhile to explore alternate ways of making filters, to see if they can be built by inductorless means, and in a manner that will permit them to be integrated.

This dissertation will propose that inductorless filters can best be built by the simulation of terminated inductor-capacitor (LC) filters, in a manner that will retain the structure and consequently the excellent properties of these classical filters. Two separate means of performing this simulation will be presented along with the results of experiments performed on filters constructed by both means. The two methods to be described are the method of inductor simulation via gyrators and the method of total simulation via state-variable techniques. The results will show that low-sensitivity inductorless filters can be built, and in a manner that will permit them to be integrated.

CHAPTER 2. DISCUSSION OF PREVIOUS WORK ON THE PROBLEM

2.1 The Filter Transfer Function

The first important step in the design of any filter is choosing a transfer function H(s) to represent the ratio of an output quantity to an input quantity of the desired filter. This transfer function is a ratio of two polynomials in the complex frequency variable s, and as a function of frequency it gives a satisfactory approximation to the desired filter response curve. Once H(s) has been chosen the next problem is to find a network which produces it, that is, to decide on how to obtain this transfer function using electronic components as building blocks. Traditional building blocks for the synthesis of passive filter circuits are inductors, capacitors, resistors, and sometimes coupled coils. The building blocks to be considered in this dissertation are resistors, capacitors, transistors and diodes.

The numerator and denominator of the transfer function can be factored as shown in Equation 2.1. When put in this form the zeros of the numerator, z_i, are called the transmission zeros or attenuation poles of the filter, and the zeros of the denominator, p_i, are called the natural frequencies.

$$H(s) = \frac{a_o + a_1 s + a_2 s^2 + \ldots a_m s^m}{b_o + b_1 s + b_2 s^2 + \ldots b_n s^n}$$

$$= \frac{a_m(s - z_1)(s - z_2) \ldots (s - z_m)}{b_n(s - p_1)(s - p_2) \ldots (s - p_n)} \qquad 2.1$$

There are many techniques in existence for the synthesis of filter transfer functions. The useful passive filter syntheses can be categorized as RC, RL, or terminated LC methods. The RC and RL methods allow natural frequencies of the transfer function only on the negative real axis of the complex frequency plane, and in practice this restricts the types of filter responses that can be approximated using finite numbers of elements. Terminated LC methods, however, permit greater freedom because the natural frequencies can be realized anywhere in the left half plane. The RC and RL methods also suffer from high insertion loss, whereas if only reactive components are used, as is the case with passive LC filters, these losses can be zero.

2.2 The Doubly-Terminated LC Filter

The most widely used and the most versatile type of passive filter is the reactive LC structure whose input and output impedances are matched to the source and load resistances at frequencies in the filter's passband. Transmission through this circuit, as will now be shown, is insensitive to small changes in all component values for frequencies in the passband of the filter.

Consider the circuit in Figure 2.1 where the filter network is entirely reactive and is placed between a source resistance R_o and a load resistance R_L. At any frequency where the input impedance of the

terminated network is R + jX the power P_N into the filter network is given by Equation 2.2.

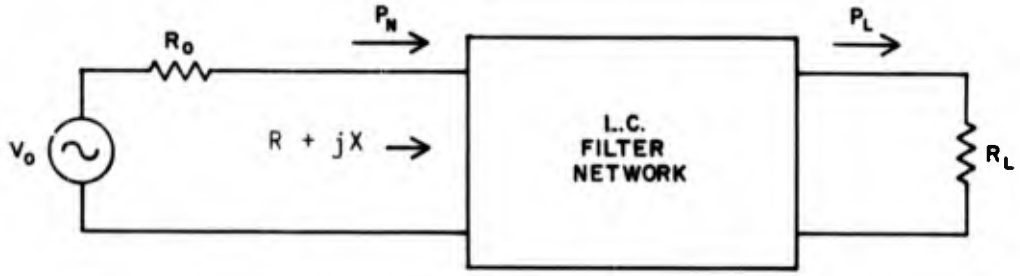

FIGURE 2.1. Doubly-Terminated LC Filter.

$$P_N = \frac{V_o^2 R}{(R + R_o)^2 + X^2} \qquad 2.2$$

As the LC filter network is composed of dissipationless components all of the power P_N must be dissipated in the load resistor R_L.

Therefore P_L, the output power = P_N

We now wish to see what happens to the output power P_L when any component value x_i in the filter network is changed from its design value. In general

$$\frac{\delta P_L}{\delta x_i} = \frac{\delta P_L}{\delta R} \cdot \frac{\delta R}{\delta x_i} + \frac{\delta P_L}{\delta X} \cdot \frac{\delta X}{\delta x_i} \qquad 2.3$$

But from Equation 2.2

$$\frac{\delta P_L}{\delta R} = V_o^2 \left[\frac{R_o^2 - R^2 + X^2}{\left\{(R + R_o)^2 + X^2\right\}^2} \right] \quad \text{and} \quad \frac{\delta P_L}{\delta X} = \frac{-V_o^2\ 2\ RX}{\left\{(R + R_o)^2 + X^2\right\}^2} \qquad 2.4$$

At frequencies of minimum loss in the passband of the filter one normally arranges to have maximum transfer of power through the filter, and this means having $R = R_o$ and $X = 0$. Therefore in the passband $\frac{\delta P_L}{\delta R} = \frac{\delta P_L}{\delta X} = 0$, and the sensitivity to any component will likewise be zero. We can also see by the following reasoning that the output impedance of the filter must be simultaneously matched to the load resistor. Maximum power is being obtained from the source, as the filter's input impedance is matched to the source resistance. The maximum available power is therefore being delivered to the load resistor because the LC filter network is dissipationless. Any change in the value of the load resistor will not result in a larger output power. Consequently the filter's output impedance must also be matched to the load resistor.

What we have just shown means that any terminated LC filter, having input and output impedances matched to the source and load resistances respectively for frequencies in its passband, will have zero first derivative of output power with respect to all components at frequencies in its passband.

This low sensitivity property, which is not present in other known filter structures, helps to explain why this filter structure is almost

universally used wherever complex filters with exacting passband specifications are required. It enables complex filters to be constructed from moderate tolerance components.

2.3 Active Filters

Interest in inductorless filters gained momentum in 1954 with the publication by Linvill [1] of a paper entitled "RC Active Filters" in which he showed that filter transfer functions could be realized via resistors, transistors, and capacitors. Linvill used the term Active Filters because the essential component of his filters is the negative impedance converter, which is an active device that provides some power gain in his filters. As will be shown in Section 4.1, one of the filter simulation techniques proposed in this dissertation involves a device that can be either active or passive, yet the filters constructed from it will not deliver any power gain. The term Inductorless Filters rather than Active Filters is consequently a more descriptive name for the filters in this dissertation.

In the past decade numerous schemes have been proposed for synthesizing active filters but they all use variations of the Linvill method, and to a greater or less degree they suffer from the same malady of unreasonably high component sensitivity.

The basic scheme proposed by Linvill and further developed by other authors [2,3,4.] consists of two RC networks, A and B, separated by a negative impedance converter (N.I.C.) as shown in Figure 2.2. This structure is used to realize a transfer function and it permits natural frequencies to be obtained anywhere in the left half of the complex frequency plane.

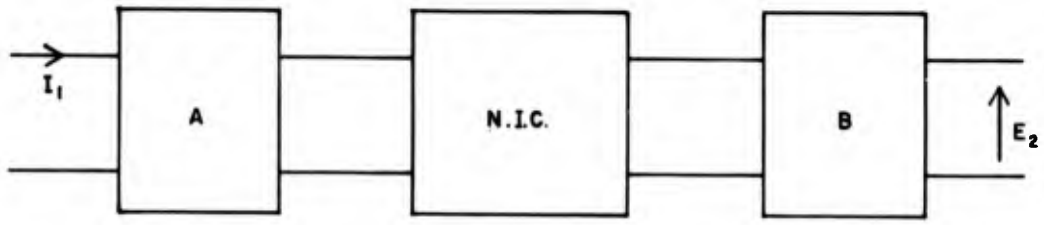

FIGURE 2.2. N.I.C. Filter Structure.

The transfer impedance of this structure is

$$Z_{21} = \frac{E_2}{I_1} = \frac{Z_{12a} Z_{12b}}{Z_{22a} - Z_{11b}} \qquad 2.5$$

where the terms in the right hand part of the equation are the open circuit impedance parameters of the two networks A and B.

The filter transfer function can be synthesized by designing the A and B networks so that the combination of their open circuit impedances in Equation 2.5 realizes the desired Z_{21}. For high order transfer functions these A and B networks will get quite complicated and the filter's sensitivity suffers.[5] It becomes more convenient to factor the numerator and denominator polynomials of H(s) into products of second order functions of s and this is the approach that has been adopted by most workers in this field.[1,5,6,7] The filter is then designed by associating one second order numerator factor with a second order denominator factor, and realizing the total second order function by the structure shown in Figure 2.2.

The complete filter is constructed by forming a tandem connection of such second order sections in a unidirectional circuit.

Each second order transfer function is designed by associating its poles and zeros with the open circuit impedance parameters of the A and B networks. If the open circuit impedances are all chosen to have the same pole frequencies, the zeros of Z_{12a} and Z_{12b} become the transmission zeros of Z_{21} and the difference between Z_{22a} and Z_{11b} determines the natural frequencies.

Synthesis procedures developed by other authors [2,6,8] also form their natural frequencies by an impedance subtraction process similar to $Z_{22a} - Z_{11b}$ in the Linvill method. Such schemes can lead to circuits with high component sensitivity as they may be realizing a small denominator impedance $Z_{22a} - Z_{11b}$ by the subtraction of two comparatively large impedances Z_{22a} and Z_{11b}. Therefore, small fractional changes in Z_{22a} or Z_{11b} can mean large fractional changes in their difference, $Z_{22a} - Z_{11b}$, and thus give a very sensitive circuit.

Sipress[5] has built a telephone channel filter by such an active synthesis technique. He obtained an excellent frequency response curve that agreed with his calculations, but the component tolerance required to preserve the passband response within 0.1 dB of its design value is of the order of 0.01%. This tolerance is over 100 times tighter than would be required of a comparable LC filter with matched terminations.

Blecher[7] has contrasted four synthesis techniques of the general Linvill type, each technique being based on splitting the transfer function into sections and realizing each section as a second order transfer

function of the general type described by Equation 2.6

$$T(s) = K_o \frac{N(s)}{(s + \sigma_c)^2 + \omega_c^2} \qquad 2.6$$

One of the synthesis procedures in Blecher's comparison is the method used by Sipress to construct his telephone channel filter. Blecher has tabulated the normalized pole sensitivities obtained with each technique. The sensitivity of a pole P_i to a component w is defined as

$$S_w^{P_i} = \frac{\delta P_i}{\frac{\delta w}{w}} \qquad 2.7$$

and the normalized pole sensitivity is defined as

$$\frac{S_w^{P_i}}{\sigma_c} \qquad 2.8$$

Blecher's tabulation shows that the normalized pole sensitivities for all four synthesis procedures can be represented by

$$\left| \frac{S_w^{P_i}}{\sigma_c} \right| = KQ \qquad 2.9$$

where Q is defined to be $\frac{\omega_c}{2\sigma_c}$ and K is a multiplier that varies between two and six for the four procedures.

Blecher's work, therefore, shows that these sensitivities are all of approximately the same order of magnitude, and, as shown by Sipress's results, the component sensitivitites of filters realized by these methods are too high to make them attractive for integrated circuit technology.

While this discussion of active filters has concentrated on those circuits which use NICs it is recognised that the circuit recently proposed by Kerwin[9] et al. has distinct sensitivity advantages; it may prove to be the best circuit to use if a filter is to be built as a unidirectional circuit.

2.4 Comparison Between Active Filters and LC Filters

It is worthwhile, therefore, to examine these active filter structures and compare them to the LC structure with matched terminations, which has been shown to have zero component sensitivity at frequencies in its passband. The basic difference depends on the fact that the LC filter operates by means of a complete interaction between its components, whereas the active filters, because of their unidirectional nature, do not. The transmission zeros of the LC filter are usually established by the resonance of one inductor and one capacitor per zero but its natural frequencies are determined by the interactions between all components in the filter. The active filters on the other hand establish their transmission zeros and natural frequencies by means of specific components, and there is no interaction between different second order functions

making up the filter. This basic difference provides a clue as to how low sensitivity inductorless filters should be made. They should try to preserve the interaction between components which is present in the LC filters, and rely on this interaction to determine the natural frequencies. A good inductorless filter technique should also avoid any subtraction of impedances, such as is used in the Linvill method to determine the natural frequencies.

The next chapter will show how these principles can be applied and used to obtain low-sensitivity inductorless filters.

CHAPTER 3. SIMULATION OF THE LOW-SENSITIVITY LC FILTER STRUCTURE

3.1 Filters by Simulation

Inductorless filters have been designed in the past by using the desired transfer function as a starting point and devising techniques for synthesizing this transfer function by inductorless means. As has been shown in Chapter 2, filters designed by these synthesis methods suffer from unacceptably high component sensitivity, especially when compared to the low sensitivity achievable with the doubly-terminated LC filter structure.

If, however, the LC doubly-terminated filter structure is simulated by methods that do not involve inductors, its ideal low sensitivity property should be retained. Simulation of the LC structure by inductorless means will then be the approach taken in this dissertation. Two independent simulation techniques will be presented. The first is simulation of the inductors only, and the second is simulation of the whole filter. The results of experiments on filters built by each of these methods will be displayed. These inductorless filters consisting of resistors, transistors, capacitors, and diodes, will be shown to have excellent component sensitivity.

3.2 Inductor Simulation Only

The first of the simulation techniques to be presented involves simulation of the inductors only, a technique first proposed by Orchard.[10] According to this scheme, all capacitors in the original LC filter cir-

cuit are retained at their design value and location in the circuit's topology; the inductors however are replaced by circuits whose external electrical properties are indistinguishable from those of inductors. When this inductance simulation is performed, the structure of the filter is undisturbed, and the voltages and currents in the filter interact just as they would in the original LC filter. There is then no reason why the excellent low sensitivity of the doubly terminated LC filter should not also be present in the filter with the simulated inductances ,the experimental results to be presented in Chapter 5 will show that this is actually the case.

The problem of implementing this inductorless filter technique resolves itself into that of designing an effective inductance simulation circuit. As the inductor is an energy storage element, an energy storage element will also be required in the simulation circuit. All energy storage in the inductorless filters will be effected via capacitance. One capacitor per inductor being simulated should be sufficient. The inductance simulation circuit can then be considered to consist of a circuit which looks inductive when it is combined with a capacitor. A gyrator loaded with a capacitor possesses this inductive property. One solution to the problem can therefore be obtained by making a good gyrator.

Tellegen[11] first proposed the gyrator as the basic non-reciprocal element of circuit theory. It is a two-port device shown schematically in Figure 3.1 and described mathematically by Equations 3.1 and 3.2. V_1 and V_2 are the instantaneous voltages appearing at the ports of the gyrator and I_1 and I_2 the instantaneous currents. In these equations

r_1 and r_2 are called the gyration resistances of the gyrator.

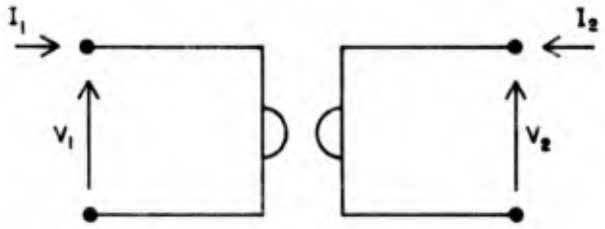

FIGURE 3.1. The Gyrator.

$$V_1 = -r_2 I_2 \qquad 3.1$$

$$V_2 = r_1 I_1 \qquad 3.2$$

When a capacitor C is placed across one port of the gyrator the other port looks inductive and the value of the inductance L thus obtained is related to the gyrator properties by Equation 3.3

$$L = C\, r_1 r_2 \qquad 3.3$$

The design of high quality gyrators will be discussed in detail in Chapter 4. The experimental results obtained when the inductors in a sophisticated filter were replaced by capacitively loaded gyrators will be presented in Chapter 5. These results show that this is a very effective way of making inductorless filters.

3.3 Simulating the Whole Filter

The second simulation technique to be discussed in this dissertation involves simulation of the complete LC filter structure rather than sim-

ulation of the inductors alone. All voltages and currents present in the original LC circuit are represented in the simulation circuit by analog equivalent voltages. The interactions that occur in the original LC circuit between its currents and voltages are performed in the simulation circuit by addition, multiplication, and integration circuits, composed of resistors, capacitors, and high gain amplifiers.

There is no direct topological correlation between the analog simulation circuit and the simulated LC circuit. The correlation between them is strictly mathematical. The same set of equations describes the relationships between the voltages and currents in the original LC filter and between their analog voltages in the simulation circuit.

One integrator will be required for each independent energy storage element in the original LC filter, and each integrator will consist of one capacitor, one resistor, and one high gain amplifier. This replacement of capacitors in the original LC circuit by an integrator in the analog circuit is a necessary complication which is caused by the fact that the simulation circuit is no longer a power transfer circuit, but is rather a voltage transfer circuit. In the original LC circuit the voltage across each capacitor is the integral of the current flowing through it. There are no corresponding currents in the analog simulation circuit and consequently the analog voltage corresponding to the voltage across a capacitor in the LC circuit is related via an integrator to the analog voltage corresponding to its current.

The complete simulation procedure just described can be applied to any type of filter circuit. This dissertation, however, will concen-

trate on the simulation of a particular type of LC circuit known as the Brune Section. The Brune Section was chosen for simulation because it can be used as a basic section in the design of low-pass, high-pass,or band-pass filters. The design of a simulation circuit for the Brune Section will be described in Chapter 6, and the experimental results obtained with analog Brune filters, as they will henceforth be called, will be described in Chapter 7. The analog Brune filters will be shown to have the low component sensitivity expected of them.

3.4 Integrable Simulation Circuits

Each of the LC filter simulation techniques just described depends on a basic circuit, either the gyrator or the Brune section. The desired filter is built up from a number of these identical circuits and this repetition can produce manufacturing economies if either circuit is integrated. The detailed circuits to be described in subsequent chapters were built from discrete components, but they were designed with eventual integration in mind. In order to facilitate this integration, the circuits were designed to be entirely direct-coupled and to consist only of transistors, diodes, resistors, and capacitors. The need for tight component value tolerances was avoided, as also was the necessity for critical matching of component values.

CHAPTER 4. THE GYRATOR

4.1 Gyrator Design

The gyrator equations in matrix form are

$$\begin{bmatrix} V_1 \\ V_2 \end{bmatrix} = \begin{bmatrix} 0 & -r_2 \\ r_1 & 0 \end{bmatrix} \begin{bmatrix} I_1 \\ I_2 \end{bmatrix} \qquad 4.1$$

For the directions of instantaneous voltages and currents shown in Figure 3.1 the instantaneous power flow P into the gyrator is given by Equation 4.2.

$$P = I_1 I_2 (r_1 - r_2) \qquad 4.2$$

This power can be positive or negative depending on the relative magnitudes of r_1 and r_2, and upon the signs of I_1 and I_2. Consequently, whenever $r_1 \neq r_2$, P can be negative for some currents I_1 and I_2, and therefore the gyrator must then be classified as an active device. On the other hand if $r_1 = r_2$, P = 0 and the gyrator is passive. The gyrators to be discussed in this dissertation will be used for inductor simulation only, where, as shown by Equation 3.3, the important quantity is the $r_1 r_2$ product: hence the relative magnitudes of r_1 and r_2 are unimportant.

Some unavoidable main-diagonal terms will be present in the gyrator matrix, Equation 4.1, of any practical gyrator. Such terms, although small compared to the off-diagonal terms, will tend to lower the quality of the gyrator. Gyrators have been built[12] by constructing a circuit

whose matrix has the correct off-diagonal terms for gyrator action, but also contains large undesirable main-diagonal terms. Negative resistances with magnitudes equal to those of the unwanted main-diagonal terms are then placed in series with the inputs of this circuit, so that resistance cancellation occurs at each port. This scheme, however, is undesirable where high quality gyrators are required, as the quality of the gyrator will depend on the degree of match between the magnitudes of the positive and negative resistances. Small percentage changes in these resistances will cause large percentage changes in the main-diagonal terms of the gyrator, and the quality of the gyrator will therefore be very sensitive to the component values used in its construction. This type of sensitivity is similar to that experienced with filters constructed from negative impedance converters as discussed in Chapter 2. Such methods of making a gyrator will not be used in this dissertation, as they would only result ultimately in filters having high sensitivities comparable to those of the NIC type filter circuits discussed in Chapter 2.

The gyrators to be discussed in this dissertation are of the controlled-source type. This type of gyrator does not involve any critical resistance-matching and it gives a low sensitivity circuit. Figure 4.1 shows the controlled-source realization of the gyrator resistance matrix, Equation 4.1.

The circuit consists of two current-controlled voltage sources. In order to obtain a practical realization of this circuit, ideal current-sensing elements that will not introduce any parasitic voltage drops at the input ports, will be required. The practical circuit should also

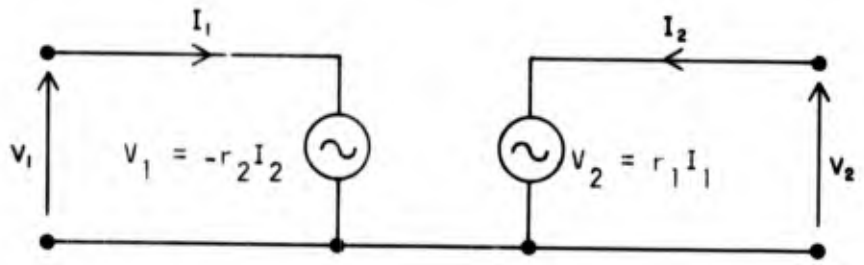

FIGURE 4.1. Current-Controlled Voltage Source Gyrator.

have good isolation between the two controlled-voltage generators.

An unsuccessful attempt was made to build a gyrator of this type using photon-coupled isolators as the current-sensing elements. The photon-coupled isolator is essentially a diode and a transistor coupled via a light beam. The diode is the current-sensing part of the device and it will cause only a very small parasitic voltage drop, as its series resistance is approximately 2Ω. The light beam being unidirectional provides good isolation between the voltage generators. The scheme was abandoned because of biasing difficulties. In any case it was felt that this scheme would not result in a practical gyrator because photon-coupled isolators do not lend themselves readily to integration.

If the gyrator resistance matrix of Equation 4.1 is transformed into the conductance matrix of Equation 4.3 an alternate method of constructing a controlled-source gyrator becomes apparent.

$$\begin{bmatrix} I_1 \\ I_2 \end{bmatrix} = \begin{bmatrix} 0 & g_1 \\ -g_2 & 0 \end{bmatrix} \begin{bmatrix} V_1 \\ V_2 \end{bmatrix} \qquad 4.3$$

$$g_1 = \frac{1}{r_1} \qquad g_2 = \frac{1}{r_2}$$

This matrix can be realized directly by the circuit of Figure 4.2.

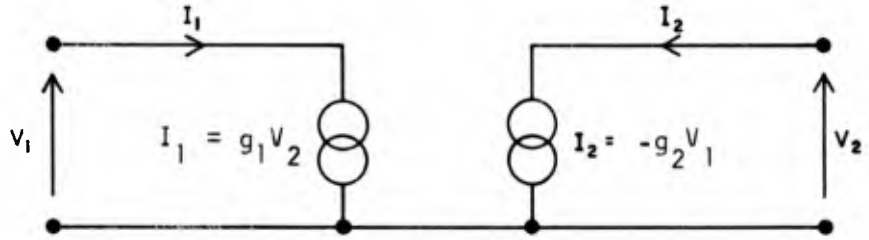

FIGURE 4.2. Voltage-Controlled Current Source Gyrator.

This gyrator circuit consists of two voltage-controlled current sources. A current source is a circuit with an infinite output impedance so a practical voltage-controlled current source is really a circuit with a very high input impedance and a very high output impedance. Ideally these impedances should be infinite as any finite impedances will tend to lower the quality of the gyrator. The effects on the gyrator of such finite impedances will now be examined in detail.

Let Equation 4.4 be the conductance matrix of the imperfect gyrator shown in Figure 4.3

$$\begin{bmatrix} G_1 & g_1 \\ -g_2 & G_2 \end{bmatrix} \qquad 4.4$$

In order to obtain a specific measure of the gyrator's quality consider the inductance obtained at port No. 1 of this gyrator when port No. 2 is loaded with a shunt capacitor to ground. The value of this

inductance is theoretically

$$L = \frac{C_2}{g_1 g_2} \qquad 4.5$$

Such an ideal inductance will be obtained only if a perfect capacitor is used and both main-diagonal terms of the gyrator matrix are zero. In practice a resistive term will be obtained at port No. 1 of the gyrator along with the desired inductance. This resistive term will result in an inductance with a finite Q. The quality of the capacitor will not substantially affect the resultant Q if high-quality capacitors ($Q \approx 10{,}000$) are used exclusively. Therefore we can consider the Q of the simulated inductance to be a direct measure of the gyrator's quality, and henceforth the term gyrator Q will be understood to mean the Q of the inductance realized when this gyrator is loaded with a perfect capacitor at one of its ports.

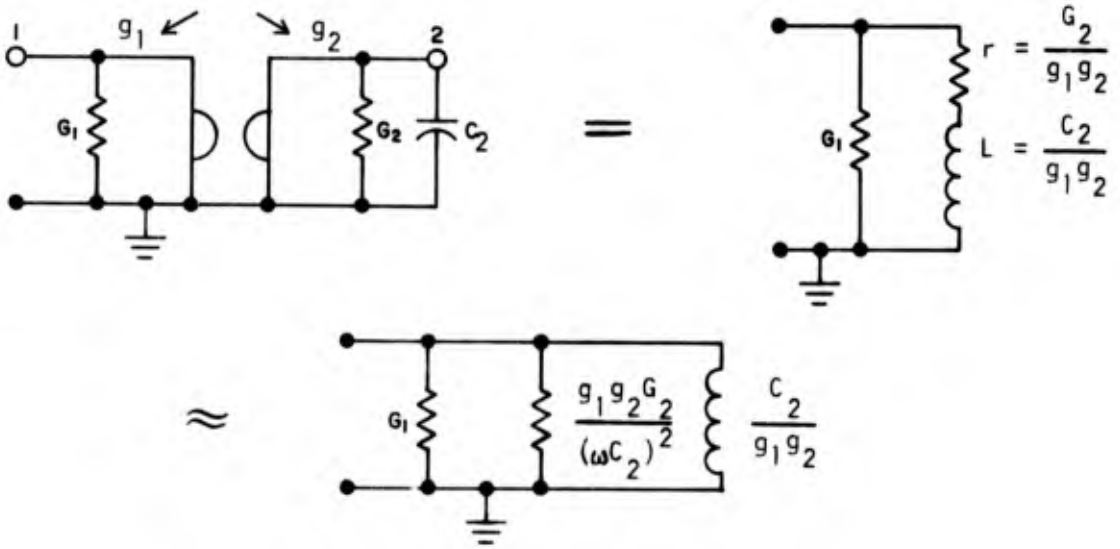

FIGURE 4.3. Simulated Inductance Obtained With Imperfect Gyrator.

As shown in Figure 4.3, imperfections in the gyrator lead to an inductance with a series resistance r and a shunt conductance G_1 exactly as in a real inductor.

The Q variation with frequency of the simulated inductance will consequently be the same as the variation of a wire wound inductor and has the form shown in Figure 4.4.

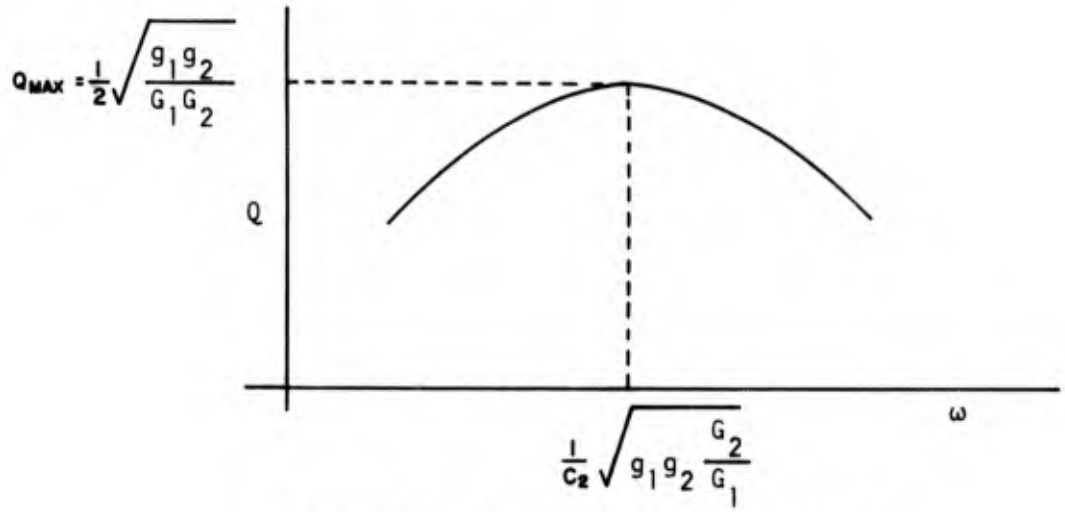

FIGURE 4.4. Q of Simulated Inductance.

The peak Q will occur when the Q due to the shunt conductance equals that due to the series resistance, i.e., when

$$\frac{\omega C_2}{g_1 g_2} \frac{g_1 g_2}{G_2} = \frac{g_1 g_2}{\omega C_2 G_1} \qquad 4.6$$

$$\text{therefore} \quad \omega^2 C_2^2 = g_1 g_2 \frac{G_2}{G_1}$$

However, when used in a resonant circuit, the equivalent inductance will be resonated with a capacitance C_1 giving

$$\omega^2 = \frac{1}{L C_1} = \frac{g_1 g_2}{C_1 C_2} \qquad 4.7$$

When $g_1 g_2$ in Equation 4.6 is replaced with $\omega^2 C_1 C_2$ from Equation 4.7 we obtain

$$\omega^2 C_2^2 = \omega^2 C_1 C_2 \frac{G_2}{G_1} \qquad 4.8$$

$$\text{therefore} \quad \frac{C_2}{C_1} = \frac{G_2}{G_1} \qquad 4.9$$

This is the condition for maximum gyrator Q. It can be stated somewhat differently that the maximum gyrator Q occurs when

$$\frac{\omega C_2}{G_2} = \frac{\omega C_1}{G_1} \qquad 4.10$$

i.e., the port Q, which is the ratio of susceptance to conductance at the port has the same value at each of the two ports. The maximum gyrator Q will be half that of each port Q.

$$Q_{max} = \frac{1}{2} \frac{\omega C_2}{G_2} \qquad 4.11$$

Substituting for ω from 4.7 we find the value of the maximum gyrator Q to be

$$Q_{max} = \frac{1}{2}\sqrt{\frac{g_1 g_2}{G_1 G_2}} \qquad 4.12$$

Note that the gyrator Q as defined above is strictly a property of the gyrator itself, even though it has meaning only when the gyrator is used along with a capacitor to simulate an inductance in a resonant circuit.

Another factor must be considered in obtaining an accurate expression for the gyrator Q, especially at high frequencies, and this is the contribution due to phase changes in the transconductances g_1 and g_2. Instead of constant transconductances, consider $g_1 g_2 e^{-j\omega T}$, where T is the sum of the time delays occurring in the two controlled sources. Neglecting the effect of time delay on the conductance G_2 as it will be very small in any case, consider the effect of this time delay on the simulated admittance.

The simulated admittance now becomes, for low enough frequencies

$$Y = \frac{g_1 g_2 e^{-j\omega T}}{j\omega C_2} \approx \frac{g_1 g_2}{j\omega C_2} - \frac{g_1 g_2 T}{C_2} \qquad 4.13$$

which gives a negative conductance in parallel with the desired simulated inductance as shown in Figure 4.5.

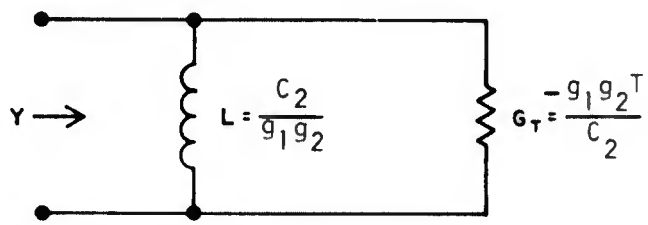

FIGURE 4.5. Conductance Caused by Gyrator Time Delay.

The time delay lowers the total value of conductance appearing at port No. 1 by an amount G_T. This causes an increase in Q and an increase in the frequency of maximum Q as seen from Figure 4.4. If T is large enough so that the net resistance in the circuit is zero, oscillation will occur. The effect of the time delay T is therefore very important as its adjustment enables any value of gyrator Q to be obtained. This time delay will have its greatest effect at the higher operating frequencies of the gyrator, where the product ωT becomes significant, as discussed below.

The actual Q of the simulated inductance is given by

$$Q = \frac{1}{\omega L G} \qquad 4.14$$

where G is the total conductance appearing across the terminals of this inductance. Combining the results obtained in Figures 4.3 and 4.5 we obtain the total conductance across the simulated inductance.

$$G = G_1 + G_2 \frac{g_1 g_2}{(\omega C_2)^2} - \frac{g_1 g_2 T}{C_2} \qquad 4.15$$

$$\text{therefore} \quad \frac{1}{Q} = \omega L \left[G_1 + G_2 \frac{g_1 g_2}{(\omega C_2)^2} - \frac{g_1 g_2 T}{C_2} \right] \qquad 4.16$$

This expression enables us to calculate the sensitivity of the gyrator Q to the time delay T. Taking the partial derivative of 1/Q with respect to T and substituting $\frac{C_2}{g_1 g_2}$ for L we obtain

$$\frac{\delta(\frac{1}{Q})}{\delta T} = -\omega \qquad 4.17$$

and

$$\delta(\frac{1}{Q}) = -\omega\delta T \qquad 4.18$$

i.e., a phase change of $\omega\delta T$ radians in the gyrator $g_1 g_2$ product causes an equal change in $1/Q$. Converting to a change in Q itself

$$\delta Q = (+\omega\delta T)Q^2 \qquad 4.19$$

If Q = 500, which is a typical value, the phase shift required to increase the Q by 50% to 750 is only 0.001 radians. Consequently, the quantities involved are seen to be very minute. This expression also shows how the problem of maintaining stable Q gets worse at high frequencies and at high Q values.

4.2 Requirements for a Practical Gyrator

From the previous analysis the requirements for a practical gyrator can be stated more specifically as follows:

1. Stable transconductances g_1 and g_2,
2. Low values of G_1 and G_2
3. Low value of time delay T
4. Whatever parasitic T does occur should be stable and in particular it should be insensitive to changes in temperature.

5. In order to have an integrable gyrator and not to limit its operating frequency range the gyrator should be a direct-coupled circuit.

For a gyrator composed of two voltage-controlled current sources, these requirements can be translated into more concrete quantities. The gyrator should be composed of two controlled sources of opposite polarity and both having high input and high output impedances. Therefore, when the controlled sources are connected to form a gyrator the complete circuit forms a negative feedback loop. This is shown schematically in Figure 4.6.

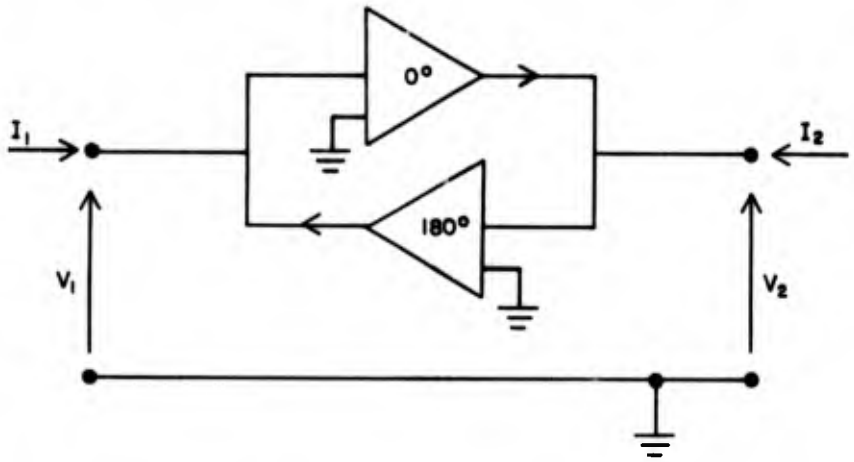

FIGURE 4.6. A Gyrator Formed by Two Voltage-Controlled Current Sources Each Having High Input and High Output Impedances.

4.3 Gyrator Using Bipolar Transistors and MOSFETs

Figure 4.7 is the circuit diagram of the gyrator developed to meet all the requirements listed in 4.2 and Figure 4.8 shows the Q values obtained. The circuit has metal-oxide-semiconductor field-effect transistors

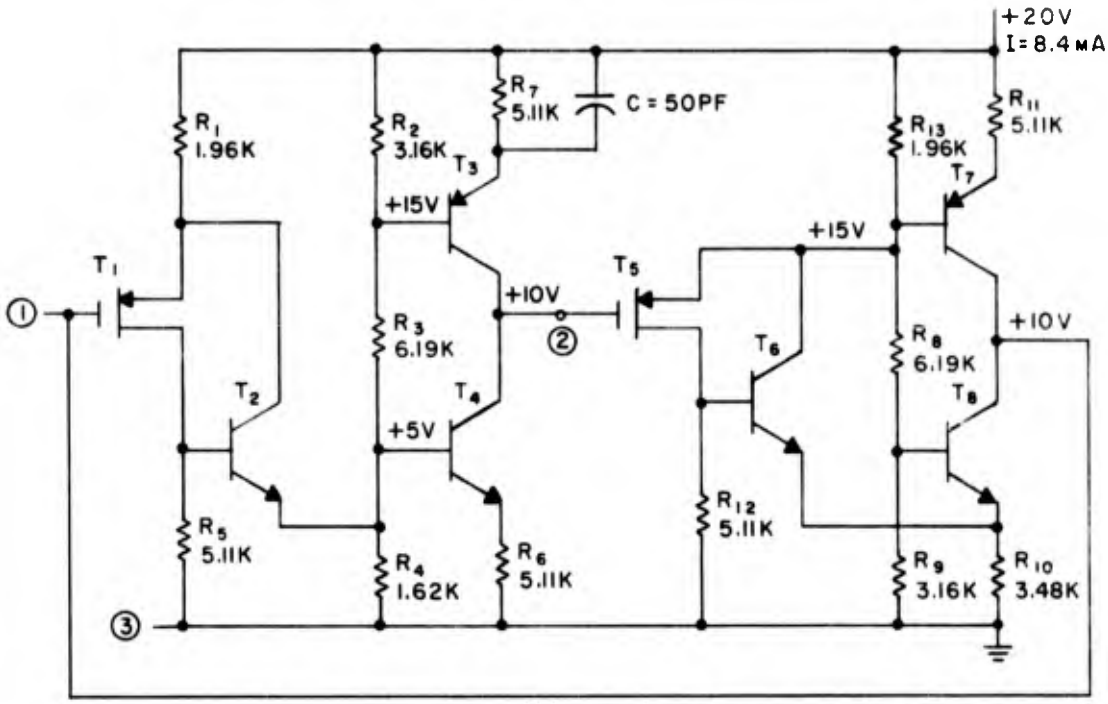

FIG. 4.7 MOSFET GYRATOR

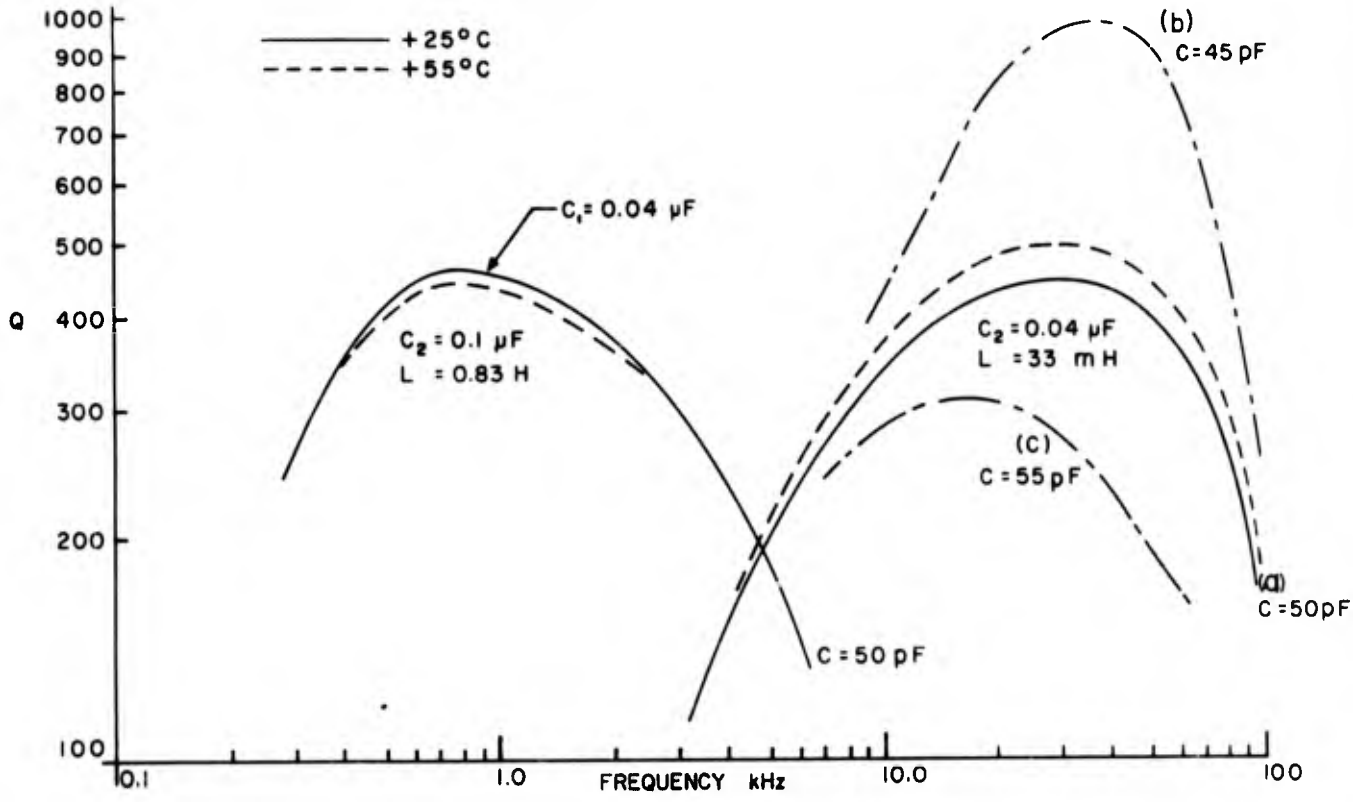

FIG. 4.8 Q OF MOSFET GYRATOR

(MOSFETs) at the input of each controlled source. These devices were used partly because of their extremely high input impedance ($\cong 10^{10}$ ohms) but mainly because they achieve this high impedance without introducing excessive and temperature-sensitive time delay to the controlled sources. This gyrator is most suitable for use at frequencies up to 100 kHz.

Darlington-pair transistors were tried on the inputs to the controlled sources in another gyrator circuit.[13] Maximum Q values of 350 were obtained with this alternate circuit and, while its performance at low frequencies was excellent, its Q was very temperature dependent at frequencies above 2 kHz. This high sensitivity of Q is due to temperature-sensitive time-delay being introduced by the Darlington pairs. This can be understood when it is considered that a very high impedance $\cong 0.5$ M Ω exists between the two transistors of such a pair, and the cutoff frequency of the input transistor is low because it is operated at negligible bias current. Consequently with such a combination the effect of temperature variations becomes very noticeable.

On the circuit diagram of Figure 4.7 the output circuit of each of the controlled sources is seen to consist of two complementary bipolar transistors. The high output impedance obtained is due to the collector output impedance of these transistors assisted by the feedback of the circuit. T_2 is used on the 1$\longrightarrow$2 controlled source to provide local feedback around the MOSFET and thus stabilize its transconductance g_m; this is required because, even though the MOSFET does not suffer from temperature-dependent time delay, its g_m is temperature sensitive. The use of T_2 along with the local source feedback of R_1 effectively stabi-

lizes the controlled source. The drive to the output of the 1⟶2 controlled source is through the emitter of T_2 to the bases of both T_3 and T_4.

The 2⟶1 controlled source is basically similar but in this case the drive to the output is taken from both the source and the drain of the MOSFET. To achieve the required 180° phase change in this controlled source, compared to the 1⟶2 controlled source, the emitter of T_6 drives the emitter of T_8. In the 1⟶2 controlled source, the source of the MOSFET was not used to drive the output as it would have had to be connected to the emitter of T_3; the low emitter-input impedance of T_3 would have meant less local feedback on T_1 and consequently the circuit would be more sensitive to variations in g_m. The use of bipolar transistors in the output circuits of the two controlled sources means that the impedances at the ports, and consequently the low frequency gyrator Q are determined by these output transistors. This is because the output impedances are of the order of 10 megohms as compared to thousands of megohms for the input impedances of the MOSFETs. Even though they can have high output impedances at their drain terminals, MOSFETs were not considered for the output circuits because they achieve this high impedance at low currents where the transconductance is also low.

An analysis of the 1⟶2 controlled source circuit gives

$$g_2 \approx \frac{g_m \dfrac{R_5R_7(R_2 + R_3) + R_2R_5R_6}{R_6R_7(R_2 + R_3)}}{g_mR_1\left[1 + \dfrac{R_5}{R_4}\dfrac{(R_2 + R_3 + R_4)}{R_2 + R_3}\right] + 1} \qquad 4.20$$

where g_m is the transconductance of the MOSFET T_1. Using the resistor values shown in Figure 1 and $g_m = 2 \times 10^{-3}$ mho, g_2 was calculated to be 0.135×10^{-3} mho.

The 2⟶1 controlled source is much more complex and g_1 is obtained from Equation 4.21

$$g_1 \approx \frac{g_m \beta \left[1 + \frac{R_{13}}{R_{11}} + \frac{R_{13}R_8}{R_9R_{11}} + \frac{(R_{13} + R_8)}{R_9} + \frac{R_{13}}{R_{10}} + \frac{R_{13}}{R_{12}} \right]}{-g_m R_{13} \beta \left[\frac{R_8}{R_9} + 1 \right] + \left[\frac{\beta R_{13} - R_8}{R_{12}} - 1 - \frac{R_{13} + R_8}{R_9} \right]} \qquad 4.21$$

where g_m is the transconductance of T_5 and β is the base to collector current gain of the bipolar transistors. Using the circuit values shown in Figure 4.7 with $g_m = 2 \times 10^{-3}$ mho and $\beta = 50$, g_1 was calculated to be 0.925×10^{-3} mho. This results in a calculated value for the g_1g_2 product of 0.125×10^{-6} mho^2, whereas the measured value was found to be 0.120×10^{-6} mho^2. The circuit does not have $g_1 = g_2$ but this was not considered to be a serious drawback as the gyrator was only required for inductor simulation where the important quantity is the g_1g_2 product.

Experiments on the circuit showed that as the values of R_5 and R_{12} were increased the greater gains from T_1 and T_5 decreased the sensitivity of the gyrator to changes in the g_m of the MOSFETs. Large values of these resistors, however, also caused the Q of the gyrator to be more temperature sensitive. The values of 5.1 kΩ shown in Figure 4.7 were found by experiment to be the best compromise.

Note that the circuit in Figure 4.7 can be operated without T_2 and T_6. When so used the Q of the gyrator is somewhat less temperature sensitive as there is one less active element in the forward path of each amplifier. With T_2 and T_6 removed, however, the circuit is more sensitive to changes in g_m. The $g_1 g_2$ product has a measured temperature coefficient of -300 ppm/°C when T_2 and T_6 are removed, whereas the complete circuit in Figure 4.7 has a temperature coefficient of <100 ppm/°C which is the temperature coefficient of the metal film resistors used in the circuit.

Figure 4.8 is a plot of the Q values obtained with this gyrator for equivalent inductances of 0.83H and 33 mH. This figure also shows that the temperature sensitivity of Q is negligible for frequencies below 1 kHz. This result was expected as the Q values at these frequencies are determined entirely by the low shunt conductances at the gyrator ports. The maximum possible drive level with this circuit is 2.0 V peak to peak when a supply voltage of +20 V is used. At greater levels the circuit becomes non-linear with a consequent decrease in Q.

The capacitor C shown in Figure 4.7 corrects for the small parasitic phase change which occurs in the basic gyrator circuit. It accomplishes this function by increasing the -3 dB frequency of the 1⟶2 controlled source from 1.1 MHz to 1.5 MHz. This capacitor can be adjusted to give a peak Q which either increases or decreases with frequency. The value of 50 pF shown in Figure 4.7 was chosen to give the same peak Q at all frequencies as is shown by Figure 4.8 (a). Figures 4.8 (b) and (c) show the Q values obtained when the capacitor C was 45 pF and 55 pF respectively.

4.4 Summary of Gyrator Design

A practical gyrator design has been demonstrated and from the experimental results it is apparent that high-Q inductances can easily be simulated by the circuit. This design achieves the desirable qualities listed in 4.2,and in order to achieve these properties it was necessary to use feedback loops. These feedback loops were needed to obtain high output impedances, and to maintain stable gyration conductances. Use of such feedback loops, however, makes it difficult to obtain a simple expression for the gyration conductances, i.e., expressions where each gyration conductance is determined essentially by only one resistor.

It appears that this MOSFET gyrator design in Figure 4.7 is a nearly optimum one for the controlled source type of gyrator because each controlled source uses just one input device and two output devices, with a third bipolar transistor per controlled source to improve the stability. Two output devices per amplifier is the minimum number possible, as one will have to act as a constant current drain for the bias current of the other.

4.5 Gyrator-Flotation Circuit

The voltage-controlled current source gyrator just described is a three-terminal device, and its common terminal is at ground potential when the gyrator is fed from a grounded power supply. Because of this the gyrator can directly simulate only inductors one of whose terminals is grounded. Many filter circuits will require inductances both of

whose terminals are floating above ground potential. A gyrator flotation circuit has been developed to permit such floating inductances to be obtained. This gyrator-flotation circuit is used in conjunction with the gyrator already described, and it enables the good quality and stability of this gyrator to be obtained in floating form.

Figure 4.9 (a) is the basic schematic diagram of the arrangement, and the detailed circuit is shown in Figure 4.9 (b). The circuit consists of a constant-current source, which feeds a constant bias current through the gyrator being floated and on into a constant-current drain. The constant-current source and drain thus effectively isolate the gyrator from ground via their high impedances, and in the detailed circuit of Figure 4.9 (b) their constant current functions are performed by the collector circuit of transistor T_1 for the source, and the collector circuit of transistor T_2 for the drain. The terminals of the gyrator are short circuited for a.c. signals by a capacitor C_2. The gyrator is therefore fed from a low impedance source for a.c. signals and from a high impedance for d.c.

Having a constant current source feeding a high impedance constant current drain will require some form of d.c. feedback in order to stabilize the bias voltage at the junction of the two devices. This feedback circuit contains a MOSFET T_4 as its sensing element so that its high input impedance will not lower the amount of isolation obtainable from the constant-current transistors T_1 and T_2. The feedback path extends from T_4 through R_6, T_3, R_8 and back to the base of T_1. This feedback circuit is decoupled for d.c. signals by the capacitor C_1.

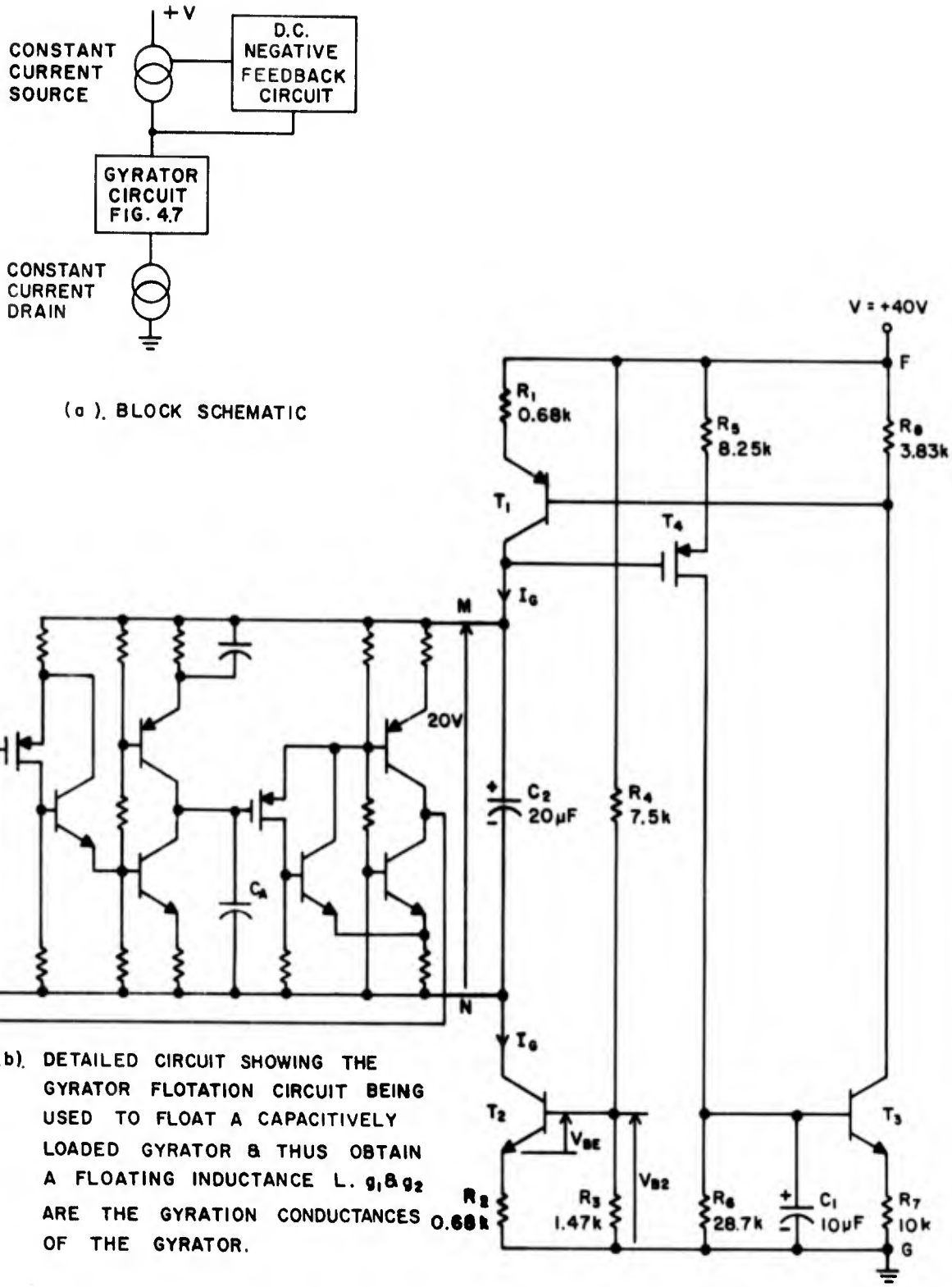

FIG. 4.9. GYRATOR FLOTATION CIRCUIT

This decoupling is necessary to prevent the feedback action from lowering the amount of isolation resistance possible.

The d.c. bias current I_G supplied to the gyrator can be obtained from equation 4.30

$$I_G = \frac{V_{B2} - V_{BE}}{R_2} \qquad 4.30$$

where V_{BE} is the base to emitter voltage of the transistor T_2 and V_{B2} is determined by the voltage-divider chain consisting of R_3 and R_4

$$I_G \cong \frac{V R_3}{R_2 (R_3 + R_4)} - \frac{V_{BE}}{R_2} \qquad 4.31$$

where V is the power supply voltage on the gyrator-flotation circuit.

The bias current I_G needed to develop the correct bias voltage of 20 V across the MOSFET gyrator terminals is 8.4 mA. The resistor values shown in Figure 4.9 (b) provide correct biasing when the MOSFET gyrator is used.

The isolation resistance R_I of this circuit is the resistance to ground from terminals M or N at a frequency where C_1 and C_2 have negligible reactance and this resistance is

$$R_I = \frac{r_c}{2 + \frac{R_8}{R_1} + \frac{R_3 R_4}{R_2 (R_3 + R_4)}} \qquad 4.32$$

For the component values shown in Figure 4.9 this is approximately $\frac{r_c}{10}$ ohms where r_c is the collector to base resistance of the transistors

T_1 and T_2. R_I of the circuit in Figure 4.9 (b) was measured at terminal M to be 120 k Ω at a frequency of 1 kHz.

The -3 dB frequency for the a.c. decoupling of the feedback circuit is obtained from Equation 4.33

$$f_{-3\ dB} \approx \frac{1}{2\pi R_6 C_1}\ Hz \qquad 4.33$$

For the component values used in Figure 4.9 (b) this frequency is about 0.5 Hz.

The Q versus frequency plots of various equivalent floating inductances measured in this circuit were similar to those shown in Figure 4.8 for the grounded MOSFET gyrator. The peak Q values obtained were approximately 350 for the floating inductors as compared to 450 for the grounded ones. This slight lowering of the peak Q is caused by the fact that the 120 k Ω of isolation from ground obtained with the circuit provides a small leakage path which lowers the Q but this is not a serious defect.

Use of this gyrator-flotation circuit provides good isolation for all frequencies greater than a few hertz. This circuit also preserves the good stability properties of the MOSFET controlled-source gyrator, and it is therefore a very effective way of realizing floating inductances.

4.6 Survey of Other Gyrator Circuits

Many gyrator circuits have been proposed since Tellegen[11] first introduced the concept and most of the earlier circuits used vacuum

tubes. Shekel[14] used negative impedance converters to cancel unwanted main diagonal terms. Bogert[15] used a feedback scheme and Sharpe[16] was the first to recognise the importance of the voltage-controlled current source. The above mentioned references however are mainly proposals and they contain very little experimental information.

There have been many semiconductor gyrator circuits developed in recent years and these circuits can be divided into two main types:

1. Voltage-controlled current source circuits
2. Circuits that use negative impedances to cancel undesirable main diagonal terms of the gyrator matrix.

As already mentioned, circuits of the second type are undesirable because the impedance-cancellation process leads to high Q sensitivity. Circuits of this second type are those in references 12,17,18,19 . Circuits of the first type are those in references 13,20,21,22,23,24 . The circuits in references 20 ,21 and 22 are of low quality and would be unsuitable for the simulation of high Q inductors. The circuit in reference 25 is also a poor quality circuit even though it proposes to use field-effect transistors in a controlled-current source configuration. It is low quality because it proposes to use field-effect transistors to obtain high output impedances as well as high input impedances. The field-effect transistor possesses high output impedance at very small bias currents thus limiting the power handling capability of such a gyrator. The circuit in reference 23 which has only very recently been disclosed is a good circuit but it is effectively the same as 13. Its basic Q is only 150 thus limiting its usefulness at low frequencies

and very stable phase shift capacitors are required to obtain high Q values at high frequencies.

The floating-inductor problem has also been tackled by Holt and Taylor[26] in a scheme consisting of two gyrators and by Holmes et al[24] in a circuit that uses voltage-controlled current sources. There are other floating-inductor circuits in existence but the two mentioned above are representative. These circuits require matched components in order to operate properly and experiments with the Holt and Taylor circuit[27] showed that the degree of matching required prohibits its use in complex filter circuits. The matching is required in these circuits because the input and output currents from the simulated floating inductance are determined by two independent circuits.

The gyrator circuit and the gyrator flotation circuit presented in this dissertation emphasize high quality and good stability in a direct-coupled integrable form. While the circuits described are somewhat complex this is the price of the good performance they provide. They permit stable high Q grounded or floating inductances to be simulated at frequencies from d.c. to 100 kHz. These properties are not claimed for any other circuit in the literature.

This dissertation also presents for the first time a complete analysis of the factors influencing the quality of a gyrator circuit.

CHAPTER 5. GYRATOR FILTERS

5.1 16.15 - 19.5 kHz Bandpass Filter

A complex bandpass filter was built with the MOSFET gyrator of Figure 4.7 for experimental verification of the proposal by Orchard [10] that low sensitivity filters could be constructed with gyrators.

The filter design chosen was a 16th degree bandpass filter with Chebyshev-passband and general stopband characteristics meeting the requirements of a typical frequency-division multiplex telephone-channel filter. The nominal passband extends from 16.15 kHz to 19.5 kHz. The filter is classified as a minimum-inductor type and the design procedure is based on the method of Watanabe [28]. The actual design of the filter was performed with the aid of a computer program developed at Lenkurt Electric Co. for this type of minimum-inductor filter.

Figure 5.1 (a) shows the design values of the basic LC filter and Figure 5.1 (b) shows the component values actually used to construct the gyrator version of this filter.

The source impedance of 1500 Ω was chosen for the filter because it resulted in the smallest deviation for all gyrators from the optimum Q condition of $C_2/C_1 = G_2/G_1 \cong 2$ (Equation 4.9). The value of 2 for the optimum capacitor ratio was obtained from the $C_2 = 0.1\mu F$ curve of Figure 4.8. This shows that the maximum Q occurs when $C_1 \cong 0.05\mu F$. The four grounded gyrators of Figure 5.2 (b) were realized by the circuit of Figure 4.7 and the three floating gyrators by the circuit of Figure 4.9 (b).

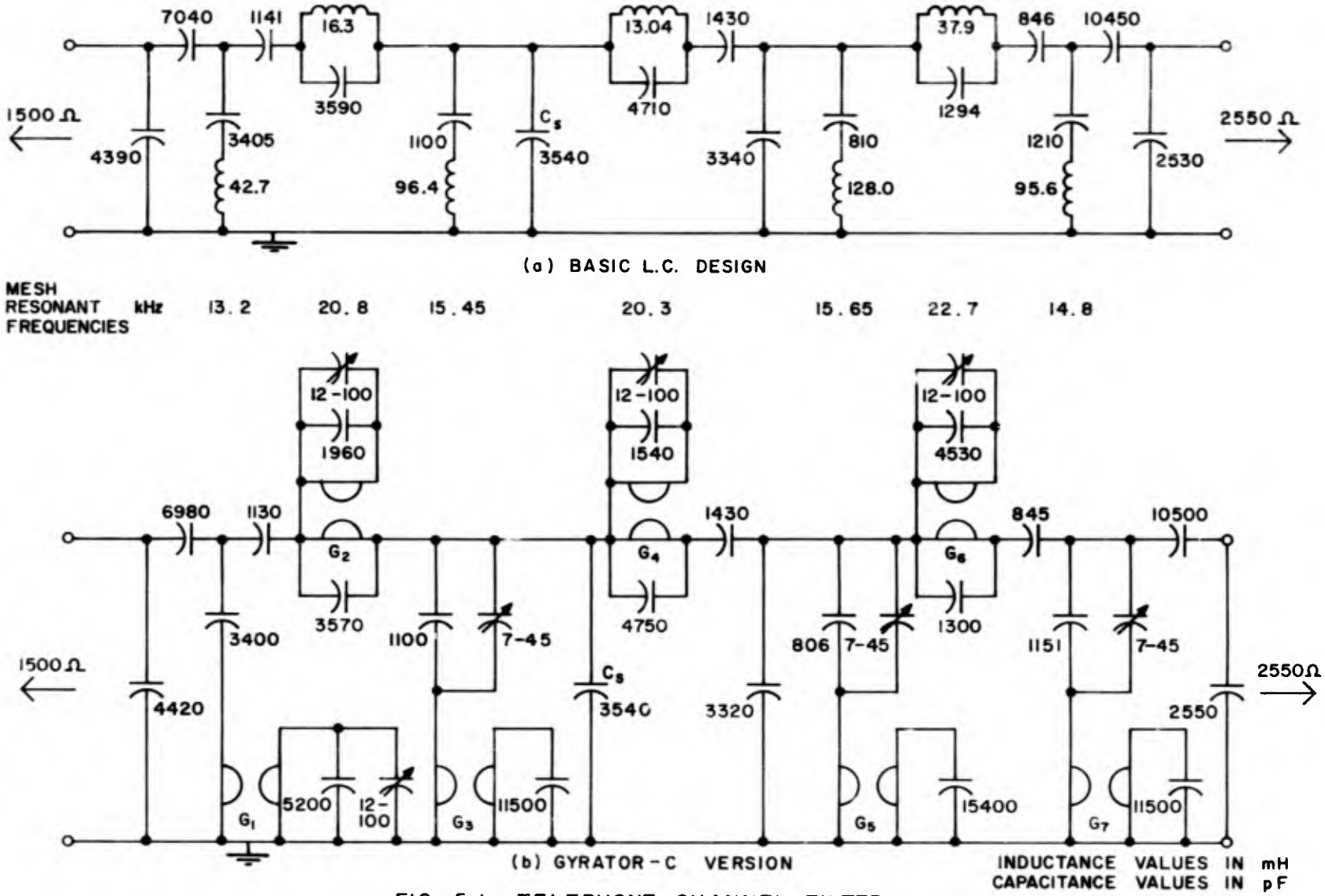

FIG. 5.1. TELEPHONE CHANNEL FILTER

The 2.2 k Ω resistors shown on Figure 5.2, the power connection diagram, enable the complete filter to operate on a supply voltage of +40 V. The MOSFET gyrators themselves are designed to operate on a supply voltage of +20 V. The 2.2 k Ω resistors in conjunction with the 47μF capacitors provide a.c. decoupling between the gyrators. The need for this decoupling becomes apparent only when measuring attenuations greater than 60 dB at the zero-transmission frequencies. The total power consumption of this filter is 3.2 watts, approximately one watt of which is wasted in the 2.2 k Ω resistors in order to preserve the convenience of a single power supply.

The filter stopband was tuned by adjusting the trimmer capacitors on each resonant mesh to obtain maximum attenuation at each of the zero-transmission frequencies. The Q adjustment capacitors, C, on each gyrator as shown in Figure 4.7 were adjusted for flattest passband response. This is not a critical adjustment and the capacitor values actually used ranged in value from 24 pF to 46 pF.

The measured frequency response curves of this filter are shown in Figures 5.3 and 5.4, and as can be seen from Figure 5.4, a very flat passband was obtained. When this measured passband response was compared to computed curves for dissipative versions of the original LC filter of Figure 5.1 (a), it was found to be equivalent to having Q values of 1000 for all inductors.

The method of measuring the filter attenuations is described in Section 5.2.

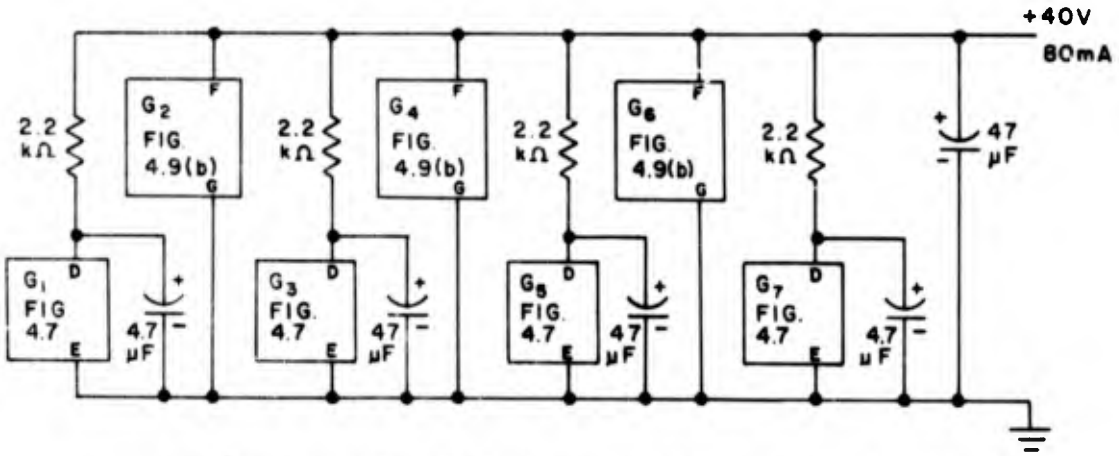

FIG. 5.2. POWER CONNECTION DIAGRAM OF GYRATOR TELEPHONE CHANNEL FILTER

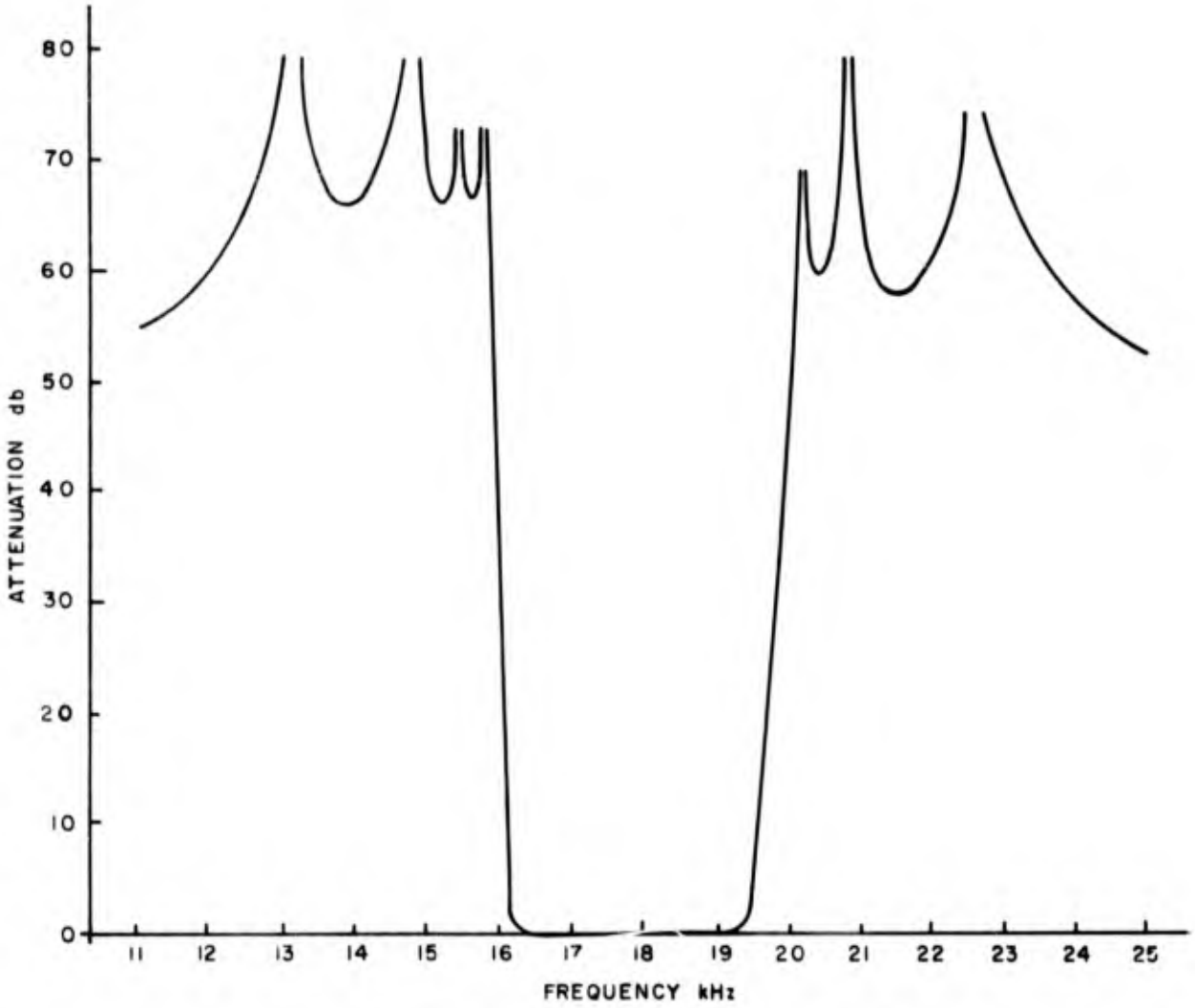

FIG. 5.3. MEASURED RESPONSE OF GYRATOR TELEPHONE CHANNEL FILTER

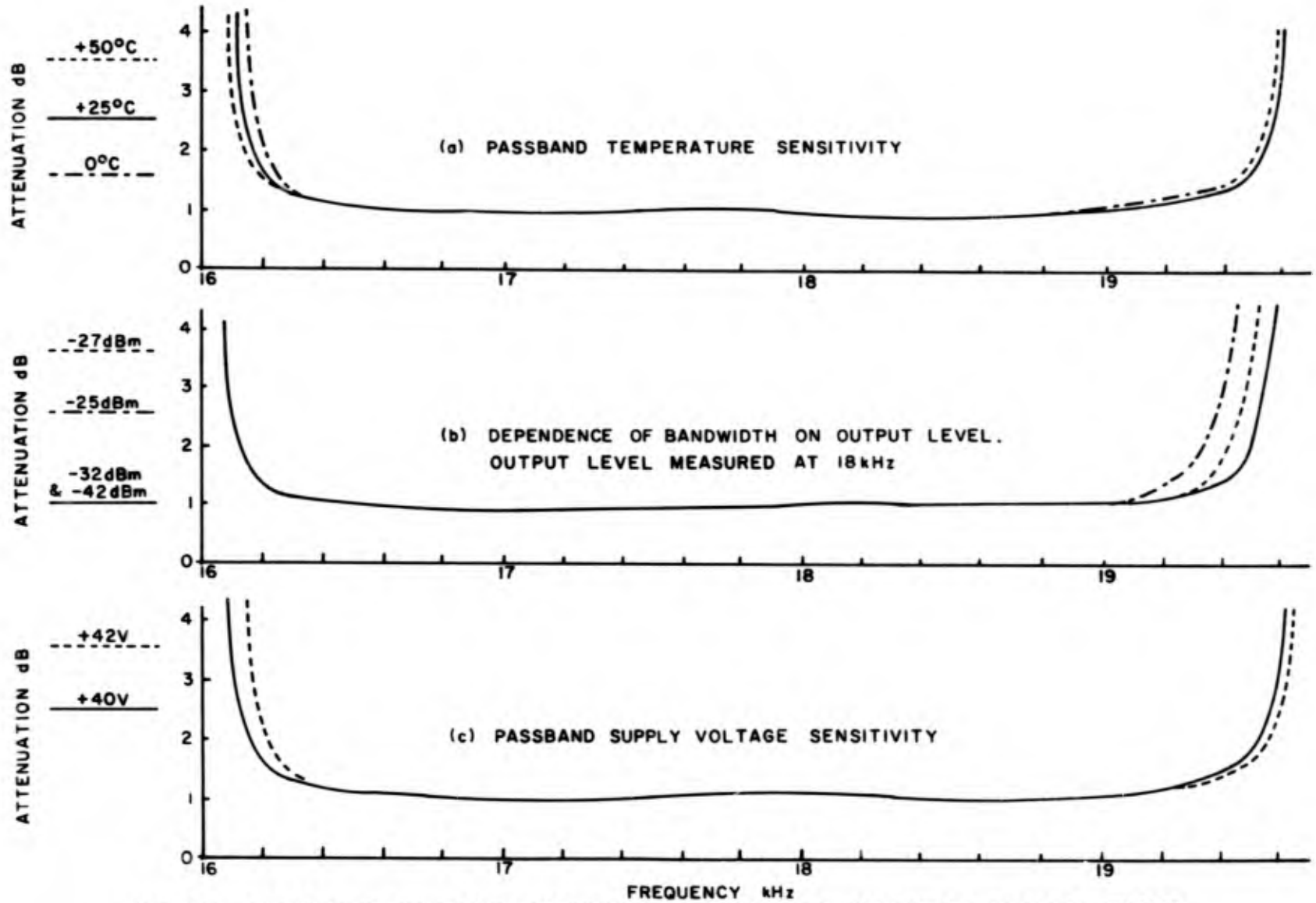

FIG. 5.4. MEASURED PASSBAND RESPONSES OF GYRATOR TELEPHONE CHANNEL FILTER

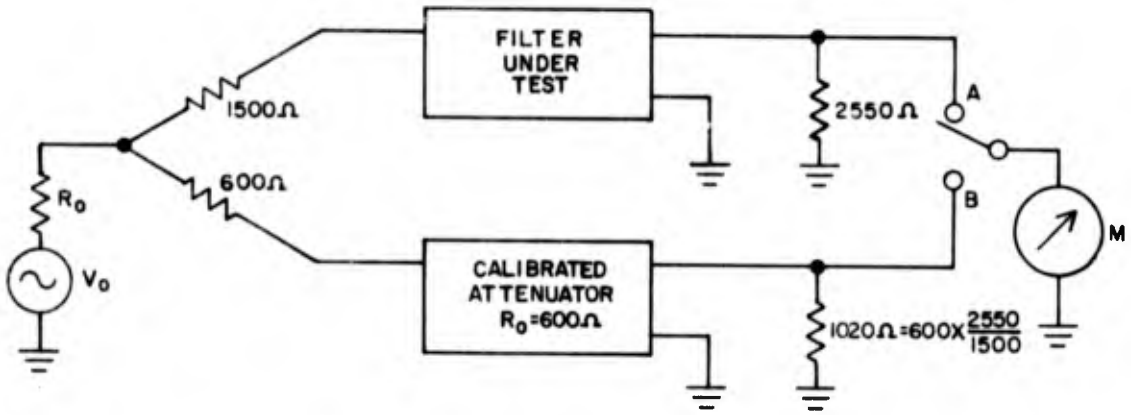

FIGURE 5.5. Filter Test Circuit.

5.2 Method of Measuring Filter Attenuations

The filter-test circuit consists of a voltage generator V_o with an internal resistance R_o and two signal paths, one through a calibrated attenuator which acts as a reference circuit, the other is through the filter under test. The attenuator has an image impedance of 600Ω. The resistor on the generator side of this attenuator equals its image impedance whereas the resistor on its load end bears the same relationship to the image impedance as the filter's load resistance does to its source resistance. The test procedure at any frequency is as follows: (See Figure 5.5) .

1. Switch the meter, M, to A and note the reading.
2. Switch the meter, M, to B and adjust the attenuator until the meter reads the same as it did in (1).
3. The attenuation of the filter is then equal to the attenuation of the attenuator as read from its calibrated dial.

Use of this circuit means that the output of the generator and the response of the meter need not be constant with frequency, as the attenuation readings are obtained from the calibrated attenuator, which

can be very accurate, as it is composed only of resistors.

5.3 Measured Sensitivity of Gyrator Filters

Computed responses of the LC channel filter of Figure 5.1 (a) showed that a uniform distribution of initial capacitor values within a ±3% range around their nominal values gives acceptable passband responses, with standard deviation nowhere exceeding 0.3 dB, provided that the inductors are adjusted to give the correct transmission-zero frequencies. Experimentally this property was observed to be true also for the gyrator capacitor version of this filter. The filter was constructed from ±1% tolerance capacitors and ±1% tolerance resistors were used in the gyrators. From experimental observations it was apparent that ±3% tolerance capacitors would have been sufficient, provided of course that the resonant circuits were tuned to give the correct zero-transmission frequencies.

The component with the highest computed passband sensitivity is C_s, the 3540 pF shunt capacitor to ground between the 15.45 kHz and 20.3 kHz resonant circuits. When this capacitance value was experimentally perturbed by +5% the change in the passband response was less than 0.1 dB as expected.

Figure 5.4 (a) shows the measured response of the filter for temperatures of 0°C and +50°C. The frequency shift in the skirts of the filter has a maximum value of -1 Hz/°C at the 16.15 kHz end of the passband, and it is linear about the response at +25°C. At the 19.5 kHz end of the passband, however, the frequency shift is less than 1 Hz/°C

and it is nonlinear about the value at +25°C. The value of 1 Hz/°C for the rate of drift of the filter skirts is equivalent to -62.4 parts per million per °C. This value is consistent with the temperature coefficients of the metal film resistors (±100 ppm/°C) and of the mica capacitors (40 ppm/°C) used to construct the filter.

The filter bandwidth was found to be independent of drive level for levels below -30 dBm, which represents an output voltage of 50 mV rms. Above -30 dBm the upper skirt of the filter decreased in frequency as shown in Figure 5.4 (b) and for a level change of +2 dB from -27 dBm to -25 dBm the upper half power frequency decreased by approximately 100 Hz. This bandwidth narrowing at high levels is caused by the large voltage which develops across the series gyrators G_2, G_4, G_6, just as it would develop across the series inductors in the equivalent LC filter. Above -30 dBm this voltage exceeds the voltage handling capacity of the MOSFET gyrator design in Figure 4.7.

The sensitivity of the filter to changes in supply voltage can be seen in Figure 5.4 (c). The filter passband width was not affected by supply voltage changes but the skirts of the filter had a uniform drift of +20 Hz per volt. This value of drift is caused by the fact that the transconductances of the MOSFETs in the gyrator design are sensitive to changes in their source-to-gate bias voltages. Changes in supply voltage will consequently be felt as changes in gyration conductances.

A 200 Hz 7th degree high-pass filter was also built using the gyrator described in Reference 13. The measured sensitivity of the filter was found to be quite low as expected, and experiments indicated

that the filter could have been constructed from ±5% tolerance components, provided that the attenuation pole frequencies were adjusted correctly. The measured frequency response of this filter was much sharper than could have been obtained with commercial quality inductors. The best commercially available inductors have Q values of 50 at 200 Hz whereas use of the gyrator enabled equivalent inductances to be obtained with Q values of 200.

These experimental results show conclusively that the sensitivity of gyrator filters is as low as the sensitivity of their LC equivalents. Gyrator filters, however, have the desirable property of allowing the Q of their inductances to be varied independently of their inductance values. The results show that excellent filters can be made by this gyrator method using commercial quality components.

CHAPTER 6. ANALOG BRUNE SECTION

6.1 Why the Brune Section?

As has already been mentioned in Section 3.3 inductorless filters can also be obtained if we simulate the complete LC filter structure with analog computer techniques. Low-pass filters of 7th degree were constructed by this total simulation method in order to test the basic principles involved. These particular filters were ladder networks and the experimental results obtained from them were very satisfactory. The measured frequency responses were exactly as calculated. However, as this total simulation technique depends very much on the type of filter being simulated, a different simulation circuit would be required for each type of LC filter structure. This can lead to complications, as it would result in a variety of simulation circuits.

Considerable economies can be obtained if different types of filters are constructed in a similar manner. The simulation techniques can of course only produce a model of an existing LC filter with known properties, so it is therefore necessary first of all to obtain some basic LC sections that can be used to construct different types of filters. The existence of suitable basic LC sections was shown by Darlington.[29,30] Darlington showed that any realizable filter transfer function can be realized by a tandem connection of simple reactive two-port networks that he designated types A, B, C, and D. The type A network consists of an LC network in the series arm of the ladder and the type B is an LC network in the shunt arm. Each of these can

provide transmission zeros anywhere on the $s = j\omega$ axis, 0 and ∞ included. The type C section is the circuit of Figure 6.1 (a) or (b). It provides a transmission zero at a frequency given by $1 + s^2 L_2 C_2 = 0$. Depending on whether L_2 in Figure 6.1 (a) is negative or positive this type C section will have a transmission zero either on the real or imaginary s axis. One negative component will be required in order to satisfy the realizability condition. The type D section realizes a tetrad of complex transmission zeros. It is more complicated than the type C section and it is mainly of theoretical interest because it contains three negative components as compared to only one in the type C section of Figure 6.1.

If we restrict our class of filters to those having transmission zeros only on the $s = j\omega$ axis, as do most practical filters, we can dispense with the Darlington type D section and also with the particular case of the type C section where L_2 is negative. If also we rely on the type A and B sections to provide transmission zeros at zero and infinity only, and let the type C section provide the transmission zeros at finite frequencies on the $s = j\omega$ axis, then only single-element type A and B sections will be required. To sum up: Any realizable filter transfer function having transmission zeros at frequencies only on the $s = j\omega$ axis can be realized by a cascade of Darlington type C sections where L_2 is positive, plus some single elements either in series or in shunt.

As will be shown in the filter realizations of Chapter 8, transmission zeros at zero or infinite frequency are most conveniently

handled by moving the series or shunt L's or C's that produce them to either the source or load ends of the filter and there simulating them along with the terminating resistances. As there are only two terminating resistances per filter this limits us to a maximum of two such zeros per filter. This however includes the majority of filter designs.

Prior to Darlington's work, Brune[31,30] had used the same circuit as Darlington's type C section in the particular case where L_2 is positive. He used this section in a synthesis procedure to show that positive reality was a sufficient condition for a function to be a driving point impedance function. Because of this prior use of the special case of the Darlington type C section in which we are interested, the circuits shown in Figure 6.1 (a) and 6.1 (b) will henceforth be referred to as Brune sections.

The Brune sections shown in Figures 6.1 (a) and (b) are not in their most useful form, but some useful equivalences can be obtained from them as shown in Figure 6.2. The equivalence in Figure 6.2 (b) is based on the Z matrix of 6.2 (a), whereas those in 6.2 (c) and (d) are based on the Y matrix. Similarly, the equivalence in Figure 6.2 (f) is based on the Z matrix of Figure 6.2 (e) and those in Figures 6.2 (g) and (h) are based on the Y matrix. Finally from the equivalences of Figures 6.2 (i) and (j) all these various Brune circuits are shown to be equivalent to each other if an extra ideal transformer is included.

Any of the circuits in Figure 6.2, therefore, satisfy our requirement for a universal filter section but we will choose that of Figure 6.2 (d) because it can be easily simulated, as will be shown in the

next section. This circuit, plus ideal transformers and series or shunt L's and C's, will be our basic building blocks for the realization of filters. The ideal transformers of course do not affect the frequency response, they are only used to obtain impedance changes.

A circuit has been constructed, which simulates the electrical properties of the Brune section of Figure 6.2 (d) by inductorless means and in a manner that permits interconnection of many such circuits.

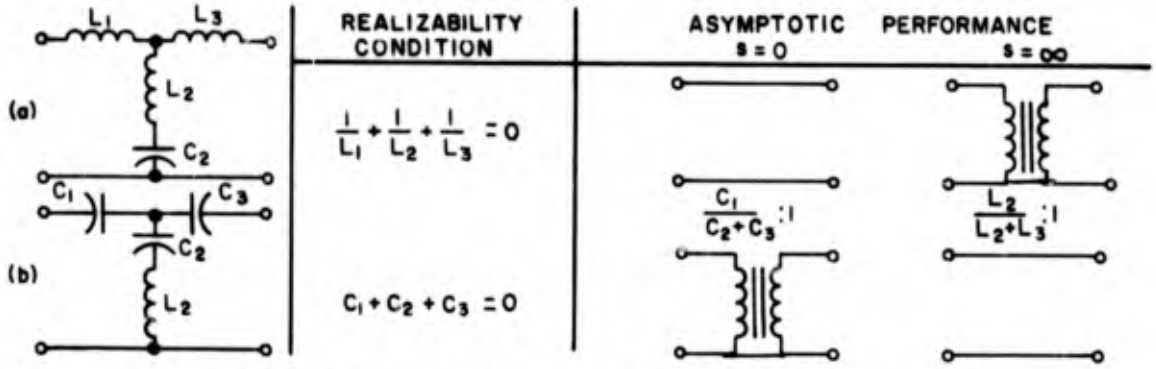

FIG 6.1. BASIC BRUNE SECTIONS

$$\underline{Z}=\begin{bmatrix} s(L_1+L_2)+\frac{1}{sC_2} & sL_2+\frac{1}{sC_2} \\ sL_2+\frac{1}{sC_2} & s(L_2+L_3)+\frac{1}{sC_2} \end{bmatrix} \qquad Y=\underline{Z}^{-1}=\begin{bmatrix} \frac{sC_2(L_2+L_3)}{L_1+L_3}+\frac{1}{s(L_1+L_3)} & \frac{-s\,L_2C_2}{L_1+L_3}-\frac{1}{s(L_1+L_3)} \\ \frac{-s\,L_2C_2}{L_1+L_3}-\frac{1}{s(L_1+L_3)} & \frac{sC_2(L_1+L_2)}{L_1+L_3}+\frac{1}{s(L_1+L_3)} \end{bmatrix}$$

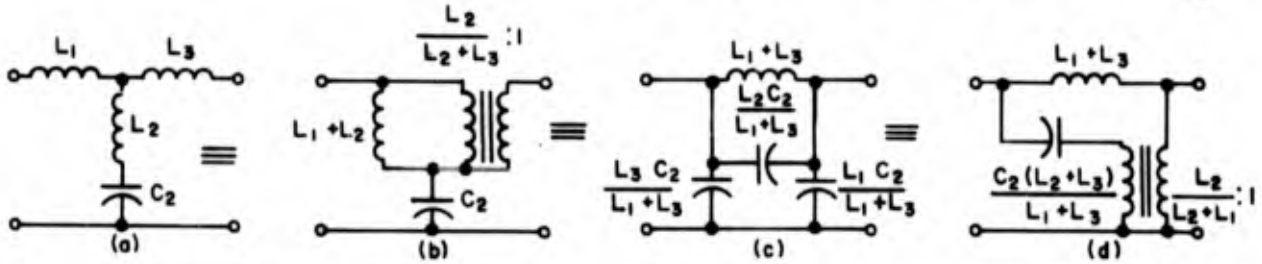

$$\underline{Z}=\begin{bmatrix} -\frac{1}{s}\frac{C_3}{C_1C_2}+sL_2 & \frac{1}{sC_2}+sL_2 \\ \frac{1}{sC_2}+sL_2 & -\frac{1}{s}\frac{C_1}{C_2C_3}+sL_2 \end{bmatrix} \qquad Y=\underline{Z}^{-1}=\begin{bmatrix} \frac{1}{sL_2}\left(\frac{C_1}{C_2}\right)^2-s\frac{C_1C_3}{C_2} & \frac{1}{s}\frac{C_1C_3}{L_2C_2^2}+\frac{sC_1C_3}{C_2} \\ \frac{1}{s}\frac{C_1C_3}{L_2C_2^2}+s\frac{C_1C_3}{C_2} & \frac{1}{sL_2}\left(\frac{C_3}{C_2}\right)^2-s\frac{C_1C_3}{C_2} \end{bmatrix}$$

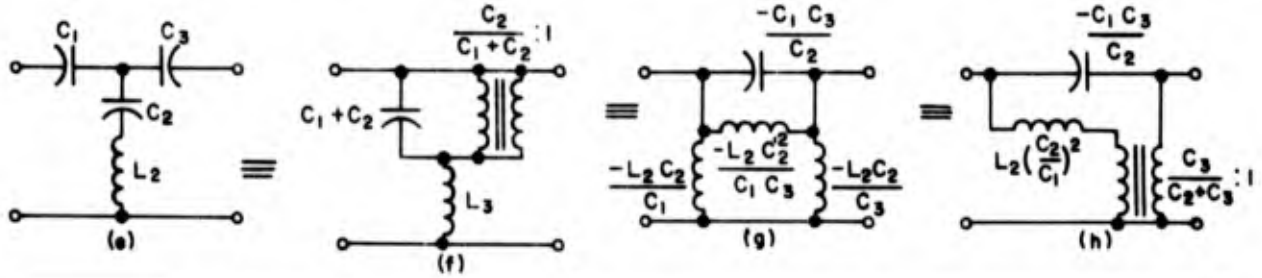

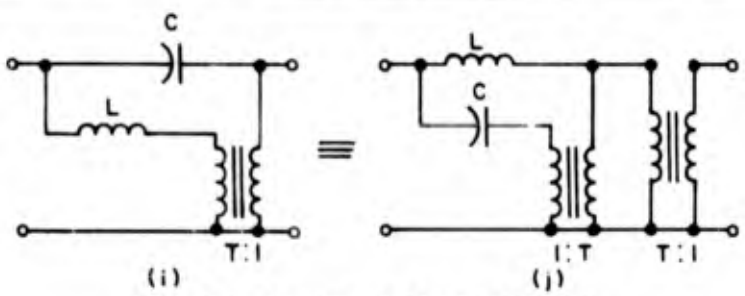

FIG. 6.2. BRUNE EQUIVALENCES

6.2 Simulating the Brune Section

In order to simulate the Brune section its defining equations must be re-arranged in a form which makes them amenable to simulation. This can be done most conveniently if we select state variables in the circuit. State variables are a means for representing the integro-differential equations of a k^{th} order dynamic system in the form of k first order differential equations. Applied to the Brune section of Figure 6.2 this means that, even though it is a second-order system, we can nevertheless describe its dynamic behavior by two first order differential equations involving two properly selected state variables. The output of the system can then be specified by two non-dynamic equations involving the inputs and these state variables.

Choose as state variables the voltage V across the capacitor and the current I through the inductor. Let V_1 and I_2 be regarded as two inputs to the circuit and V_2 and I_1 as outputs. The Brune section is then completely described by the matrix Equations 6.1 and 6.2, which are in the so-called state variable normal form.[32]

$$\begin{bmatrix} sV \\ sI \end{bmatrix} = \begin{bmatrix} 0 & -\frac{1}{CT} \\ \frac{1}{LT} & 0 \end{bmatrix} \begin{bmatrix} V \\ I \end{bmatrix} + \begin{bmatrix} 0 & \frac{1}{CT} \\ \frac{T-1}{LT} & 0 \end{bmatrix} \begin{bmatrix} V_1 \\ I_2 \end{bmatrix} \qquad 6.1$$

$$\begin{bmatrix} V_2 \\ I_1 \end{bmatrix} = \begin{bmatrix} -\frac{1}{T} & 0 \\ 0 & \frac{T-1}{1} \end{bmatrix} \begin{bmatrix} V \\ I \end{bmatrix} + \begin{bmatrix} \frac{1}{T} & 0 \\ 0 & \frac{1}{T} \end{bmatrix} \begin{bmatrix} V_1 \\ I_2 \end{bmatrix} \qquad 6.2$$

The equations in this normal form are not very amenable to simulation but if they are re-arranged as Equations 6.3 - 6.6 it is easy to see how they can be simulated.

$$V_2 = \frac{V_1 - V}{T} \qquad 6.3$$

$$-(T-1)I = \frac{T-1}{sL}(V_2 - V_1) \qquad 6.4$$

$$V = \frac{1}{sC}\frac{(I_2 - I_1)}{T-1} \qquad 6.5$$

$$I_1 = \frac{1}{T}\left[I_2 - I\left\{-(T-1)\right\}\right] \qquad 6.6$$

These equations are simulated by the circuit of Figure 6.5 where the elements of this circuit are the Difference Integrator and the Difference Amplifier circuits of Figure 6.4. The terms on the left-hand side of the above four equations are the outputs of the Difference Integrators and Difference Amplifiers.

As has been mentioned already, the simulation circuit of Figure 6.5 has two inputs and two outputs. In a filter type application, however, we will have only one independent input and the circuitry external to

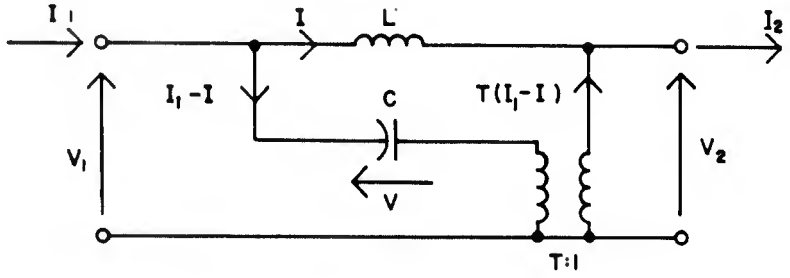

FIG. 6.3 THE BRUNE SECTION

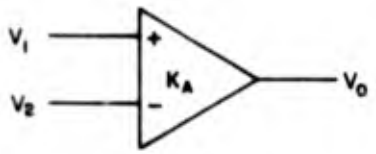

$V_0 = K_A(V_1 - V_2)$

(a) DIFFERENCE AMPLIFIER
(SCHEMATIC)

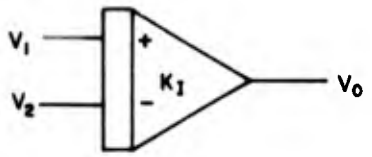

$V_0 = \frac{K_I}{S}(V_1 - V_2)$

(b) DIFFERENCE INTEGRATOR
(SCHEMATIC)

FIG. 6.4

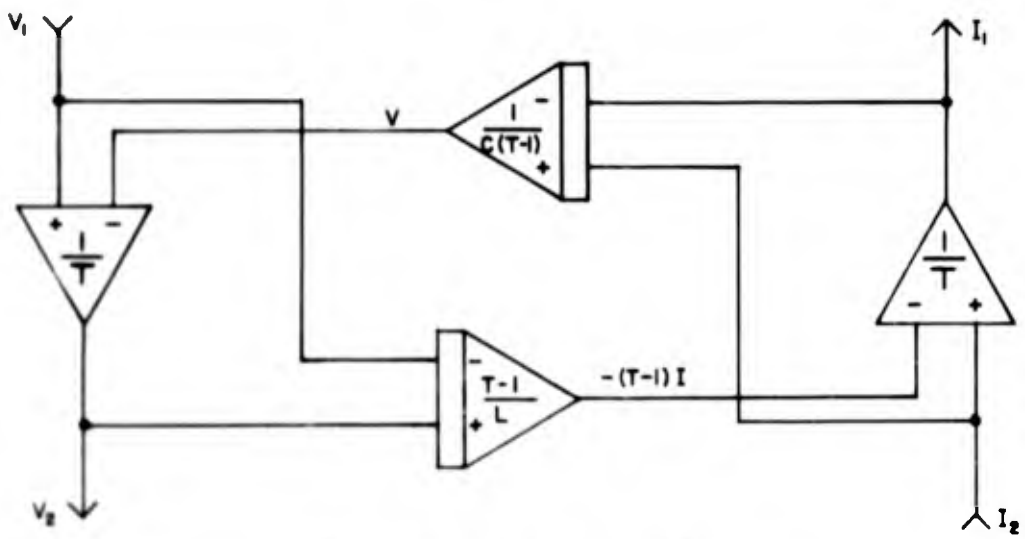

FIG. 6.5 ANALOG BRUNE SECTION
(SCHEMATIC)

the simulated Brune section must properly represent this fact. The reduction from two independent variables to one results from including the effect of the terminating resistances on the Brune section.

If the load resistance is equal to one ohm then $I_2 = V_2$ and this can be simulated by just connecting together the V_2 and I_2 terminals. For the case of a one ohm source resistance and an e.m.f. of V_o we have $V_1 = V_o - I_1$ and this expression can be simulated by a Difference Amplifier as shown in Figure 6.6 (b). The analog Brune section complete with terminations is then shown in Figure 6.6 (b). We now see that it has just one independent input V_o and the output is V_2. Terminating resistances, other than one ohm, can be simulated by an amplifier at the load end and by appropriate scaling at the source end. Note that even though Figures 6.5 and 6.6 are drawn for the special case of $T > 1$ the analog Brune circuit can be re-arranged for $T < 1$ if the inputs to each of the two Difference Integrators are reversed.

6.3 Properties of the Simulated Brune Section

It is interesting to note the mechanism for achieving a transmission zero with this analog Brune section. The LC Brune section itself will have a transmission zero at a frequency on the $s = j\omega$ axis and this property must also be present in the analog Brune circuit. For the analog circuit, as shown in Figure 6.5, the zero of transmission will mean that $V_2 = 0$. Using Equation 6.3 it therefore follows that $V_1 = V$, i.e., the transmission zero is being formed by a voltage cancellation process, which occurs at the input to the left hand Difference Amplifier.

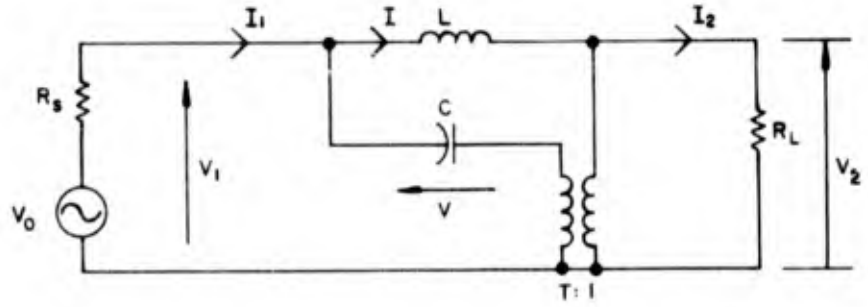

FIG. 6.6 (a). BRUNE SECTION WITH TERMINATIONS

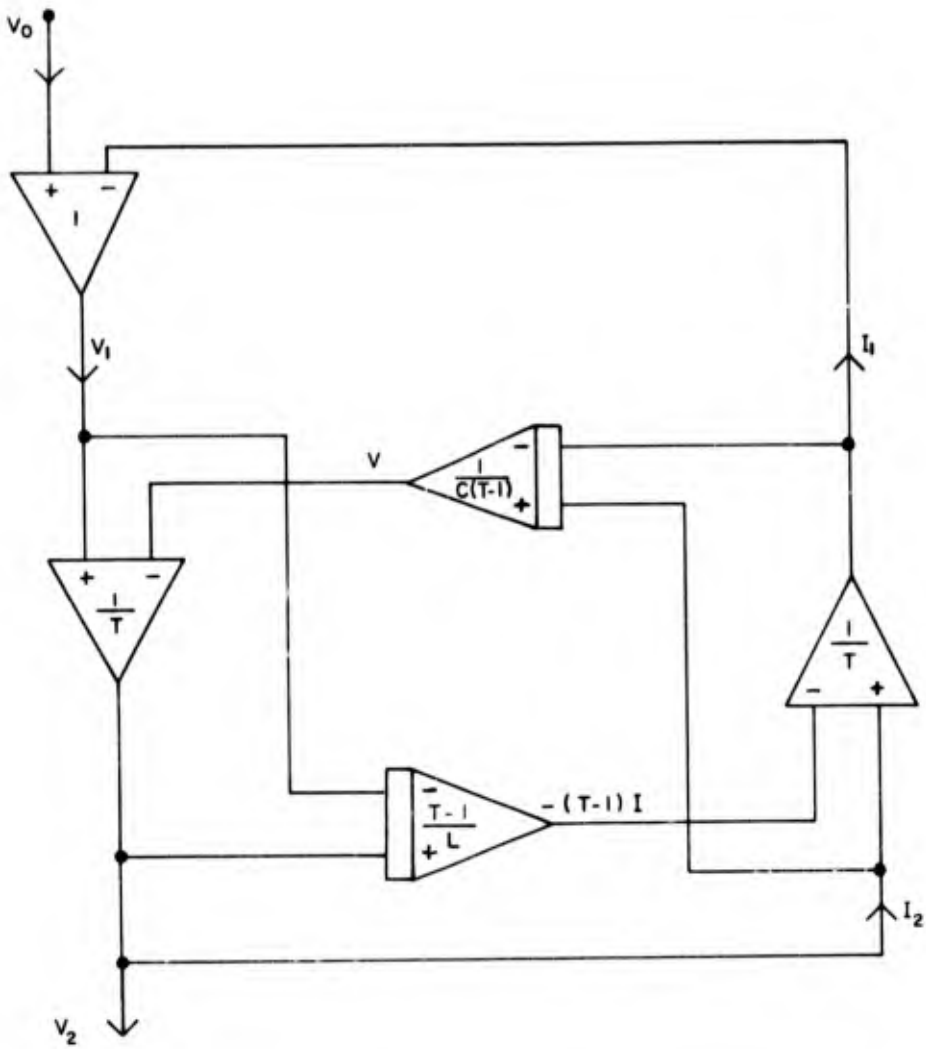

FIG. 6.6 (b). ANALOG BRUNE SECTION WITH TERMINATIONS. $R_S = R_L = 1\ \Omega$

As $V_2 = 0$ and $I_2 = 0$, V is then obviously formed by the double integration of V_1. This can be seen by tracing the circuit path through the Difference Integrators in Figure 6.5.

$$\text{Therefore} \qquad V = -\frac{V_1}{s^2 L\, C\, T} \qquad 6.7$$

but as $V = V_1$ the frequency at which the transmission zero occurs is given by Equation 6.8

$$s = \pm j \sqrt{\frac{1}{LCT}} \qquad 6.8$$

Due to the symmetry of the circuit, we see that a similar transmission zero could occur at the input to the right-hand Difference Amplifier if I_2 were considered to be an independent input. The expression for the transmission zero frequency would still be Equation 6.8 but the transformer ratio T in this expression would now correspond to the gain of the left-hand Difference Amplifier in Figures 6.5 and 6.6. At first glance it would appear that this reverse direction transmission zero is relatively unimportant as it cannot affect the poles of loss of the desired filter. However, it does have an effect on the natural modes of the filter, because these natural modes are formed by the interactions that take place between all components in the filter. Experiments performed on filters constructed from analog Brune sections showed that variations in the gain of the right-hand Difference Amplifier of Figure 6.5 changed the position of the attenuation poles of the filter. Variations in the gain of the left-hand Difference Amplifier only

affected the passband response of the filter, thereby showing the effect of this gain on the natural modes of the filter. This ambiguity in the transformer turns ratio T, which is determined by two independent methods on the analog circuit, means that transmission in both forward and reverse directions must be considered when the filter is being tuned.

Another interesting property of the analog Brune circuit can be observed if we consider the circuit in Figure 6.5 when there is only one input V_1 to the circuit and I_2 is zero. In this case we have

$$V = (V_2 - V_1) \frac{1}{s^2 LCT} \qquad 6.9$$

By eliminating V_2 with the aid of Equation 6.3 we can find Equation 6.10

$$\frac{V}{V_1} = \frac{\frac{1-T}{LCT^2}}{s^2 + \frac{1}{LCT^2}} \qquad 6.10$$

This equation shows that the Brune section now has a natural mode at a frequency given by Equation 6.11

$$s = \pm j \sqrt{\frac{1}{LCT^2}} \qquad 6.11$$

Therefore its natural frequency $= \frac{1}{\sqrt{T}}$ (its transmission zero frequency).

This natural frequency only occurs when there is no I_2 input and its presence emphasizes the need for a proper termination on the analog

Brune section. In terms of the original LC Brune section the appearance of the natural frequency is equivalent to having a circuit made from an ideal inductor, an ideal capacitor, and an ideal transformer, with no terminating or loss resistances whatsoever. Such a circuit would also be expected to oscillate.

The transmission zero and natural mode frequencies are present in both the original LC circuit and also in the analog Brune circuit but the way in which they are determined in the analog circuit suggests some precautions that must be taken in order to obtain good filters. These precautions are correct reverse direction tuning and good terminations.

The next topic which will be treated in Chapter 7 is the means adopted to obtain a practical realization of Figure 6.5 in integrable form.

CHAPTER 7. INTEGRABLE BRUNE SECTION

7.1 Desirable Properties for an Integrable Brune Section

In order to obtain a practical realization of the Brune section we need, first of all, to realize the Difference Amplifier and the Difference Integrator circuits of Figure 6.4 in an integrable form. These circuits can be constructed from high gain amplifiers using standard analog computer techniques.[33] The amplifiers conventionally used for such applications have high impedance differential inputs and the a.c. properties of the circuits, in which they are used, are determined exclusively by the feedback components external to the amplifiers themselves.

A fifth degree low-pass filter was constructed from such amplifiers and the results obtained were not entirely satisfactory. Constructing the Brune section from standard operational amplifier circuits required a total of eleven external resistors and two capacitors per Brune section. The measured frequency response of the filter was as calculated, but it did suffer from a higher component sensitivity than had been expected. A tolerance of !.5% was required of the resistors in order to maintain the passband response correct to 0.1 dB and this was excessive.

This high sensitivity occurred in the parts of the circuitry primarily concerned with the subtraction of voltages corresponding to the right hand sides of Equations 6.3 - 6.6. The right hand sides of Equations 6.3 - 6.6 all involve subtractions of two quantities and to perform such subtractions with standard operational amplifier circuits

requires the use of matched resistors as a minimum of three attached components per amplifier will be required. The experience gained with this Brune filter showed that it would be advisable to strive for circuits that could realize the circuit functions of Figure 6.4 without requiring any component matching.

Ideally we would like to have the circuit operations of Figure 6.4 determined by the ratios of just two impedances. For this reason circuits were developed to perform the circuit functions with the minimum number of two attachments. These circuits are shown in Figure 7.1.

Work on the operational-amplifier Brune filter pointed out other trouble areas and also some desirable features that should be incorporated in an integrable Brune circuit. They can be listed as follows:

(a) It should realize the circuit without requiring any matched components.

(b) The circuit functions of Figure 6.4 should be performed by basic circuits that contain only wide tolerance components, the a.c. properties being completely determined by the ratios of two high quality attached components.

(c) The points to which the attached resistors are connected should have nominally equal d.c. potential, so that the attached resistors will not disturb the biasing of the circuits.

(d) All input and output points of the analog Brune section should be at the same d.c. potential, so that connecting

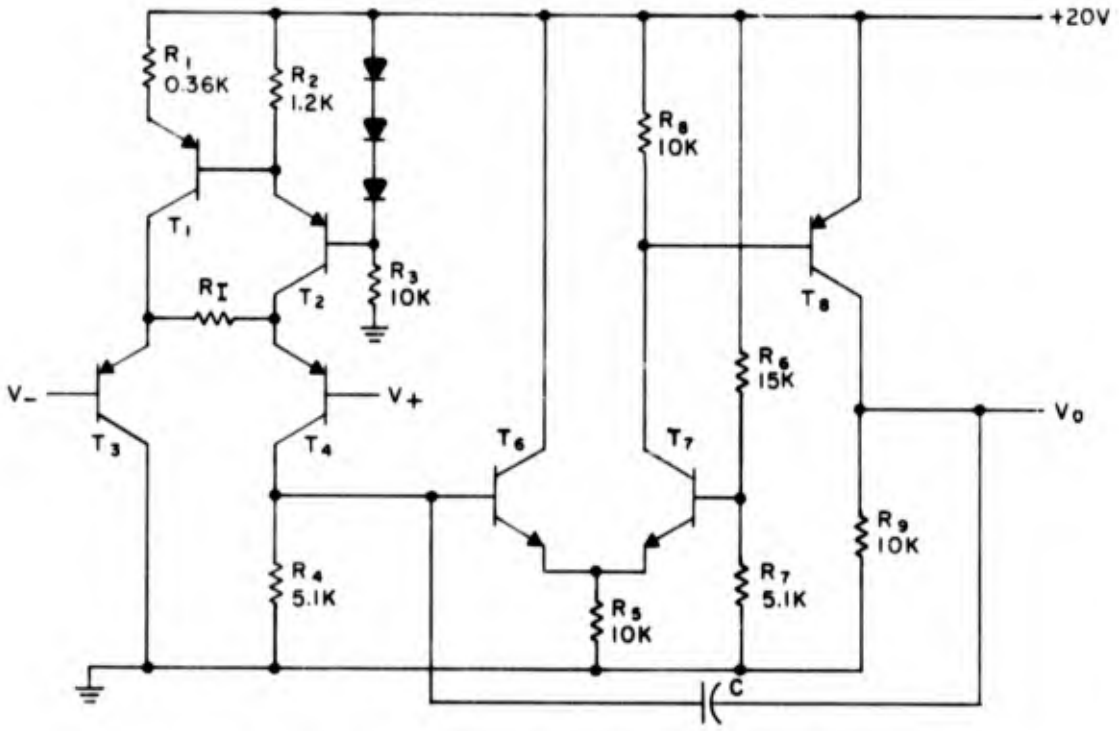

FIG 7.1(a) DIFFERENCE INTEGATOR $V_o \approx \frac{1}{SR_I C}(V_+ - V_-)$

R_I IS R_L OR R_c, & C IS C_L OR C_c OF FIG 7.2

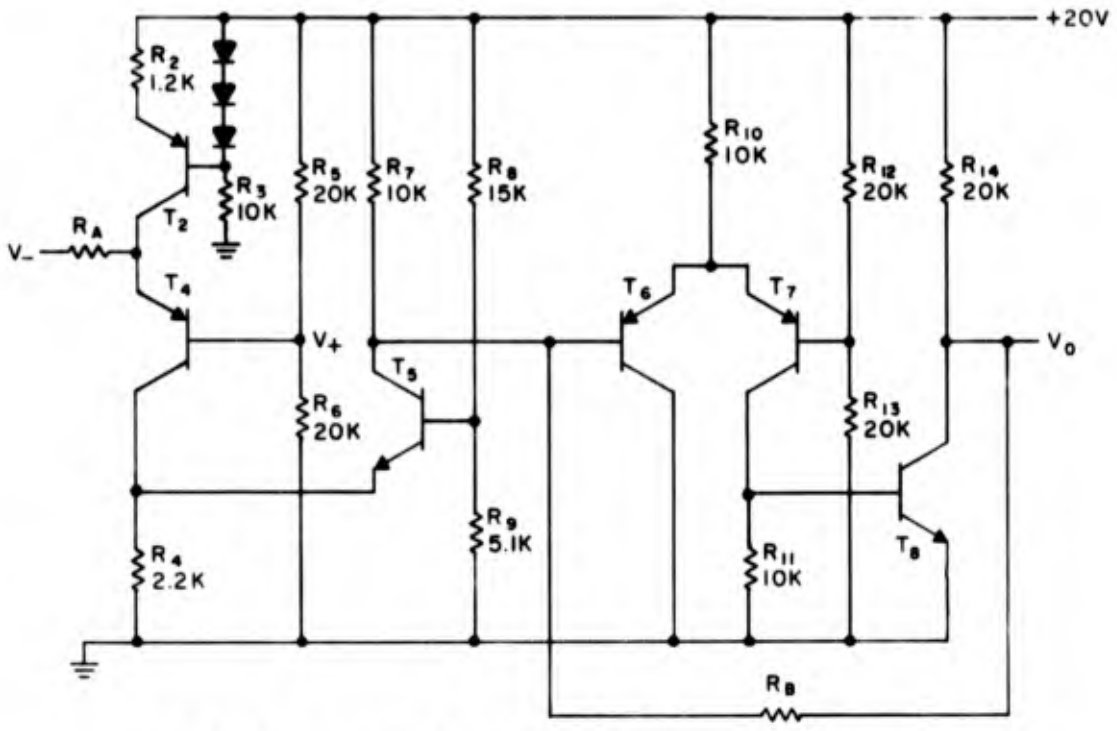

FIG 7.1(b) DIFFERENCE AMPLIFIER $V_o \approx \frac{R_B}{R_A}(V_+ - V_-)$

a number of Brune sections together will not disturb the biasing of any one.

(e) There should be a well defined mechanism for establishing the bias on each analog Brune section so as to have independent biasing circuits for each section.

7.2 A.C. Properties of the Developed Circuits

Figures 7.1 (a) and (b) show the two basic circuits that were developed to satisfy the above requirements. Figure 7.1 (a) is the circuit designed to realize the Difference Integrator of Figure 6.4 (b) and the circuit in Figure 7.1 (b) realizes the Difference Amplifier. Figure 7.2 shows the complete analog Brune section constructed from the circuits in Figure 7.1. The a.c. properties of this section are determined almost exclusively by the attached components R_L, C_L, R_C, C_C, two R_A resistors, and two R_B resistors.

To understand the operation of the circuits in Figure 7.1 consider, first of all, the operation of the Difference Integrator circuit, Figure 7.1 (a). T_1 and T_2 in this circuit are constant current sources that supply the bias currents for the input circuit. The voltages to be subtracted are applied at the bases of transistors T_4 and T_3. The base of T_4 is the non-inverting input and the base of T_3 is the inverting input of the circuit. Call these input voltages V_+ and V_- respectively. As the emitters of T_4 and T_3 will have essentially the same a.c. potential as their bases, the a.c. input difference voltage $V_+ - V_-$ will appear across the high quality attached resistor R_I. A current I_I whose value

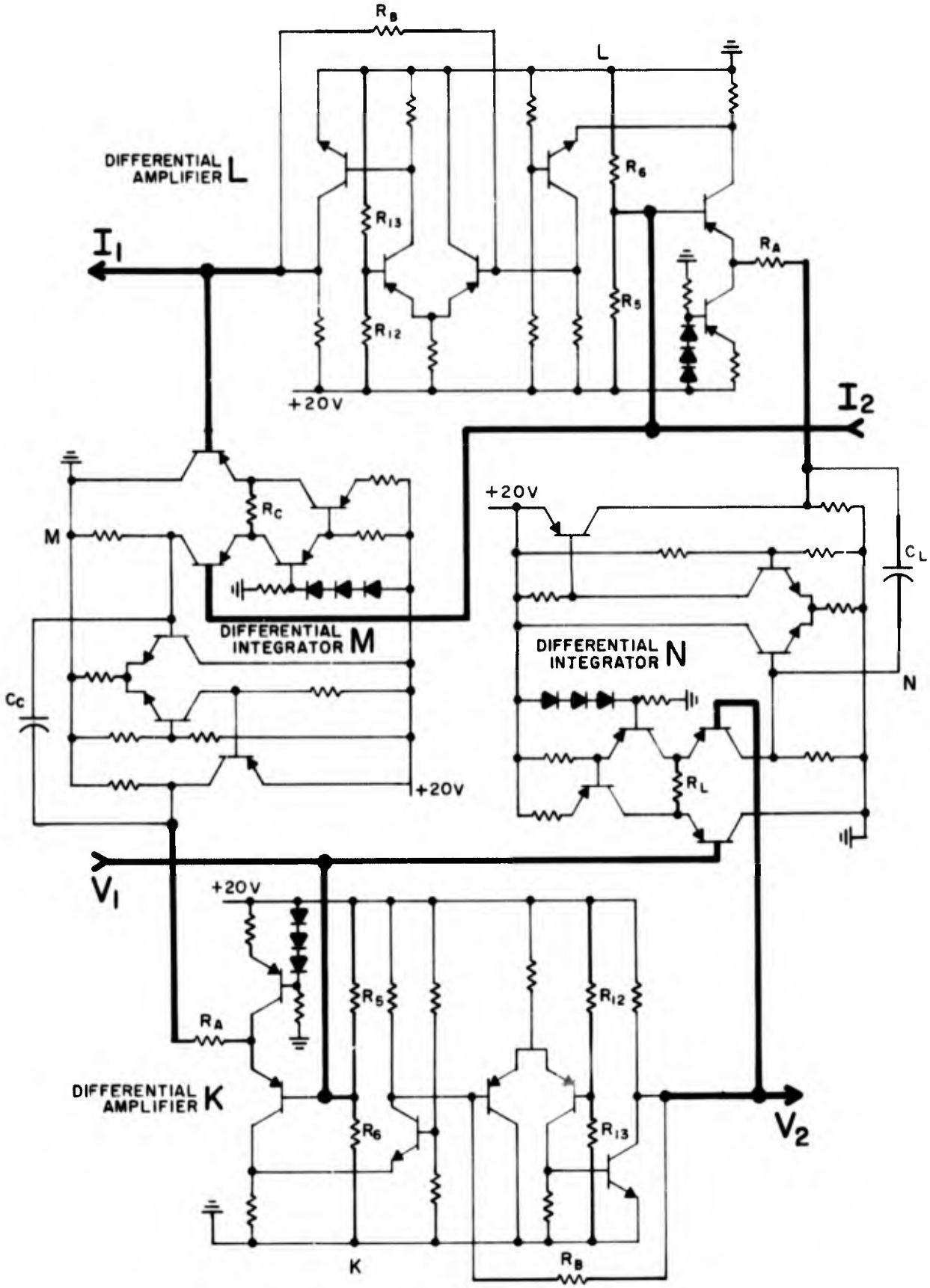

FIG. 7.2. ANALOG BRUNE SECTION

is given by Equation 7.1 will flow in R_I due to this a.c. difference voltage.

$$I_I = \frac{V_+ - V_-}{R_I} \qquad 7.1$$

This current I_I flows away from R_I through the emitter of T_4. If α is the emitter-to-collector current gain of T_4, and is approximately equal to 1, the current flowing out of the collector of T_4 due to the input difference voltage is

$$I_{C4} = -\alpha \frac{(V_+ - V_-)}{R_I} \cong -\frac{(V_+ - V_-)}{R_I} \qquad 7.2$$

Now consider the portion of the circuit consisting of T_6, T_7, and T_8. This circuit is just a high-gain amplifier having an open-loop gain of 65 dB. Negative feedback is applied across this amplifier via a high quality attached capacitor C. Because of the high open-loop gain of the amplifier, combined with negative feedback through the attached capacitor, the input impedance of the amplifier-capacitor combination is very low. This impedance will be considerably lower than R_4, and consequently almost all of the current flowing away from the collector of T_4 will flow into this impedance. The low input impedance of the amplifier capacitor combination means that the base of T_6 is at approximately zero a.c. potential. The input impedance of the amplifier alone at this point is still quite high so almost all the current from the collector of T_4 must flow through the feedback capacitor C. The voltage that this current will develop across the capacitor C must be the output voltage V_0

and

$$V_0 = \alpha \frac{(V_+ - V_-)}{R_I} \frac{1}{sC} = \frac{1}{sR_I'C}(V_+ - V_-) \cong \frac{1}{sR_IC}(V_+ - V_-) \qquad 7.3$$

The output is therefore the integral of the input difference voltage.

The Difference Amplifier circuit of Figure 7.1 (b) operates in a similar manner. To perform the Difference Amplifier function we cannot just replace the capacitor C of Figure 7.1 (a) with a resistor R_B, as there would be a d.c. voltage across this resistor and consequently the biasing of the circuit would be dependent on the value of R_B. T_1 and T_3 of Figure 7.1 (a) can be dispensed with, as their main function is to allow both the V_- and the V_+ inputs to have the same d.c. bias potential. Note that on Figure 7.2 the V_- and the V_+ inputs to the Difference Integrators M and N have the same d.c. bias potential whereas the inputs to the Difference Amplifiers K and L differ by the emitter to base voltage drop ($\cong$0.6V) of their input transistor. This topic of biasing will be explained in greater detail in Section 7.3. The Difference Amplifier, Figure 7.1 (b), also contains an extra transistor T_5 that is not possessed by the Difference Integrator of Figure 7.1 (a). This transistor provides a d.c. voltage shift so that there will be no d.c. potential across R_B and the d.c. output potential will therefore be equal to the value present at the two input points. The current out of the T_5 collector, however, will be approximately α times the value out of the T_4 collector. Therefore

$$V_0 = \alpha^2 \frac{(V_+ - V_-)}{R_A} R_B = \frac{R_B}{R_A'}(V_+ - V_-) \approx \frac{R_B}{R_A}(V_+ - V_-) \qquad 7.4$$

From the descriptions of the circuits just given the two circuits Figure 7.1 (a) and 7.1 (b) are seen to be almost identical. A modified form of the Difference Amplifier circuit, Figure 7.1 (b), could have been used for both the Difference Amplifier and the Difference Integrator functions. Two separate circuits were used as the circuits were simpler and, because of reasons (b) and (c) mentioned below, a better integrator was obtained.

From these simplified descriptions of the two circuits they are seen to perform the desired functions. The multiplying factor is not quite proportional to a resistor ratio, and this is due to a number of reasons. The effect of α, the emitter to collector current gains of the transistors, has already been mentioned but there are also some other small perturbing factors that can be considered as modifying the effective α.

(a) The small emitter resistance of T_4 will add to R_A and its relative importance gets worse at low R_A values.

(b) The resistor R_4, even though it is large compared to the emitter input resistance of T_5, will still draw off some a.c. current.

(c) R_7 will similarly draw off some a.c. current.

(d) If R_A is large it becomes comparable to the collector impedance of T_2. The current to T_4 is then no longer determined solely by $\frac{(V_+ - V_-)}{R_A}$.

Because of all these small perturbing factors, some experiments were performed on both the Difference Integrator and the Difference Amplifier circuits in order to determine correction factors for these effects. The results of the experiments are plotted in Figure 7.3. Figure 7.3 shows the values of resistors R_A and R_I required in order to obtain effective resistance values R_A' and R_I' for the Difference Amplifier and Difference Integrator respectively where

$$V_0 = \frac{1}{sR_I'C}(V_+ - V_-) \qquad 7.5$$

for the Difference Integrator, and

$$V_0 = \frac{R_B}{R_A'}(V_+ - V_-) \qquad 7.6$$

for the Difference Amplifier.

For a value of $R_I' = 3\ k\Omega$ the value of R_I required is $2.9\ k\Omega$ for the Difference Integrator and $R_A = 2.7\ k\Omega$ is required for the Difference Amplifier to realize an $R_A' = 3\ k\Omega$. If the emitter-to-collector current gain of the transistors were the only contributing factor, these results would correspond to a value of $\alpha = 0.967$ which is not too unreasonable as the transistors actually used had a minimum $\alpha = 0.98$.

Some experiments were performed on the Difference Amplifier circuit of Figure 7.1 (b) in order to determine its effectiveness in forming a transmission zero which, as shown by Equation 6.3 and Figure 7.2, will occur when the circuit has equal a.c. inputs V_+ and V_-. The experiments were performed by monitoring the current out of the collector of T_4 for

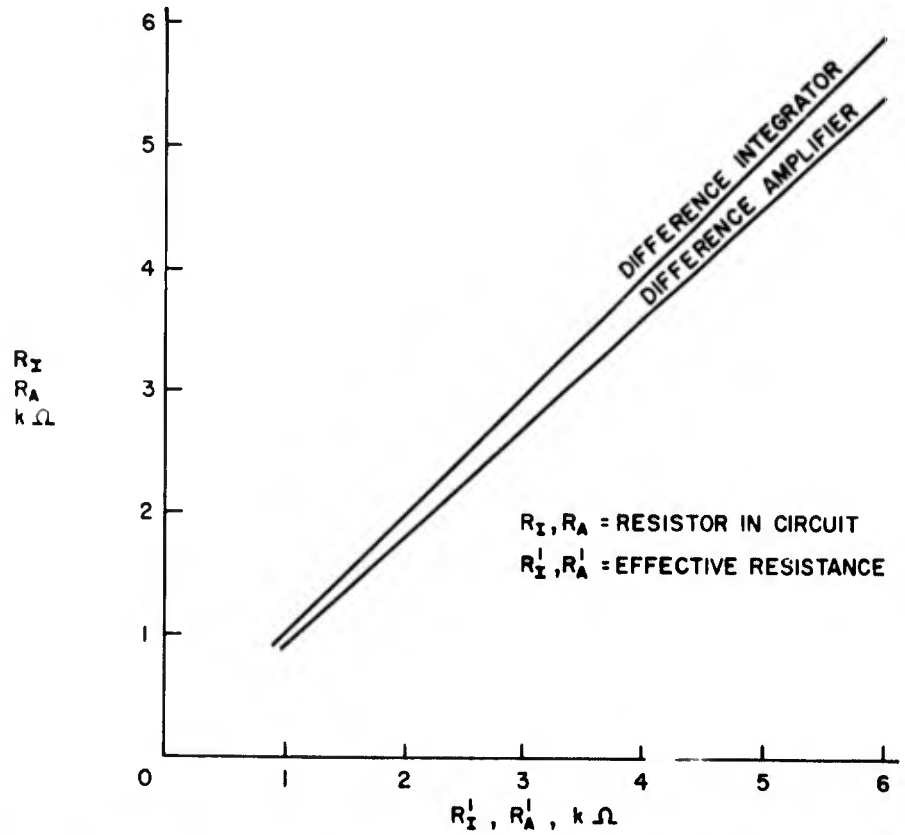

FIG. 7.3 CORRECTION CHART FOR INPUT RESISTOR ON FIG. 7.1 (a) & (b)

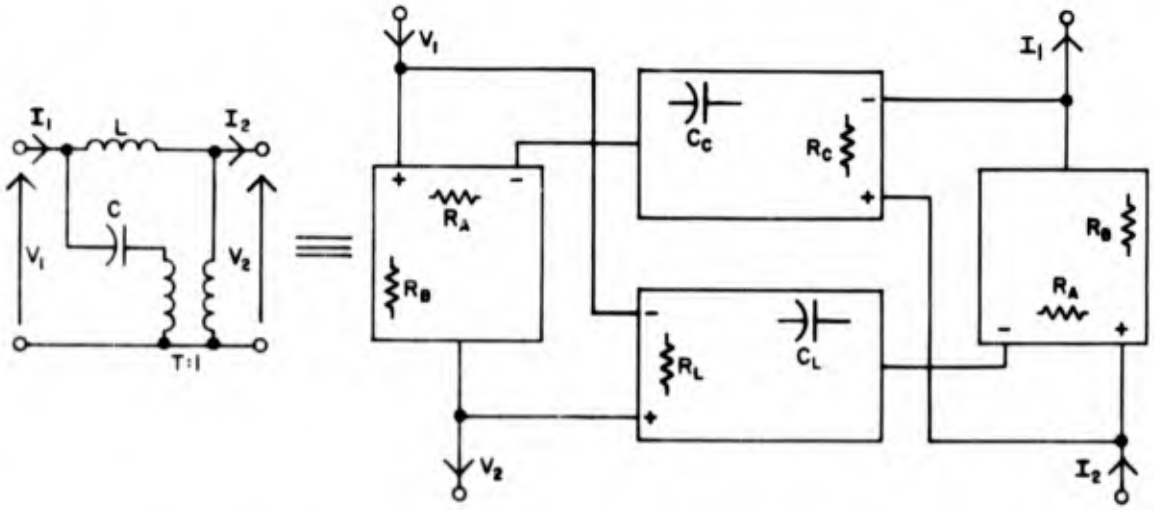

$$R_L' C_L = \frac{L}{T-1} \qquad R_B = \frac{R_A'}{T} \qquad R_C' C_C = C(T-1)$$

FIG. 7.4 ANALOG BRUNE SECTION, DESIGN EQUATIONS

the two cases listed below. The currents were monitored by measuring the voltage across R_4

(a) When a voltage V_+ was applied to T_4 and $V_- = 0$

(b) When the two inputs were at the same a.c. potential, i.e., $V_- = V_+$ = the value used in experiment (a).

If V_a and V_b are the voltages obtained from each of these two experiments the ratio $\frac{V_b}{V_a}$ is then a measure of the effectiveness of the subtracting circuit. The measured results obtained at a frequency of 1 kHz were

$$\frac{V_b}{V_a} = 0.00056 \text{ when } R_A = 3\ k\Omega$$

$$\frac{V_b}{V_a} = 0.0018 \text{ when } R_A = 10\ k\Omega$$

It is inadvisable to make R_A much less than 1.0 kΩ as its value approaches the emitter resistance of T_4, but for effective null operation R_A should be as low as possible, otherwise the current to T_4 is no longer determined solely by $\frac{V_+ - V_-}{R_A}$. A compromise value for R_A is 3.0 kΩ.

7.3 Biasing of the Analog Brune Section

The biasing of the complete Brune section can be explained by referring to Figure 7.2. Figure 7.2 shows the Difference Integrators and Difference Amplifiers interconnected to form the Analog Brune

circuit of Figure 6.5. The Difference Integrators are labelled M and N. The Difference Amplifiers are labelled K and L.

The power supply voltage for the Brune circuit is +20 V and the voltage at the interconnect points is chosen to be +10 V. All input and output points of the four circuits K, L, M, and N must therefore be biased at +10 V.

The two Difference Amplifiers K and L contain the resistor pairs R_5R_6 and $R_{12}R_{13}$. These resistor pairs establish the bias reference voltages of +10 V at their junctions. The references are thus determined by resistance ratios which facilitates integration of the circuit.

There are two inputs to the analog Brune section, V_1 and I_2. As can be seen from Figure 7.2 the V_1 entry point achieves its correct bias voltage directly from the R_5R_6 resistor pair in the K amplifier. The output of the high-gain amplifier section of K is strapped to its input via the feedback resistor R_B which therefore refers the output voltages to the +10 V established by the junction of the $R_{12}R_{13}$ pair in the K amplifier. The non-inverting input terminal of the N integrator is connected to the output of the K amplifier and the inverting input terminal is connected to the R_5R_6 pair of amplifier K. Both inputs to the integrator N are therefore firmly biased.

The I_2 input is directly connected to the R_5R_6 pair on amplifier L thereby establishing its bias and also the bias for the non-inverting input terminal of integrator M. The I_1 output is firmly tied to the $R_{12}R_{13}$ pair on the L amplifier by the feedback resistor R_B.

This leaves the outputs of the two integrators M and N not directly biased,but because of the d.c. negative feedback present in the

simulated Brune section they will assume the d.c. voltages present at the non-inverting terminals of the K and L amplifiers respectively.

The biasing for the complete simulated Brune section circuit is therefore determined and it is seen to be referred in all cases to resistor ratios. The biasing is not dependent on the connection of other Brune sections and direct interconnection of many such analog Brune sections is therefore possible.

As the outputs of the K and L amplifiers have their bias voltages established via the feedback resistors R_B it is desirable to keep the resistances R_B as low as possible. This can be arranged if we design the filter circuits so that the Brune transformer-ratio T is greater than unity. If this is done, R_B will always be less than 3 kΩ as it has been already decided to keep R_A close to 3 kΩ.

This new Brune section achieves all of the desirable requirements listed at the beginning of this chapter. The detailed equivalence between the new analog Brune section and the basic LC Brune section can be seen in Figure 7.4. Note the simple expressions obtained and the fact that this section requires only six resistor attachments, whereas eleven were required per section when operational amplifiers were used.

In the expressions shown in Figure 7.4 the resistances R'_L and R'_C are the two special cases of the Difference Integrator resistance R'_I. The actual resistor values R_L and R_C required in the circuits of Figure 7.1 in order to achieve these effective values are obtained from the Difference Integrator curve of Figure 7.3. The resistor values R_A

are similarly found by using the Difference Amplifier curve of Figure 7.3.

As can be seen from the design equations in Figure 7.4 the $R'_L C_L$ product becomes infinite and $R'_C C_C$ equals zero when T = 1. The circuit cannot properly handle this special case but this does not present much of a problem as the LC filter design can generally be varied to ensure that T is never in the range of approximately 0.9 to 1.1.

CHAPTER 8. FILTER REALIZATIONS WITH THE ANALOG BRUNE SECTION

8.1 Low-Pass Filters

A fifth degree elliptic function low-pass filter with a cut-off frequency of 20 kHz was constructed from the analog Brune sections of Figure 7.2. The component sensitivity of this filter was found to be much less than the same filter realized with operational amplifiers, which was previously mentioned in Section 7.1.

The filter design in normalised units as obtained from a handbook[34] (filter no. C 0515, $\theta = 54^{o}$, page 88) is shown in Figure 8.1 (a). The filter was arranged in the Brune form of Figure 8.1 (b) by leaving the shunt capacitor at the load end unchanged, finding the other capacitor values for the two Brune sections by means of the realizability condition in Figure 6.1 (a) and finally using the equivalences in Figure 6.2 (c) and (d). This particular type of Brune realization, with the attenuation pole of the filter at infinity caused by a shunt capacitor, was chosen because such a shunt capacitor can be easily simulated at the source end of the filter as shown in Figure 8.1 (c). One-port components causing attenuation poles at zero or infinite frequency in Brune filters are most easily simulated by moving them to the source or load ends in this manner. Figure 8.1 (c) shows the filter constructed from analog Brune sections. The component values in Figure 8.1 (c) were obtained by using the design equations of Figure 7.4 and the correction chart, Figure 7.3. The 36.04 kHz attenuation pole frequency of the filter was tuned by R_6 for the forward direction of

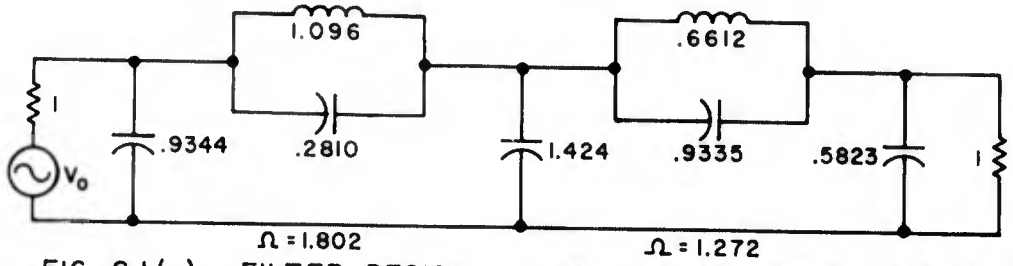

FIG. 8.1(a) FILTER DESIGN C 05 15 θ = 54° FROM HANDBOOK [34]

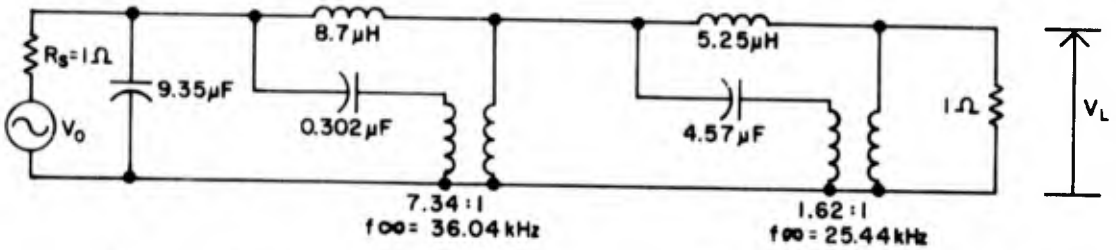

FIG. 8.1(b). 20 kHz LOW-PASS FILTER IN BRUNE FORM. FROM FIG. 8.1(a).

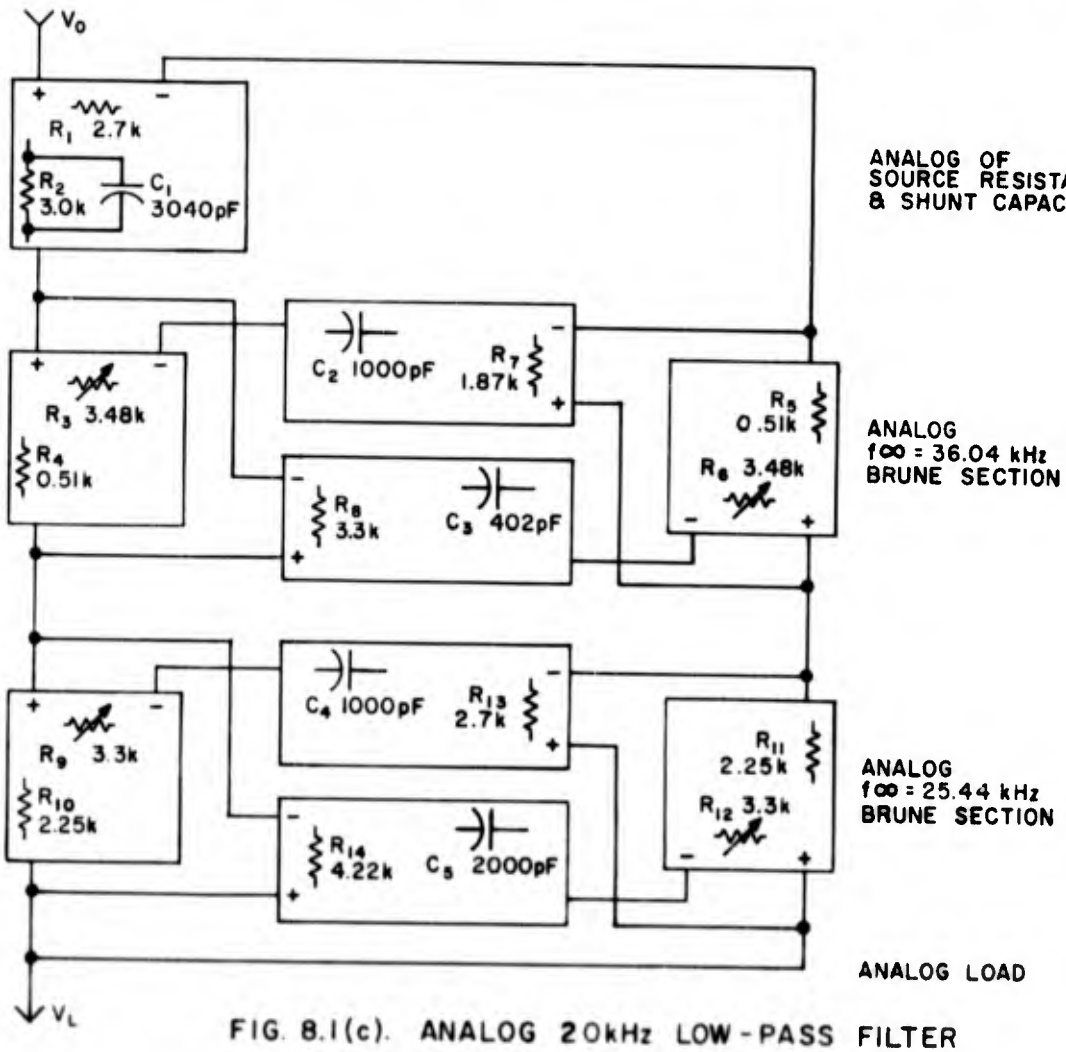

FIG. 8.1(c). ANALOG 20kHz LOW-PASS FILTER

transmission and by R_3 for the reverse direction. The 25.44 kHz attenuation pole frequency was tuned by R_{12} for the forward direction and by R_9 for the reverse direction. Figure 8.2 (a) shows the measured frequency response of the filter to be exactly as calculated. Table 8.1 shows the results of a sensitivity experiment performed on the filter. The experiment was performed by paralleling each component in turn with 10 times its impedance value, thereby perturbing each component value by -9%. Apart from the unavoidable sensitivities to R_1 and R_2 all other components have very low sensitivities especially in the lower frequencies of the passband. Changing R_1 or R_2 is equivalent to changing simultaneously both R_s, the source resistance, and V_o the open circuit source voltage. Changing these quantities would be expected to produce a change in the output voltage V_L even on the original LC filter of Figure 8.1 (a). Therefore we can say that the components of the filter itself, apart from those determining the source conditions, have very low sensitivities as expected,and the low sensitivity of the LC structure has not been lost in the transition from the real to the simulated circuit.

The low sensitivities of Table 8.1 represent a marked improvement over the values obtained from the same low-pass filter made with commercially available operational amplifiers in the Brune sections. The resistor matching problem, encountered in the operational amplifier Brune sections mentioned in Section 7.1, produced output level changes of 0.6 dB at 5 kHz for -9% perturbations in component values, and this occurred for four resistors per Brune section or for a total of eight resistors in the whole filter.

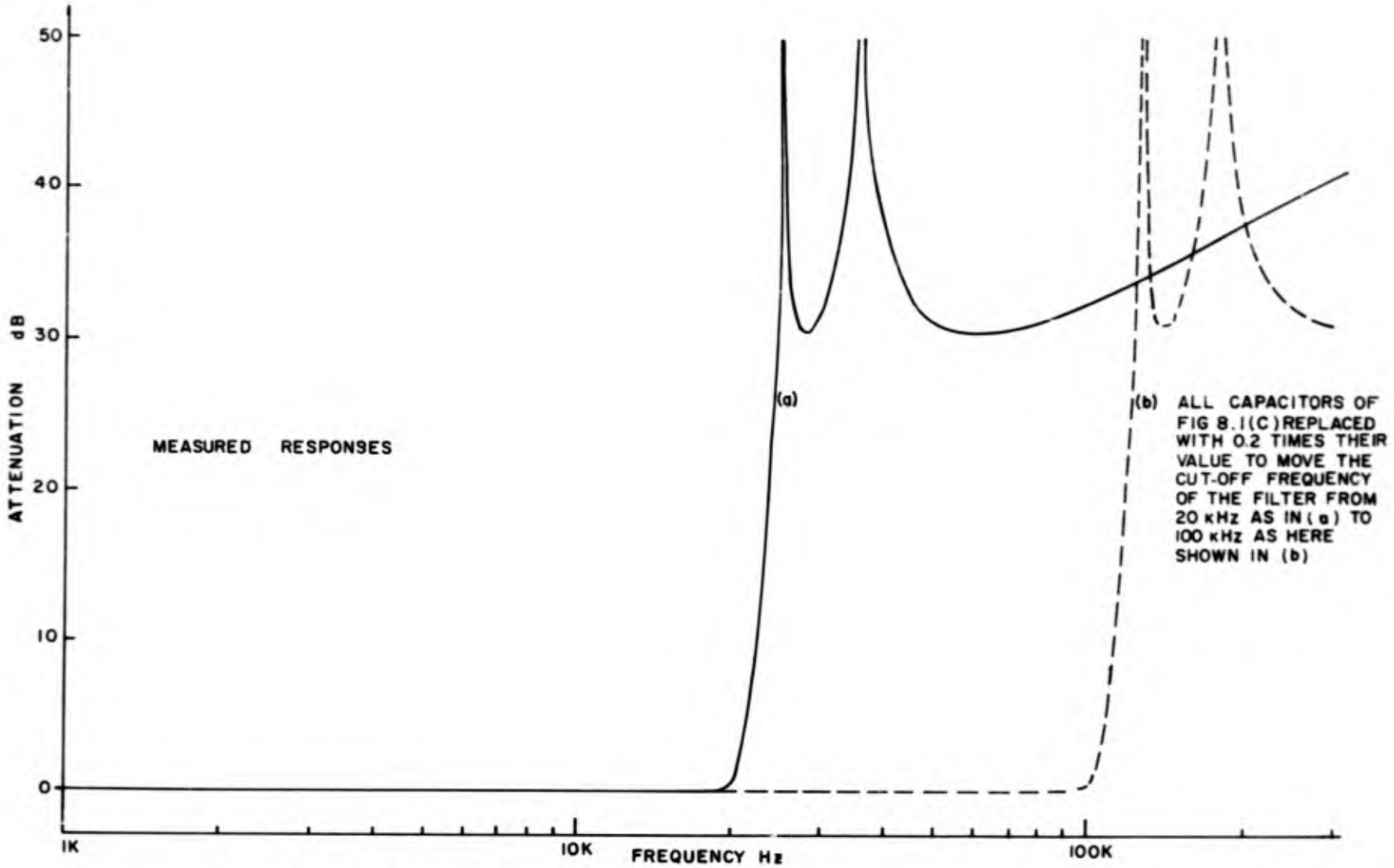

FIG. 8.2. LOW-PASS FILTERS USING ANALOG BRUNE SECTION

FREQUENCY kHz	5	10	15	18	20	21
MEASURED ATTENUATION IN dB WHEN ALL COMPONENTS ARE AT THEIR DESIGN VALUES SHOWN IN FIG.8·1(C)	0	0	0	0	+0.2	+2.0

PERTURBED COMPONENT	MEASURED ATTENUATION IN dB WHEN EACH COMPONENT WAS SEPARATELY PERTURBED BY −9%					
R_1	−0.35	−0.3	−0.4	−0.45	−0.1	+1.6
R_2	+0.4	+0.4	+0.35	+0.3	+0.7	+2.5
R_3	0.	0	+0.05	+0.25	+0.2	+0.8
R_4	+0.05	+0.1	−0.1	−0.1	+1.7	+5.0
R_5	0	+0.1	+0.2	+0.5	+1.5	+5.0
R_6	+0.05	+0.1	−0.1	−0.1	+0.1	+1.2
R_7	0	0	0	+0.1	0	+0.5
R_8	+0.05	+0.1	0	0	+0.25	+1.3
R_9	+0.05	+0.15	+0.15	+0.3	+0.9	+2.6
R_{10}	0	0	−0.25	−0.4	−0.5	+1.6
R_{11}	+0.05	+0.1	+0.3	+0.7	+3.1	+7.5
R_{12}	+0.05	+0.05	−0.15	−0.1	−0.3	−0.4
R_{13}	0	+0.05	−0.05	0	+0.2	+1.2
R_{14}	+0.05	+0.1	0	+0.05	+0.1	+0.7
C_1	0	+0.1	0	0	+0.2	+2.6
C_2	+0.05	+0.1	0	0	+1.1	+4.2
C_3	0	0	0	+0.1	+0.7	+3.4
C_4	0	+0.05	0	0	+0.7	+4.2
C_5	0	0	0	0	+1.5	+5.8

TABLE 8.1

COMPONENT SENSITIVITY EXPERIMENT ON 20 kHz LOW-PASS FILTER OF FIGURE 8.1(C). EACH COMPONENT WAS PERTURBED BY-9%

The biasing of the filter performed as expected and all interconnect voltages were within $\pm$0.3 V of +10 V even though the basic circuits, Figures 7.1 (a) and (b), of the analog Brune sections were constructed from $\pm$5% tolerance resistors. Correct frequency response was maintained when R_4 of either the Difference Integrator, Figure 7.1 (a), or of the Difference Amplifier, Figure 7.1 (b), was perturbed by -15% and these resistors were found to be the most sensitive biasing resistors in the analog Brune circuits. The filter could tolerate larger perturbations in the R_4 resistors if the corresponding R_2 resistors were changed simultaneously, thus demonstrating that the biasing of the circuit is dependent mainly on resistor ratios and not on absolute values. With the -15% perturbation in the value of R_4 a lower maximum undistorted output level was obtained from the filter.

When all components were at their design values the maximum undistorted output voltage obtainable from the filter was 0.4 V peak to peak. The limitation on this level is caused by the resonant rise in voltage that occurs at the output of the Difference Integrator containing C_3 and R_8. For the 0.4 V peak to peak output condition this voltage at the output of the C_3R_8 Difference Integrator has a maximum resonant voltage of 7 V peak to peak at 21 kHz. The output of this integrator corresponds to the current in the 8.7μH coil of Figure 8.1 (b). Resonant current peaks are to be expected in components such as this at frequencies close to the passband edge, where the natural modes of the filter have their greatest effect. A similar effect occurred in the gyrator channel filter, where the limitation on drive

level was caused by the high voltages developed across the floating gyrators.

In order to check the high frequency capability of the filter, all the capacitors in the filter were replaced with 1% tolerance capacitors whose values were one fifth their former magnitude. The filter was not retuned and the frequency response curve of Figure 8.2 (b) was measured. This is the same type of response as before but the cut-off frequency is now 100 kHz. The filter circuit therefore performed exactly as expected.

8.2 20 kHz High-Pass Filter

To test the capability of the analog Brune circuit on a high-pass filter the dual of the low-pass prototype filter in Figure 8.1 (a) was converted into a 20 kHz high-pass filter and arranged in Brune form as shown in Figure 8.3 (a). The conversion to Brune form was accomplished by using the equivalences described in Figures 6.2 (e) and (j). The series capacitor in this filter required to provide the attenuation pole at zero frequency was moved to the source end where it could be simulated along with the source resistance. As can be seen in Figure 8.3 (b), the analog filter circuit, this simulation of the series capacitor was accomplished by a Difference Amplifier having a series connected resistor and capacitor in place of its R_B.

The two extra transformers, obtained in converting both Brune sections as shown in Figure 6.2 (j), were combined into one with a turns ratio of 1:11.9. As can be seen from Figure 8.3 (b) this transformer was simulated by means of a pair of high-gain amplifiers and four

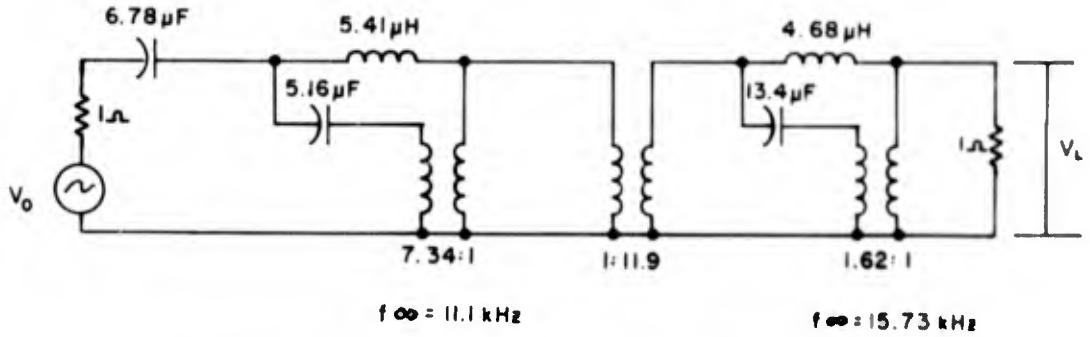

FIG. 8.3 (a) 20kHz HIGH-PASS FILTER

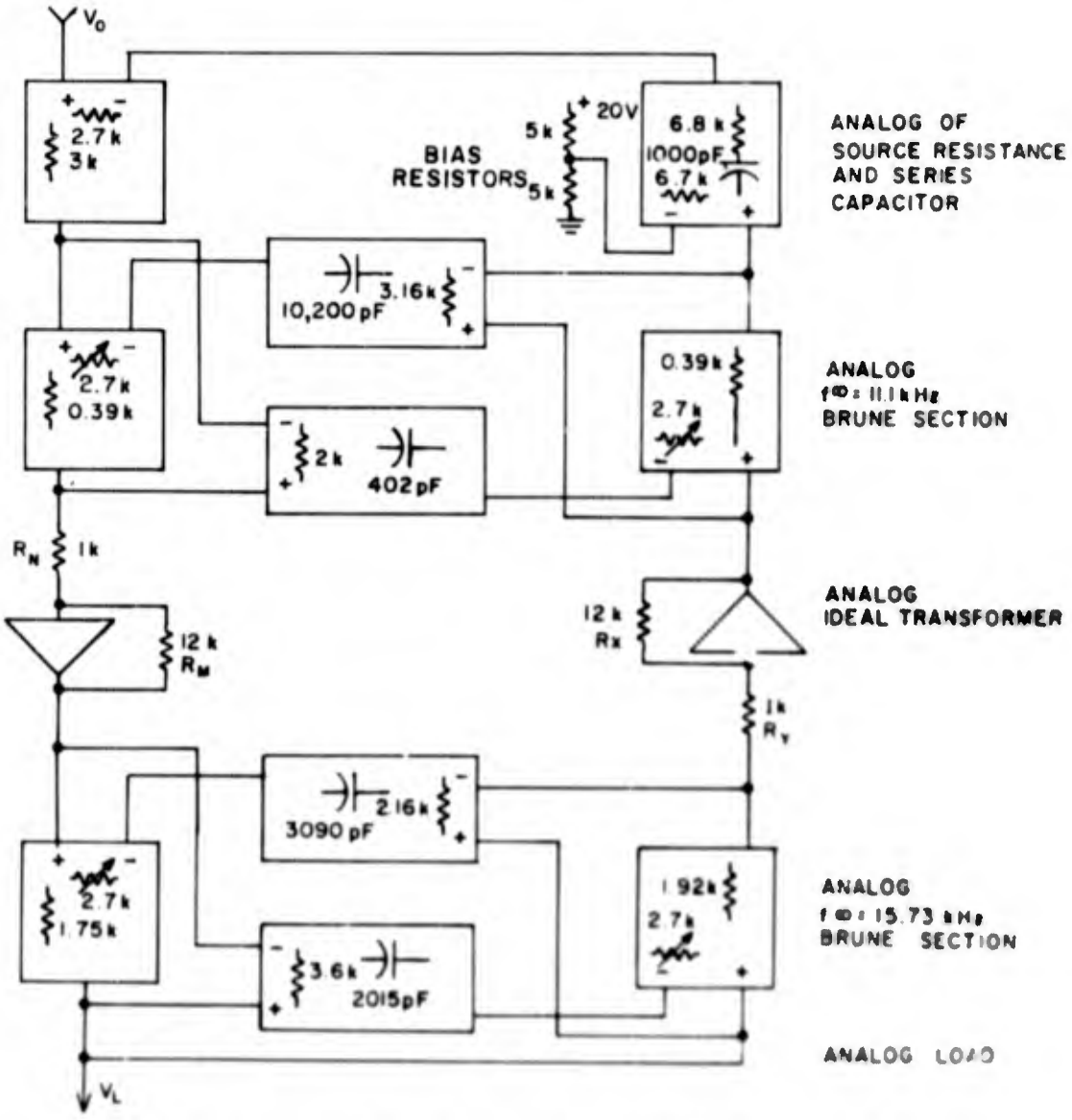

FIG 8.3 (b) ANALOG 20kHz HIGH-PASS FILTER

attached resistors. Figure 8.4 shows the details of these amplifiers and how they simulate a transformer. The analog ideal transformer in Figure 8.4 (b) has two inputs V_1 and I_2 just as in the analog Brune section. The outputs are related to the inputs in the ideal transformer Figure 8.4 (a) by the same turns ratio T. and in the analog equivalent circuit, Figure 8.4 (b), by two independent ratios T_V and T_I which correspond to a voltage and a current ratio respectively. This ambiguity is undesirable, as T_V should always equal T_I but it is unavoidable, and experimental results showed that the match between T_V and T_I is not critical. In the filter of Figure 8.3 (b) the resistors $R_M R_N R_X R_Y$ used to determine T_V and T_I had a tolerance of $\pm 5\%$.

Each amplifier in Figure 8.4 (b) introduces a phase change of 180°, but since no phase change is introduced between V_2 and I_2 or between V_1 and I_1 the operation of the simulation circuit is not disturbed.

Figure 8.5 shows the measured frequency response of the high-pass filter which is exactly as calculated. The measured attenuation increases slightly at frequencies above 150 kHz. This is caused by parasitic effects; a similar slight attenuation increase would be expected from the parasitic effects in an LC filter.

8.3 16.15 - 19.5 kHz Band-Pass Filter

A band-pass telephone channel filter was designed in a ladder structure by using series resonant circuits in its shunt arms and inductors (some with negative values) in its series arms as shown in Figure 8.6. The design was performed with the aid of a filter design computer program developed at Lenkurt Electric Co. The calculated frequency

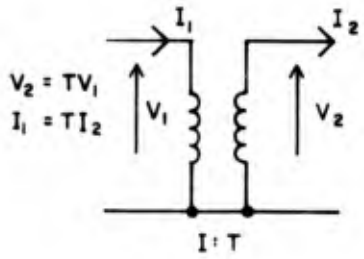

FIG. 8.4 (a) IDEAL TRANSFORMER

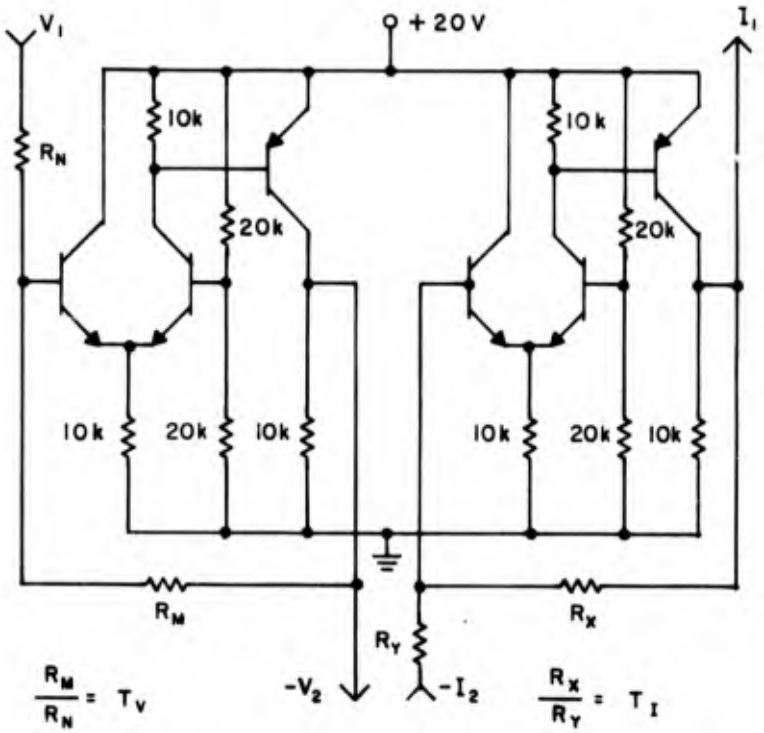

FIG. 8.4 (b) ANALOG EQUIVALENT OF IDEAL TRASFORMER

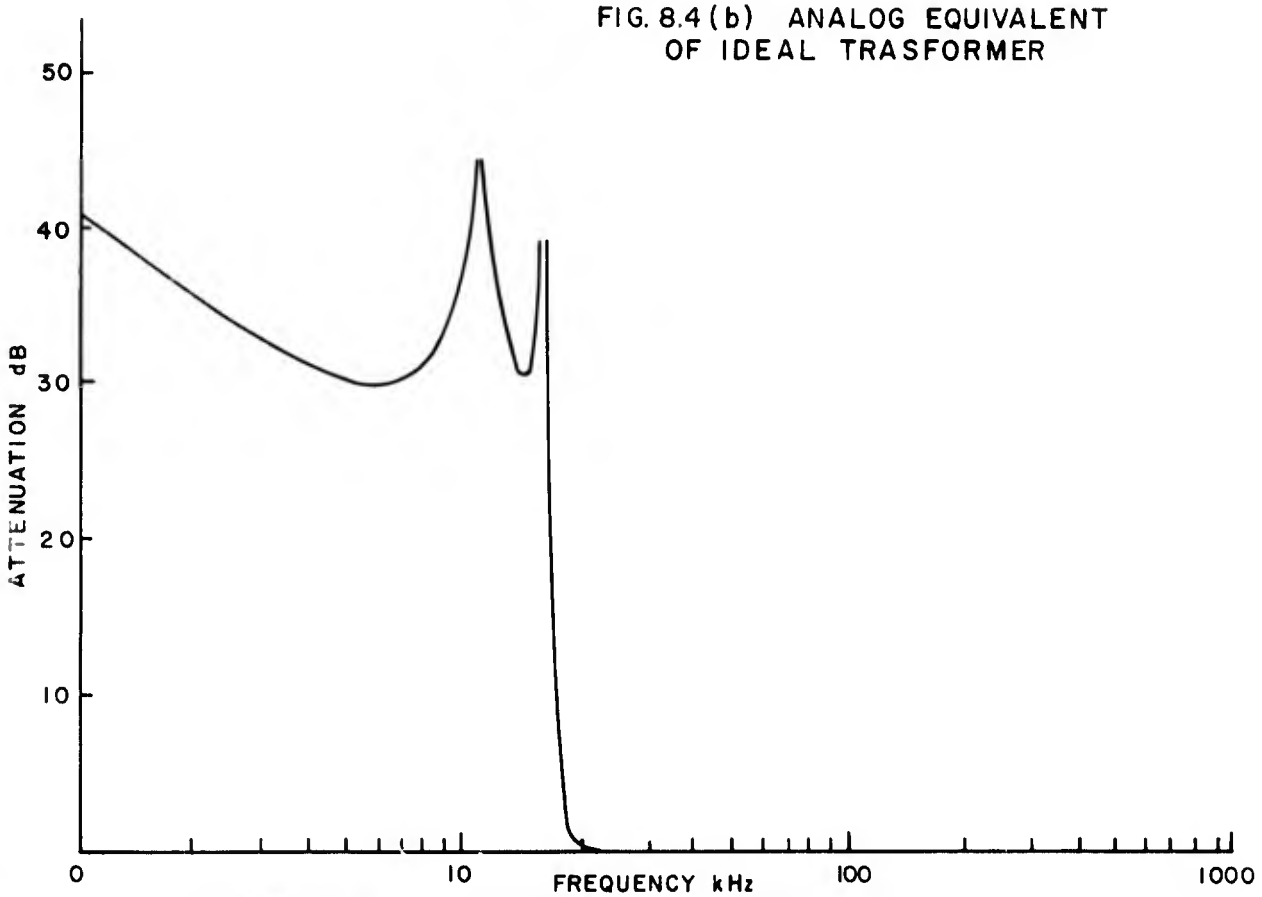

FIG. 8.5 20kHz HIGH-PASS FILTER USING ANALOG BRUNE SECTIONS (FIG. 8.3 (b))

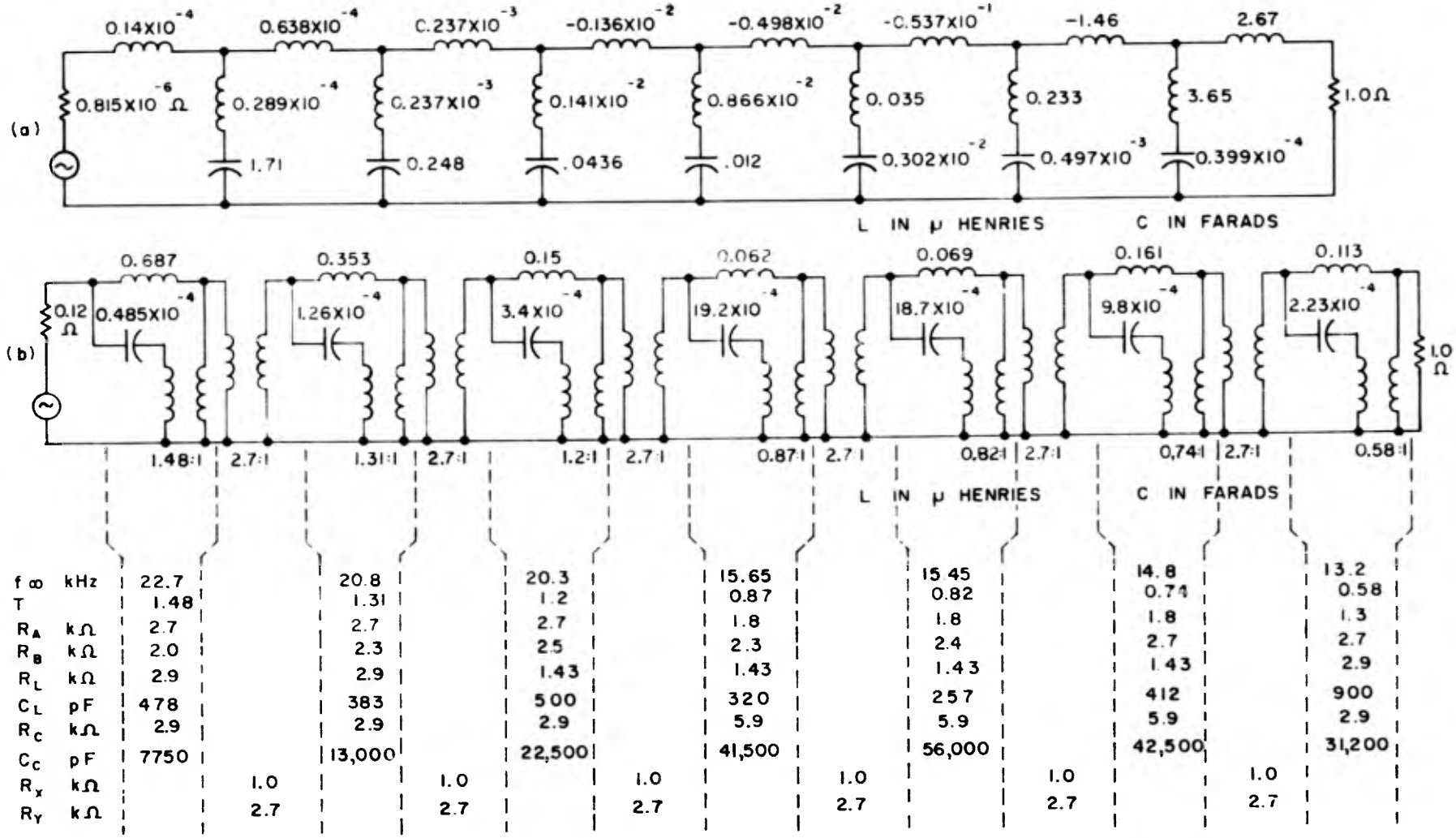

FIG. 8.6 TELEPHONE CHANNEL FILTER & TABLE OF COMPONENT VALUES USED TO CONSTRUCT THE FILTER WITH ANALOG BRUNE SECTIONS

response of the filter was similar to that of the filter described in Chapter 5 and the calculated pass-band is shown in Figure 8.7 (a).

As already mentioned in Section 6.1 it is theoretically possible with Brune sections and some one-port networks to realize any filter transfer function having poles of loss on the real frequency axis. The realization, however, may be a very impractical one as it may require a large spread of L/C ratios in its Brune sections. The above mentioned band-pass filter did prove to be such an impractical design.

The computed component values for the filter are shown in Figure 8.6 (a) and it is evident from this circuit that there is a serious impedance problem with the filter. The large change in Brune section L/C ratios that occurs through the filter means that the terminating resistances differ by a factor of approximately 10^6. Several designs of the filter were tried by changing around the positions of the various attenuation poles in the filter but the magnitude of impedance change was not greatly affected. With such a large impedance change the filter can hardly be considered as a good LC doubly terminated design and it would be difficult to construct even with coupled coils. Even though the filter design was an impractical one it was decided to construct it in analog form in order to see how the simulation technique would perform with this type of difficult circuit.

The circuit was arranged in the Brune form shown in Figure 8.6 (b) by using the equivalences of Figure 6.2 (a) and (d), and it was constructed from analog Brune sections by using the component values tabulated in Figure 8.6. Figure 8.7 (b) shows the measured frequency response of the

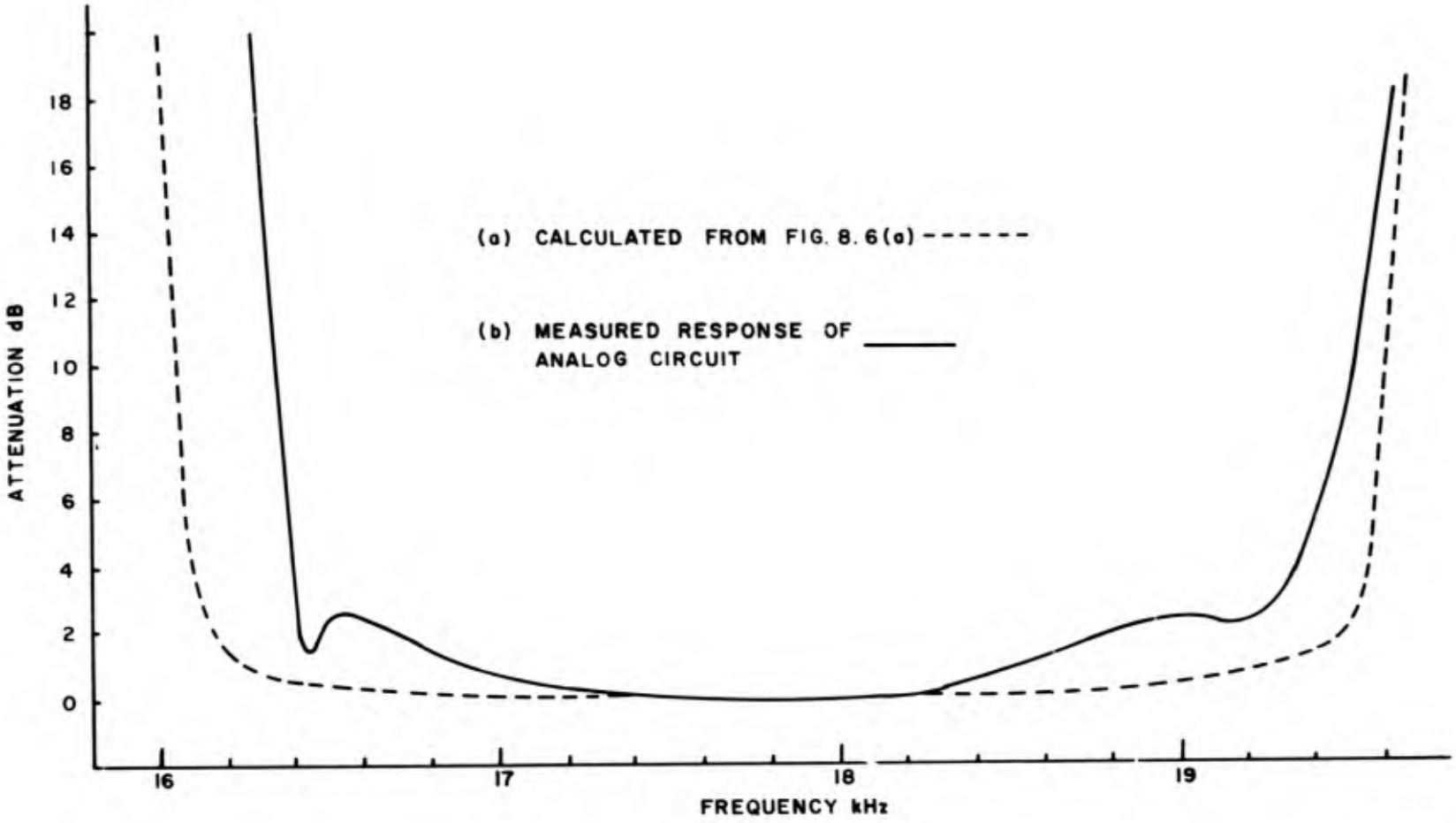

FIG. 8.7 RESPONSES OF TELEPHONE CHANNEL FILTER IN FIG. 8.6

analog circuit. This response is not very good as can be seen by comparing it to the calculated curve of Figure 8.7 (a).

The poor frequency response can be attributed to the impedance change that occurs in the filter. This impedance change requires that analog transformers be used in order to make the circuit realizable. The analog Brune circuits however cannot operate properly when such a large impedance transformation is being effected by the analog transformers, because the signal loss incurred in passing through these transformers in both directions of transmission means that the I_2 input to each analog Brune section as shown in Figure 7.2 is very small. Each Brune section therefore has to function with almost a single input, V_1, and as shown by Equation 6.11 this is an undesirable condition as it accentuates the tendency towards oscillation. Using Equation 6.11 the natural modes for all Brune sections are computed to fall in the passband of the filter. The result of these natural modes falling in the passband is to give a very noisy output from the filter. This noisy output prevented the filter from being properly tuned, even though a selective meter with a -3 dB bandwidth of ± 3.5 Hz was used. This incorrect tuning accounts for much of the poor passband response of Figure 8.7 (b).

Another design of the filter was tried where the turns ratio of the transformers was < 1, i.e., the impedance build up occurred from load to source end. Biasing problems were encountered with the analog version of this design as the high loop gain from the V_2 output of one analog Brune section through the filter and back to its I_2 input tended

to lock the bias of the filter in a condition where one transistor was shut off. This bias locking occurred when the circuit was switched on and consequently no frequency responses could be measured.

8.4 Conclusions on Analog Brune Filters

The results on the low-pass and high-pass filters of Sections 8.1 and 8.2 have shown that excellent low sensitivity filters can be made by the technique of simulating a good LC doubly terminated filter design. The results on the band-pass filter in Section 8.3, however, have also shown that the simulation technique will behave poorly when simulating a bad LC filter design. This poor performance shows up as noisy output or bias instability.

By a good LC filter design is meant, one that does not require large transformer ratios in order to keep approximately the same L/C ratio in all its resonant LC pairs used to determine the attenuation pole frequencies. When these L/C ratios, which are related to the impedance level of the filter, are not the same,moderate impedance changes can be taken care of with ideal transformers. An example of this is the 11.9:1 transformer used in the high-pass filter of Section 8.2. When large transformation ratios are required,two defects can become quite noticeable in the analog circuit. If the transformer ratios are such that the source impedance of the filter is less than its load impedance the analog circuits become very noisy, and if, on the other hand, the transformers are such that the load impedance is the smaller of the two impedances the biasing becomes unstable. This biasing problem becomes

a difficult one to resolve when it is remembered that all circuits in the analog filter are direct coupled.

The secret of good analog Brune filter design is therefore to have a good LC design in Brune form to start with. When this good design is simulated with analog Brune sections all the advantages of the analog technique can be obtained. These advantages are, completely integrable standard filter sections constructed from low tolerance components, with the a.c. properties determined by high quality attachments.

CHAPTER 9.

COMPARISON OF INDUCTOR-SIMULATION TO TOTAL-FILTER-SIMULATION TECHNIQUES

9.1 Suitability of Basic LC Section for Simulation

The most important consideration in either the inductor-simulation or the analog-Brune techniques is that the filter to be simulated be a suitable subject for application of the appropriate technique. In the analog Brune technique the most important requirement is to have an approximately equal L/C ratio in all Brune sections.

A similar requirement appears in circuits where the Inductor-Simulation Technique is used. For inductor simulation via gyrators the maximum resonant circuit Q occurs when the capacitors on both sides of the gyrator satisfy Equation 4.9 which is $\frac{C_2}{C_1} = \frac{G_2}{G_1}$. Combining this equation with Equation 4.5 the optimum L/C ratio is found to be

$$\left(\frac{L}{C}\right)_{opt} = \frac{G_2}{G_1 g_1 g_2} \qquad 9.1$$

and this is entirely a function of the gyrator. The impedance level of the filter can be adjusted so that the resonant LC pairs of the filter have their L/C ratios close to the optimum as given by Equation 9.1.

In the telephone channel filter described in Chapter 5 the ratio

$$\frac{\text{highest value of } \frac{L}{C} \text{ ratio}}{\text{lowest value of } \frac{L}{C} \text{ ratio}}$$

was computed for the seven resonant LC pairs of the filter that determine the attenuation pole frequencies, and this ratio was found to be equal to 57. This is quite a low value when compared to the value of 54×10^8 computed for the same ratio on the telephone channel filter of Figure 8.6 (a). This wide difference helps explain why the gyrator filter could be built and the analog Brune filter could not. This ratio can be interpreted as a figure of merit to determine a circuit's suitability for simulation.

As the LC telephone channel filter circuit of Figure 5.1 is a good subject for simulation it would be an interesting project for future research in this area to devise a method of simulating this type of filter structure by inductorless means. If this is done, however, generality will probably have to be sacrificed, as there would no longer be a basic section such as the Brune that could be used for low-pass, high-pass, or band-pass filters. This filter structure could be simulated by the same general state variable techniques used in Chapter 6.

9.2 Biasing

The Inductor Simulation method is by far the better inductorless filter technique when considered from a bias point of view. The biasing of its active circuitry is entirely self contained at each gyrator. The gyrators are isolated from one another by the filter capacitors which consequently are performing a very useful dual role. The analog Brune filters on the other hand are entirely direct coupled and consequently their reliability suffers. Failure of one component could

disrupt the entire filter, as the biasing of the whole filter would be upset, whereas failure of a component in a gyrator can only upset one simulated inductance value.

9.3 Noise Performance

The noise performances of the telephone channel filter made from gyrators, Figure 5.1, and from analog Brune sections, Figure 8.6, were compared for two different bandwidths and the results are tabulated below

Noise Bandwidth	30 Hz - 20 kHz	16 kHz - 20 kHz
Dynamic Range of Gyrator Filter	57 dB	> 70 dB
Dynamic Range of Analog Brune Filter	37 dB	41 dB

The dynamic range is defined as the ratio of the maximum undistorted signal output to the zero signal noise output of the filter. Both filter designs had approximately the same maximum output level of 50 mV. rms. The tabulated results, therefore, show the amount of rms noise voltage below 50 mV. rms., obtained in the two bandwidths, when there is no signal input to the filter.

The small difference between the values of dynamic range for the two bandwidths of the analog Brune filter, Figure 8.6, confirm the theory proposed in Section 8.3, that the noise is being accentuated by the natural modes of the individual analog Brune sections.

Noise did not create any problems in the high-pass or low-pass analog Brune filters of Sections 8.1 and 8.2. All the frequency responses of these filters were measured with a meter having a response flat to 4 MHz, thus showing that the dynamic ranges of these filters were greater than 60 dB for a noise bandwidth of 4 MHz.

9.4 Directions for Future Research

The inductor simulation technique shows the greatest promise for future research on inductorless filters and future work in this field should be directed towards obtaining simpler inductor simulation circuits whose a.c. properties would be dependent on only two resistors. This dissertation has discussed inductor simulation by means of controlled source gyrators only,but there are other types of gyrator circuits such as those of references 35 and 36 that deserve further study. There are also inductor simulation circuits that cannot be classified as gyrators, such as those of references 37 and 38 and some useful further work may be undertaken along these lines, although circuits that involve matched components, such as that in reference 38 are not at all attractive. However, none of the gyrator circuits that have been published to date has performance equal to that of the controlled-source circuit described in this dissertation, and its performance is felt to be the minimum acceptable for high quality filters at frequencies below 100kHz.

The analog Brune filters of Chapter 8 have shown that the low sensitivity property of terminated LC filters is preserved, if their structure is simulated by analog means. While the Brune section is a

theoretically versatile filter section its practical usefulness is somewhat restricted, as has been shown in Section 8.3. There are many other types of valuable LC doubly terminated filter structures and some useful work could therefore be done in applying the total filter simulation technique to them.

Both of the inductorless filter techniques described in this dissertation were very successful in that they showed conclusively how low sensitivity inductorless filters could be built when the LC doubly terminated structure is simulated by inductorless means. This fact is the major contribution of this dissertation.

Both of the techniques described are suitable for integration. The integration process for any high quality filter will have to be a thin film technique as this is the only technology presently available that can produce resistors and capacitors with temperature coefficients less than 100 ppm/°C. This order of temperature coefficient will be required in order to maintain stable attenuation pole frequencies. The best one can hope to get in this respect for any inductorless filter is to have the attenuation pole frequencies determined solely by RC products. Both techniques just described do this. The gyrator will need to have all of its resistors made by stable thin film techniques. The analog Brune section on the other hand can have most of its resistors made by the more economical monolithic process and only the six resistors per section that determine its a.c. properties need to be thin film. The most important consideration, however, is that both techniques contain a basic circuit that can be common to all filters and therefore enable them to be produced economically.

REFERENCES

1. Linvill, J. G., "RC Active Filters," Proc. of I.R.E., 1954, 42, pp. 555-564.

2. Yanagisawa, T., "RC Active Networks Using Current Inversion Type Negative Impedance Converters," I.R.E. Trans., 1957, CT-4, pp. 140-144.

3. Kinariwala, B. K., "Synthesis of Active RC Networks," Bell System Tech. J., 1959, 38, pp. 1269-1316.

4. Sipress, J. M., "Synthesis of Active RC Networks," I.R.E. Trans., Sept., 1961, CT-8, pp. 260-269.

5. Sipress, J. M., "Synthesis and Sensitivity of Active RC Networks," D.E.E. Dissertation, Polytechnic Institute of Brooklyn, N.Y., June, 1960.

6. Sallen, R.P., and Key, E.L., "A Practical Method of Designing RC Active Filters," I.R.E. Trans., 1955, CT-2, pp. 74-85.

7. Blecher, F. H., "Application of Synthesis Techniques to Electronic Circuit Design," I.R.E. International Conv. Record, 1960, 8, PT 2, pp. 210-217.

8. Horowitz, I. M., "Optimum Design of Single Stage Gyrator RC Filters with Prescribed Sensitivity," I.R.E. Trans., CT-8, June, 1961, pp. 88-94.

9. Kerwin, W. J., Huelsman, C. P., and Newcomb, R. W., "State Variable Synthesis for Insensitive Integrated Circuit Transfer Functions," Stanford University Center for Systems Research, Tech. Report No. 6560-10, December, 1966.

10. Orchard, H. J., "Inductorless Filters," Electronics Letters, Vol. 2, No. 6, June, 1966.

11. Tellegen, B. D. H., "The Gyrator, A New Electric Network Element," Philips Res. Rept., 1948, pp. 81-101.

12. Ghausi, M. S., and McCarthy, F. D., "A Realization of Transistor Gyrators," Semiconductor Prod. Solid State Technol., 1964, 5, (10), pp. 13-17.

13. Sheahan, D. F., and Orchard, H. J., "High-Quality Transistorized Gyrator," Electronics Letters, Vol. 2, No.7, July, 1966, pg. 274.

14. Shekel, J., "The Gyrator as a 3-Terminal Element," Proc. of I.R.E., Vol. 41, August, 1953, pp. 1014-1016.

15. Bogert, B. P., "Some Gyrator and Impedance Inverter Circuits," Proc. of I.R.E., Vol. 43, July, 1955, pp. 793-796.

16. Sharpe, G. E., "The Pentode Gyrator," I.R.E. Trans., CT-4, Dec., 1957, pp. 321-323.

17. Harrison, T. J., "A Gyrator Realization," I.R.E. Trans., CT-10 June, 1963, pg. 303.

18. Yanagisawa, T., and Kawashima, Y., "Active Gyrator," Electronics Letters, Vol. 3, No. 3, March, 1967, pp. 105-107.

19. Yanagisawa, T., "Realization of a Lossless Transistor Gyrator," Electronics Letters, Vol. 3, No. 4, April, 1967, pp. 167-168.

20. New, W., and Newcomb, R., "An Integratable Time Variable Gyrator," Proc. of IEEE, Vol. 53, No. 12, Dec., 1965, pp. 2161-2162.

21. Newcomb, R. W., and Rao, T. N., "Direct Coupled Gyrator Suitable for Integrated Circuits and Time Variation," Electronics Letters, 1966, 2, pg. 250.

22. Shenoi, B. A., "Practical Realization of a Gyrator Circuit and RC Gyrator Filters," Trans. IEEE, 1965, CT-12, pp. 374-380.

23. Holmes, W. H., Gruetzmann, S., and Heinlein, W. E., "High Performance Direct Coupled Gyrators," Electronics Letters, Vol. 3, No. 2, Feb., 1967, pp. 45-46.

24. Holmes, W. H., Gruetzmann, S., and Heinlein, W. E., "Direct Coupled Gyrator with Floating Ports," Electronics Letters, Vol. 3, No. 2, Feb., 1967, pp. 46-47.

25. Warner, R. M., "Three Field-Effect Transistor Gyrators," U.S. Patent No. 3,255,364, June 7, 1966.

26. Holt, A.G.J., and Taylor, J., "Method of Replacing Ungrounded Inductors by Grounded Gyrators," Electronics Letters, June, 1965, Vol. 1, No. 4, pg. 105.

27. Sheahan, D. F., and Orchard, H. J., "Gyrator Flotation Circuit," Electronics Letters, Vol. 3, No. 1, January, 1967.

28. Wantanabe, H., "Synthesis of Band-Pass Ladder Network," I.R.E. Trans., CT-5, Dec., 1958, pp. 256-264.

29. Darlington, S., "Synthesis of Reactance Four-Poles Which Produce Prescribed Insertion-Loss Characteristics," J. Math. Phys., MIT, 18: 257-353, 1939.

30. Tuttle, D. F., "Electric Networks," McGraw Hill, 1965.

31. Brune, O., "Synthesis of a Finite Two-Terminal Network Whose Driving-Point Impedance is a Prescribed Function of Frequency," Journal of Mathematics and Physics, 10: 191-236, 1931.

32. Schwartz, R. J., and Friedland, B., "Linear Systems," McGraw Hill, 1965.

33. Burr-Brown Research Corporation, "Handbook of Operational Amplifier Applications," 1963.

34. Saal, R., "Der Entwurf Von Filtern mit Hilfe des Kataloges Normierter Tiefpasse," Telefunken, G.M.B.H., 1961.

35. Jost, W., "Die Realizierung des Idealen Gyrators mit zwei Operations-verstarkern," Archiv der Elektrischen Ubertragung, Band 21, Heft 3, March, 1967, pp. 152-157.

36. Riordan, R.H.S., "Simulated Inductors Using Differential Amplifiers," Electronics Letters, Vol. 3, No. 2, Feb., 1967, pp. 50-51.

37. Lampard, D. G., and Rigby, G. A., "The Application of a Positive Immittance Inverter to the Design of Integrated Selective Filters," Proc. of IEEE, Vol. 55, No. 6, pp. 1101-1102, June, 1967.

38. Keen, A. W., and Peters, J. L., "Inductance Simulation With a Single Differential-Input Operational Amplifier," Electronics Letters, Vol. 3, No. 4, April, 1967, pp. 136-137.

JOINT SERVICES ELECTRONICS PROGRAM
STANFORD ELECTRONICS LABORATORIES
REPORTS DISTRIBUTION LIST
March 1967

DEPARTMENT OF DEFENSE

Dr. Edward M. Reilley
Asst. Director (Research)
Office of Defense Res & Eng
Department of Defense
Washington, D.C. 20301

Office of Deputy Director
(Research and Information Rm 3D1037)
Department of Defense
The Pentagon
Washington, D.C. 20301

Director
Advanced Research Projects Agency
Department of Defense
Washington, D.C. 20301

Director for Materials Sciences
Advanced Research Projects Agency
Department of Defense
Washington, D.C. 20301

Headquarters
Defense Communications Agency (333)
The Pentagon
Washington, D.C. 20305

Defense Documentation Center
Attn: TISIA
Cameron Station, Bldg. 5
Alexandria, Virginia 22314 (20 cys)

Director
National Security Agency
Attn: Librarian C-332
Fort George G. Meade, Maryland 20755

Weapons Systems Evaluation Group
Attn: Daniel W. McElwre
Department of Defense
Washington, D.C. 20305

National Security Agency
Attn: R4-James Tippet
Office of Research
Fort George G. Meade, Maryland 20755

Central Intelligence Agency
Attn: OCR/DD Publications
Washington, D.C. 20505

Institute for Defense Analyses
400 Army-Navy Drive
Arlington, Virginia 22202

Office of the Dir. of Defense
Research and Engineering
Advisory Group on Electron Devices
346 Broadway, 8th Floor
New York, New York 10013

DEPARTMENT OF THE AIR FORCE

AFRSTE (Col. Kee)
Hqs. USAF
Room 1D-429, The Pentagon
Washington, D.C. 20330

Col. A. Swan
Aerospace Medical Div.
Brooks AFB, Texas 78235

AUL3T-9663
Maxwell AFB, Alabama 36112

AFFTC (FTBPP-2)
Technical Library
Edwards AFB, California 93523

Space Systems Division
Air Force Systems Command
Attn: SSSD
Los Angeles Air Force Station
Los Angeles, California 90045

NOTE: 1 CY TO EACH ADDRESSEE UNLESS OTHERWISE INDICATED

Maj. Charles Waespy
Technical Div
Deputy for Technology
SSD, AFSC Los Angeles, Calif. 90045

SSD (SSTRT/Lt. Starbuck)
AFUPO
Los Angeles, California 90045

DET #6, OAR (LOOAR)
Air Force Unit Post Office
Los Angeles, California 90045

Systems Engineering Group (RTD)
Technical Information Reference Branch
Attn: SEPIR
Directorate of Engineering Standards & Technical Information
Wright-Patterson AFB, Ohio 45433

ARL (ARIY)
Wright-Patterson AFB, Ohio 45433

AFAL
Wright-Patterson AFB, Ohio 45433
Attn: Dr. H. V. Noble
Attn: Mr. Peter Murray

AFAL (AVT)
Wright-Patterson AFB, Ohio 45433

AFAL (AVTE/R.D. Larson)
Wright-Patterson AFB, Ohio 45433

Commanding General
Attn: STEWS-WS-VT
White Sands Missile Range
New Mexico 88002 (2 cys)

RADC (EMLAL-1)
Attn: Documents Library
Griffiss AFB, New York 13442

Academy Library (DFSLB)
U.S. Air Force Academy
Colorado 80840

Lt. Col. Bernard S. Morgan
FJSRL, USAF Academy
Colorado Springs, Colorado 80912

APGC (PGBPS-12)
Eglin AFB, Florida 32542

AFETR Technical Library
(ETV, MU-135)
Patrick AFB, Florida 32925

AFETR (ETLLG-1)
STINFO Officer (For Library)
Patrick AFB, Florida 32925

Dr. L. M. Hollingsworth
AFCRL(CRN)
L.G. Hanscom Field
Bedford, Mass. 01731

AFCRL (CRMXLR)
AFCRL Research Library, Stop 29
L.G. Hanscom Field
Bedford, Mass. 01731

Department of the Air Force
AFSC Scientific and Technical Liaison Office
111 East 16th Street
New York, New York 10003

Col. Robert E. Fontana
EE Dept.
AF Institute of Technology
Wright-Patterson AFB, Ohio 45433

Col. A. D. Blue
RTD(RTTL)
Bolling AFB, Wash. D.C. 20332

ESD (ESTI)
L.G. Hanscom Field
Bedford, Mass. 01731 (2 cys)

Dr. I. R. Mirman
AFSC(SCT)
Andrews AFB, Md. 20331

Col. J. D. Warthman
AFSC(SCTR)
Andrews AFB, Md. 20331

Lt. Col. J. L. Reeves
AFSC(SCBB)
Andrews AFB, Md. 20331 (2 cys)

AEDC (ARO, Inc.)
Attn: Library/Documents
Arnold AFB, Tenn. 37389

European Office of Aerospace Res.
Shell Building
47 Rue Cantersteen
Brussels, Belgium (2 cys)

Lt. Col. R. Kalsich
Chief, Electronics Div. (SREE)
Directorate of Engineering Sci.
Air Force Office of Sci. Res.
1400 Wilson Boulevard
Arlington, Virginia 22209 (5 cys)

DEPARTMENT OF THE ARMY

U.S. Army Research Office
Attn: Physical Sciences Division
3045 Columbia Pike
Arlington, Virginia 22204

Commanding General
U.S. Army Materiel Command
Attn: AMCRD- TP
Washington, D.C. 20315

Commanding General
U.S. Army Strategic Communications Command
Washington, D.C. 20315

Commanding Officer
U.S. Army Materials Research
Watertown Arsenal
Watertown, Massachusetts 02172

Commanding Officer
U.S. Army Ballistics Research Lab.
Attn: V.W. Richards
Aberdeen Proving Ground
Aberdeen, Maryland 21005

Commandant
U.S. Army Air Defense School
Attn: Missile Sciences Div.
C & S Dept.
P.O. Box 9390
Fort Bliss, Texas 79916

Commanding Gereral
U.S. Army Missile Command
Attn: Technical Library
Redstone Arsenal, Alabama 35809

Commanding General
Frankford Arsenal
Attn: SMUFA-L6000 (Dr. Sidney Ross)
Philadelphia, Pa. 19137

U.S. Army Munitions Command
Attn: Technical Information Branch
Picatinney Arsenal
Dover, New Jersey 07801

Commanding Officer
Harry Diamond Laboratories
Attn: Dr. Berthold Altman(AMXDO-TI)
Connecticut Ave. and Van Ness Street N.W.
Washington, D.C. 20438

Commanding Officer
U.S. Army Security Agency
Arlington Hall
Arlington, Virginia 22212

Commanding Officer
U.S. Army Limited War Laboratory
Attn: Technical Director
Aberdeen Proving Ground
Aberdeen, Maryland 21005

Commanding Officer
Human Engineering Laboratories
Aberdeen Proving Ground,
Maryland 21005

Director
U.S. Army Engineer Geodesy,
Intelligence and Mapping
Research and Development Agency
Fort Belvoir, Virginia 22060

Commandant
U.S. Army Command and General Staff College
Attn: Secretary
Fort Leavenworth, Kansas 66270

Dr. H. Robl, Deputy Chief Scientist
U.S. Army Research Office (Durham)
Box CM, Duke Station
Durham, North Carolina 27706

Commanding Officer
U.S. Army Research Office (Durham)
Attn: CRD-AA-IP (Richard O. Ulsh)
Box CM, Duke Station
Durham, North Carolina 27706

Librarian
U.S. Military Academy
West Point, New York 10996

The Walter Reed Institute of Res.
Walter Reed Medical Center
Washington, D.C. 20012

CO, U.S. Army Electronics R and D Activity
White Sands Missile Range
N.M. 88002

Commanding Officer
U.S. Army Engineering R & D Lab.
Attn: STINFO Branch
Fort Belvoir, Virginia 22060

Dr. S. Benedict Levin, Director
Institute for Exploratory Research
U.S. Army Electronics Command
Fort Monmouth, New Jersey 07703

Director
Institute for Exploratory Research
U.S. Army Electronics Command
Attn: Mr. Robert O. Parker
Executive Secretary,
JSTAC (AMSEL-XL-D)
Fort Monmouth, New Jersey 07703

Commanding General
U.S. Army Electronics Command
Fort Monmouth, New Jersey 07703
Attn: AMSEL-SC
RD-D
RD-G

Commanding General
U.S. Army Electronics Command
Fort Monmouth, New Jersey 07703
Attn: RD-GF
RD-MAT
XL-D
XL-E
XL-C
XL-S
HL-D
HL-CT-R
HL-CT-P
HL-CT-L
HL-CT-O
HL-CT-1
HL-CT-A
NL-D
NL-A
NL-P
NL-R
NL-S
KL-D
KL-E
KL-S
KL-T
KL-SM
VL-D
WL-D

NOTE: 1 CY TO EACH SYMBOL LISTED INDIVIDUALLY ADDRESSED

DEPARTMENT OF THE NAVY

Chief of Naval Research
Attn: Code 427
Washington, D.C. 20360 (3 cys)

Naval Electronics Systems Command
ELEX 03
Falls Church, Va. 22046 (2 cys)

Naval Ship Systems Command
SHIP 031
Washington, D.C. 20360

Naval Ship Systems Command
SHIP 035
Washington, D.C. 20360

Naval Ordnance Systems Command
ORD 32
Washington, D.C. 20360 (2 cys)

Naval Air Systems Command
AIR 03
Washington, D.C. 20360 (2 cys)

Commanding Officer
Office of Naval Research Branch Office
Box 39, Navy No. 100 F.P.O.
New York, New York 09510 (2 cys)

Office of Naval Res. Branch Office
Attn: Deputy Chief Scientist
1076 Mission Street
San Francisco, California 94103
(2 cys)

Commanding Officer
Office of Naval Research Branch Office
219 South Dearborn Street
Chicago, Illinois 60604 (3 cys)

Commanding Officer
Office of Naval Research Branch Office
1030 East Green Street
Pasadena, Calif. 91101

Commanding Officer
Office of Naval Res. Branch Office
207 West 24th Street
New York, New York 10011

Commanding Officer
Office of Naval Res. Branch Office
495 Summer Street
Boston, Massachusetts 02210

Director, Naval Research Laboratory
Technical Information Officer
Washington, D.C.
Attn: Code 2000 (8 cys)

Commander
Naval Air Development and Material Center
Johnsville, Pennsylvania 18974

Librarian
U.S. Naval Electronics Laboratory
San Diego, California 95152 (2 cys)

Commanding Officer and Director
U.S. Naval Underwater Sound Lab.
Fort Trumbull
New London, Connecticut 06840

Librarian
U.S. Navy Post Graduate School
Monterey, California 93940

Commander
U.S. Naval Air Missile Test Center
Point Mugu, California 93041

Director
U.S. Naval Observatory
Washington, D.C. 20390

Chief of Naval Operations
OP-07
Washington, D.C. 20360 (2 cys)

Director, U.S. Naval Security Group
Attn: G43
3801 Nebraska Ave.
Washington, D.C. 20390

Commanding Officer
Naval Ordnance Laboratory
White Oak, Maryland 21502 (5 cys)

CO, Naval Ord. Lab
Corona, Calif. 91720

Commanding Officer
Naval Ordnance Test Station
China Lake, California 93555

Commanding Officer
Naval Avionics Facility
Indianapolis, Indiana 46206

Commanding Officer
Naval Training Device Center
Orlando, Florida 32813

U.S. Naval Weapons Laboratory
Dahlgren, Virginia 22448

Weapons Systems Test Division
Naval Air Test Center
Patuxtent River, Maryland 20670
Attn: Library

Head, Tech. Div.
U.S. Naval Counter Intelligence
Support Center
Fairmont Bldg.
4420 N. Fairfax Dr.
Arlington, Va. 22203

OTHER GOVERNMENT AGENCIES

Mr. Charles F. Yost
Special Assistant to the Director
of Research
National Aeronautics and Space Admin.
Washington, D.C. 20546

Dr. H. Harrison, Code RRE
Chief, Electrophysics Branch
National Aeronautics and Space Admin.
Washington, D.C. 20546

Goddard Space Flight Center
National Aeronautics and Space Ad.
Attn: Library, Documents Section
Code 252
Greenbelt, Maryland 20771

NASA Lewis Research Center
Attn: Library
21000 Brookpark Road
Cleveland, Ohio 44135

National Science Foundation
Attn: Dr. John R. Lehmann
Division of Engineering
1800 G Street, N.W.
Washington, D.C. 20550

U.S. Atomic Energy Commission
Division of Tech. Information Ext.
P.O. Box 62
Oak Ridge, Tenn. 37831

Los Alamos Scientific Laboratory
Attn: Reports Library
P.O. Box 1663
Los Alamos, New Mexico 87544

NASA Scientific & Technical
Information Facility
Attn: Acquisitions Branch (S/AK/DL)
P.O. Box 33
College Park, Maryland 20740 (2 cys)

Commandant (E-2)
U.S. Coast Guard Headquarters
Library, Station 5-2
Washington, D.C. 20226

National Aeronautics and Space Admin.
Electronics Research Center
AT/Library
575 Technology Square
Cambridge, Massachusetts 02139

Federal Aviation Agency
Information Retrieval Branch, HQ-630
800 Independence Avenue, S.W.
Washington, D.C. 20553

U.S. Department of Commerce
National Bureau of Standards
Publications Editor
Center for Computer Sciences and
Technology
Washington, D.C. 20234

U.S. Department of Commerce
Environmental Science Services Admin.
Institute for Telecommunication
Sciences and Aeronomy
Boulder, Colorado 80301

NON-GOVERNMENT AGENCIES

Director
Research Laboratory of Electronics
Massachusetts Institute of Tech.
Cambridge, Massachusetts 02139

Polytechnic Institute of Brooklyn
Attn: Mr. Jerome Fox
Research Coordinator
333 Jay Street
Brooklyn, New York 11201

Director
Columbia Radiation Laboratory
Columbia University
538 West 120th Street
New York, New York 10027

Director
Coordinated Science Laboratory
University of Illinois
Urbana, Illinois 61803

Director
Electronics Research Laboratory
University of California
Berkeley, California 94720

Director
Electronic Sciences Laboratory
University of Southern California
Los Angeles, California 90007

Professor A.A. Dougal, Director
Laboratories for Electronics and
Related Sciences Research
University of Texas
Austin, Texas 78712

Division of Engineering and
Applied Physics
210 Pierce Hall
Harvard University
Cambridge, Massachusetts 02138

Director
Stanford Electronics Labs
Stanford University
Stanford, Calif. 94720

Director
Microwave Laboratory
Stanford University
Stanford, California 94305

Director
Information Processing and Control
Systems Laboratory
Northwestern University
Evanston, Illinois 60201

Director
Electronic Systems Res. Laboratory
Purdue University
Lafayette, Indiana 47907

Aerospace Corporation
Attn: Library Acquisition Group
P.O. Box 95085
Los Angeles, California 90045

Professor Nicholas George
California Institute of Technology
Pasadena, California 91109

Aeronautics Library
Graduate Aeronautical Laboratories
California Institute of Tech.
1201 E. California Boulevard
Pasadena, California 91109

Director, USAF Project RAND
Via: Air Force Office Liaison Office
The RAND Corporation
Attn: Library
1700 Main Street
Santa Monica, California 90406

The Johns Hopkins University
Applied Physics Laboratory
Attn: Boris W. Kuvshinoff
Document Librarian
8621 Georgia Avenue
Silver Spring, Maryland 20910

Hunt Library
Carnegie Institute of Technology
Schenley Park
Pittsburgh, Pa. 15213

Dr. Leo Young
Stanford Research Institute
Menlo Park, California 94025

Mr. Henry L. Bachmann
Assistant Chief Engineer
Wheeler Laboratories
122 Cuttermill Road
Great Neck, New York 11021

School of Engineering Sciences
Arizona State University
Tempe, Arizona 85281

University of California at
Los Angeles
Department of Engineering
Los Angeles, California 90024

California Institute of Technology
Pasadena, Calif. 91109
Attn: Documents Library

University of California
Attn: Library
Santa Barbara, California 93106

Carnegie Institute of Technology
Electrical Engineering Dept.
Pittsburgh, Pa. 15213

New York University
College of Engineering
New York, New York 10019

Syracuse University
Dept. of Electrical Engineering
Syracuse, New York 13210

Yale University
Engineering Department
New Haven, Connecticut 06520

Airborne Instruments Laboratory
Deer Park, New York 11729

Bendix Pacific Division
11600 Sherman Way
North Hollywood, California 91605

Lockheed Aircraft Corp.
P.O. Box 504
Sunnyvale, California 94088

Raytheon Co.
Attn: Librarian
Bedford, Mass. 01730

Emil Schafer, Head
Electronics Properties Info Center
Hughes Aircraft Co.
Culver City, Calif. 90230

Texas Instruments Inc.
Library Acquisitions Center,
M/S - 284
P.O. Box 5474
Dallas, Texas 75222

The University of Wisconsin
College of Engineering
Dept. of Electrical Engineering
Madison, Wisconsin 53706

General Electric Company
Research and Development Center
P.O. Box 8
Schenectady, New York 12301

The University of Adelaide
Barr Smith Library
Adelaide, South Australia

Westinghouse Electric Corporation
Electronic Tube Division
Box 284
Elmira, New York 14902

Fairchild Research & Development Lab.
4001 Junipero Serra Boulevard
Palo Alto, California 94304

Bell Telephone Laboratories
Electron Device Laboratory
Mountain Avenue - Room 2A-229
Murray Hill, New Jersey 07971

Purdue University Libraries
Periodicals Checking Files
Lafayette, Indiana 47907

Ampex Corporation
401 Broadway
Redwood City, California 94063

General Precision, Inc.
Librascope Group
808 Western Avenue
Glendale, California 91201

Sperry Rand Research Center
North Road
Sudbury, Massachusetts 01776

Westinghouse Electric Corporation
Defense and Space Center
Aerospace Division - MS-393
P.O. Box 746
Baltimore, Maryland 21203

Lockheed Propulsion Company
Scientific & Technical Library
P.O. Box 111
Redlands, California 92373

University of Utah
Dept. of Electrical Engineering
Microwave Device and Physical
Electronics Laboratory
Merrill Engineering Building
Salt Lake City, Utah 84112

Director of Research
AeroChem Research Laboratories, Inc.
P.O. Box 12
Princeton, New Jersey 08540

Director of Research
Motorola, Inc.
Semiconductor Products Division
5005 East McDowell Road
Phoenix, Arizona 85008

International Business Machines Corp.
Electronics Systems Center
Oswego, New York 13827

Stevens Institute of Technology
Department of Physics
Castle Point Station
Hoboken, New Jersey 07030

The University of Michigan
Institute of Science and Tech.
Technical Documents Service
Box 618
Ann Arbor, Michigan 48107

Hughes Aircraft Company
Library
500 Superior Avenue
Newport Beach, California 92663

Director
Engineering Design Center
Case Institute of Technology
10900 Euclid Avenue
Cleveland, Ohio 44106

Director
Speech Communications Research
Lab., Inc.
115 West Figueroa Street
Santa Barbara, California 93104

Baird-Atomic Inc.
Library
33 University Road
Cambridge, Massachusetts 02138

Director
Electronics Defense Laboratories
Sylvania Electric Products, Inc.
Library
P.O. Box 205
Mountain View, California 94040

TRW Systems, Inc.
Semiconductor Technology Section
Microelectronics Center
Bldg. 68, Room 2734
One Space Park
Redondo Beach, California 09278

ITT Corporation
ITT Electron Tube Division
Vice-President - Engineering
Box 100
Easton, Pennsylvania 18043

Sylvania Electronics Systems
Director of Engineering
Eastern Operation
100 First Avenue
Waltham, Massachusetts 02154

TRW Semiconductors, Inc.
Research Director
14520 Aviation Boulevard
Lawndale, California 90260

Director
Communication & Display R&D
Research & Development Center
Westinghouse Electric Corporation
Pittsburgh, Pennsylvania 15235

Raytheon Company
Semiconductor Library
350 Ellis Street
Mountain View Operation
Mountain View, California 94040

McGill University
Department of Electrical Engineering
Montreal, Canada

North Carolina State University
School of Engineering
Dept. of Electrical Engineering
Box 5275
Material Science Laboratory
Raleigh, North Carolina 27607

ITT Semiconductors
Product Laboratory
1801 Page Mill Road
Palo Alto, California 94304

Raytheon Company
Microwave and Power Tube Division
Waltham, Massachusetts 02154

National Biomedical Res. Foundation
8600 Sixteenth Street
Silver Springs, Maryland 20910

University of Nevada
College of Engineering
Dept. of Electrical Eng.
Reno, Nevada 89507

University of California
Lawrence Radiation Laboratory
Technical Information Division
Berkeley, California 94720

LFE Electronics
Electronics Division of Laboratory
for Electronics Inc.
1075 Commonwealth Avenue
Boston, Massachusetts 02215

ITT Federal Laboratories
500 Washington Avenue
Technical Library
Nutley, New Jersey 07110

Raytheon Company
Research Division Library
28 Seyon Street
Waltham, Massachusetts 02154

The University of Oklahoma
College of Engineering
School of Electrical Engineering
Norman, Oklahoma 73069

Hughes Aircraft Company
Hughes Research Laboratory
3011 Malibu Canyon Road
Malibu, California 90265

The University of Wisconsin
Laboratory of Neurophysiology
Medical School
283 Medical Sciences Building
Madison, Wisconsin 53706

Federal Scientific Corporation
615 West 131st Street
New York, New York 10027

The University of Santa Clara
The School of Engineering
Dept. of Electrical Engineering
Santa Clara, California 95053

Sprague Electric Company
Research and Development Laboratories
North Adams, Massachusetts 01247

Worcester Polytechnic Institute
Dept. of Electrical Engineering
Worcester, Massachusetts 01609

Westinghouse Electric Corporation
Research Laboratories
Churchill Borough
Pittsburgh, Pennsylvania 15235

International Business Machines Corp.
Monterey & Cottle Roads
San Jose, California 95114

University of Notre Dame
Dept. of Electrical Engineering
Notre Dame, Indiana 46556

Radio Corporation of America
RCA Engineering Library
Moorestown, New Jersey 08057

Lockheed-Georgia Company
Department 72-34, Zone 400
Research Information
Marietta, Georgia

Varian Associates
Technical Library
611 Hansen Way
Palo Alto, California 94303

Princeton University
School of Engineering and
Applied Science
Princeton, New Jersey 08540

Vice President
Bell Telephone Laboratories, Inc.
Murray Hill, New Jersey 07971

University of Illinois
Dept. of Electrical Engineering
Urbana, Illinois 61801

Mr. John J. Sie, President
Micro State Electronics Corp.
152 Floral Avenue
Murray Hill, New Jersey 07971

University of Alberta
Department of Physics
Edmonton, Alberta
Canada

Staff Vice President
Materials and Device Research
Radio Corporation of America
David Sarnoff Research Center
Princeton, New Jersey 08540

Information Technology Library
AUERBACH Corporation
121 North Broad Street
Philadelphia, Pennsylvania 19107

Philco Corporation
Module Engineering Department
Microelectronics Division
504 South Main Street
Spring City, Pennsylvania 19475

Motorola, Inc.
Government Electronics Division
8201 East McDowell Road
Scottsdale, Arizona 85252

Librarian
Microwave Associates, Inc.
Northwest Industrial Park
Burlington, Massachusetts 01803

Professor A. S. Vander Vorst
Laboratoire d'Electronique
Universite de Louvain
94, Kardinaal Mercierlaan
Heverlee - Leuven, Belgium

United Aircraft Corporation
Norden Division
Technical Library
Norwalk, Connecticut 06851

Watkins-Johnson Company
3333 Hillview Avenue
Stanford Industrial Park
Palo Alto, California 94304

The Ohio State University
Dept. of Electrical Engineering
2024 Neil Avenue
Columbus, Ohio 43210

University of Florida
College of Engineering
Dept. of Electrical Engineering
Gainesville, Florida 32603

Georgia Institute of Technology
Price Gilbert Memorial Library
Atlanta, Georgia 30332

Sandia Corporation
Technical Library
P.O. Box 5800, Sandia Base
Albuquerque, New Mexico 87115

Cornell Aeronautical Laboratory, Inc.
of Cornell University
P.O. Box 235
Buffalo, New York 14221

The University of Western Australia
Dept. of Electrical Engineering
Nedlands, Western Australia

Radio Corporation of America
Manager of Engineering
415 South 5th Street
Harrison, New Jersey 07029

General Telephone & Electronics
Laboratories, Inc.
208-20 Willets Point Boulevard
Bayside, New York 11360

The Boeing Company
Office of the Vice President
Research and Development
P.O. Box 3707
Seattle, Washington 98124

Professor R.E. Vowels, Head
School of Electrical Engineering
The University of N.S.W.
Box 1 P.O.
Kensington, N.S.W. Australia

The George Washington University
School of Engineering and Applied Sci.
Department of Electrical Engineering
Washington, D.C. 20006

AUTONETICS
Research and Engineering Division
Technical Information Center
P.O. Box 4173
3370 Miraloma Avenue
Anaheim, California 92803

Martin-Marietta Corporation
Martin Company, Baltimore Division
Chief of Libraries
Baltimore, Maryland 21203

Sperry Gyroscope Company
Division of Sperry Rand Corporation
Head, Engineering Department
Countermeasures Engineering
Great Neck, New York 11020

Rensselaer Polytechnic Institute
Dept. of Electrical Engineering
Russell Sage Laboratory
Troy, New York 12181

General Electric Company
Liaison Engineer
Computer Laboratory
P.O. Box 1285
Sunnyvale, California 94088

Electro-Optical Systems, Inc.
Micro-Data Operations
300 North Halstead Street
Pasadena, California 91107

Manager Systems Engineering
Radio Corporation of America
Communications Systems Division
Front and Market Streets, Bldg. 17C-6
Camden, New Jersey 08102

Engineering Librarian
Varian Associates
LEL Division
Akron Street
Copiague, New York 11726

Dr. Alan M. Schneider
University of California, San Diego
Department of the Aerospace and
Mechanical Engineering Sciences
P.O. Box 109
La Jolla, California 92038

University of Illinois
Dept. of Computer Science
Digital Computer Laboratory
Room 230
Urbana, Illinois 61803

University of Chicago
Institute for Computer Research
5640 South Ellis Avenue
Chicago, Illinois 60637

Scientific Advisor
Lockheed Electronics Company
Military Systems
Plainfield, New Jersey 07060

California Institute of Technology
Jet Propulsion Laboratory
Library Supervisor
4800 Oak Grove Drive
Pasadena, California 91103

UNCLASSIFIED
Security Classification

DOCUMENT CONTROL DATA - R & D

(Security classification of title, body of abstract and indexing annotation must be entered when the overall report is classified)

1. ORIGINATING ACTIVITY *(Corporate author)*
Stanford Electronics Laboratories
Stanford University, Stanford, California

2a. REPORT SECURITY CLASSIFICATION
Unclassified

2b. GROUP

3. REPORT TITLE
INDUCTORLESS FILTERS

4. DESCRIPTIVE NOTES *(Type of report and inclusive dates)*
Technical Report - (also a Ph.D. Dissertation)

5. AUTHOR(S) *(First name, middle initial, last name)*
Desmond Francis Sheahan

6. REPORT DATE	7a. TOTAL NO. OF PAGES	7b. NO. OF REFS
September 1967	100	38

8a. CONTRACT OR GRANT NO.	9a. ORIGINATOR'S REPORT NUMBER(S)
Nonr-225(83)	
b. PROJECT NO. NR 373 360	TR No. 6560-15
c.	9b. OTHER REPORT NO(S) *(Any other numbers that may be assigned this report)*
d.	SEL-67-086

10. DISTRIBUTION STATEMENT
Qualified requesters may obtain copies from DDC. Foreign announcement and dissemination are limited.

11. SUPPLEMENTARY NOTES	12. SPONSORING MILITARY ACTIVITY
	Joint Services Electronics Program (U.S. Army, Navy, and Air Force)

13. ABSTRACT In recent years integrated circuit technology has been used in the construction of many types of miniaturized electronic systems but it has not, as yet, found much application to the precision, electrical filters used by the telephone industry at frequencies up to a few hundred kilohertz. These filters require very high quality inductors, and those presently available are heavy, bulky items. Great savings in the size and weight of telephone systems would be obtained if suitable inductors could be made by integrated circuit techniques, but so far this has not been possible. One alternative is to make the filters by using those components which are available in integrable form. Various schemes have been proposed for doing this, but most of them require component tolerances too tight to be practical. Many of the schemes use negative impedance converters in circuits whose transmission properties are determined by a critical match between a positive and a negative impedance; as a result of this matching process the transmission properties are very sensitive to component tolerances. The conventional, doubly terminated, inductor-capacitor filter, on the other hand is relatively insensitive to component tolerances, and it is proposed in the dissertation that this desirable property be retained by making an integrated circuit which simulates, in an inductorless fashion, the detailed behavior of the LC filter structure. Two distinct methods are described. The first of these uses exactly the conventional LC filter structure and merely replaces each inductor by an integrable circuit that behaves like an inductor. The circuit takes the form of a frequency-independent, two-port network which, when terminated at one port by a capacitor, presents an inductive behavior at the other port. This impedance inverting network, or gyrator, can be constructed from a pair of controlled sources. The dissertation analyzes this type of

DD FORM 1 NOV 65 1473

UNCLASSIFIED
Security Classification

14. KEY WORDS	LINK A		LINK B		LINK C	
	ROLE	WT	ROLE	WT	ROLE	WT
ELECTRIC FILTERS INTEGRATED CIRCUITS GYRATORS						

ABSTRACT (Cont)

gyrator, derives a set of requirements for high-quality performance and describes a specific circuit which meets them. Experiments on a complex band-pass filter confirm that it is possible to obtain low sensitivity filters by this means. The second method simulates the LC filter structure by making a complete model in the manner of an analog computer. Conventional analog computer circuitry proved inadequate and it was necessary to devise two special circuits to perform, very precisely, the operations of subtraction and integration. These were designated the Difference Amplifier and the Difference Integrator. In an attempt to produce a universal circuit arrangement that would be applicable to all classes of filter, these basic units were used to build the principal canonical tandem section due to Darlington and Brune. These simulated Brune sections were used to construct a low-pass, a high-pass, and a band-pass filter. Experiments on these filters showed that this also is a suitable way to produce low sensitivity filters.

It was found for both techniques, that, in order for the simulation to be successful, the original LC design should not have widely different L/C ratios in its resonant circuits. The dissertation compares the two techniques from several points of view and notes that the inductor simulation technique has a distinct practical advantage in that the filter capacitors isolate the bias circuits of the separate gyrators. The two techniques are completely integrable as they use only resistors, capacitors, transistors and diodes. The tolerance and stability required of the resistors and capacitors can be achieved with modern thin-film technology. Both techniques clearly show that complex filters can now be built in integrable form.